THE IN-SERVICE NON-DESTRUCTIVE EVALUATION OF WOODEN TRANSMISSION LINE POLES

B.P.PRESTAGE

AUGUST 1997

Submitted to the University of Cape Town in

full fulfilment of the requirements

for the Degree of Master of Science

in

Mechanical Engineering.

SUPERVISOR

Professor J Gryzagoridis

I, Brendan Paul Prestage, submit this thesis in full fulfilment of the requirements for the Degree of Master of Science in Mechanical Engineering. I state that it has not been submitted in this or any similar form for any degree at this or any other university.

Brendan Paul Prestage

University of Cape Town

August 1997

ABSTRACT

This thesis covers the research undertaken on behalf of the ESKOM TRI Group into the In-service Non-Destructive Evaluation of Wooden Transmission Line Poles. The aim of this work was the development of an effective pole tester that could be used to test the integrity of wooden transmission line poles in situ. The pole testing method that ESKOM uses at present is both time and labour intensive and it is envisaged that this research will contribute to the establishment of a faster, cheaper and more effective alternative.

The research began with a literature survey of past investigations. Previous research in this area followed two distinct approaches. The first approach concentrated on mechanical testing procedures. For example the physical bending of the pole and measuring its bending stress (the effect that this bending has on the single fibres in the pole is not documented). The present ESKOM pole tester follows this approach. The second approach has been in the field of true "non-destructive" testing. Procedures using x-rays, magnetic resonance imaging and vibration analysis have all been considered in the past by investigators.

The present investigation followed the approach of vibrations analysis. The process involved impacting the pole and measuring its vibration response. The response was then used to analyse the pole's behaviour. The state of integrity of the pole determined its vibration characteristics. Thus a pole

without groundline decay was found to have higher modal frequencies than one with decay. This approach was applied to the testing of pole samples in an attempt to formulate a suitable testing procedure. The pole samples were subjected to a number of tests and a comparison between all was attempted. The results obtained did not allow a reasonable comparison.

The work continued by artificially degrading the wooden poles and it was found that by removing material in the groundline area, the modal frequencies had decreased. Although one cannot correlate a direct strength value for a particular pole from these data, a "history" of the pole can be obtained over a period of time. This will allow for a preventative maintenance programme.

The test procedure was finally applied to a full length pole. It was found that groundline degradation had a significant impact on the maximum bending moment that the pole could withstand while exhibiting a very small percentage shift in frequency.

The conclusion drawn from this work is that vibration analysis may be used as a technique in the non-destructive evaluation of wooden poles, but that the procedure would have to be "fine-tuned" to cater for the in-service poles

ACKNOWLEDGEMENTS

The author would like to thank the following for their assistance with this project:

Professor J. Gryzagoridis for his technical guidance during the supervision of this project. His patience, understanding and help with the structure of this thesis, are gratefully acknowledged.

Messers J. Retief and D. van der Westhuyzen for their help in completing this thesis.

My parents and girlfriend for their unselfish patience and moral support.

CONTENTS

LIST OF FIGURES

LIST OF TABLES

LIST OF PHOTOGRAPHS

1 INTRODUCTION

Over the last century the use of wooden poles for the support of transmission lines has become a world-wide practice. This wide usage has led to increased research into maintaining these poles and most importantly in determining their fitness for purpose. It is hoped that the contents of this thesis will contribute to these efforts.

The main reasons for the use of wooden poles include low weight, good workability for framing and boring and the potential for long service as compared to other materials such as concrete, steel or fibreglass poles.

However, the use of wood does have its disadvantages. These include the fact that wood is biodegradable and has highly variable strength properties. Utility companies continue to investigate the properties of wooden poles and possible ways of prolonging the in-service life of these poles. The poles that are used are chemically preserved but even this does not prevent pole failure due to excessive rot. The approach of most utilities has been to incorporate a preventative maintenance plan that ensures that the poles maintain a level of condition/strength. This has lead to further research into methods of determining the in-service "state" of the poles and the necessary minimum levels.

This project was undertaken on behalf of the Technology Research Investigations (TRI) Division of ESKOM. ESKOM has up to now used a

mechanical test procedure that applies a bending moment to the pole, transverse to the direction of the transmission line. By measuring the deflection and the force applied, the maximum bending moment at the point at which the outer fibres fail (the proportional limit), is determined. This procedure has been found to be cumbersome, time consuming, labour intensive and does not allow one to test any other construction configuration besides a single pole such as a stayed pole, corner pole or H-frame support.

ESKOM also investigated the possibility of testing the wooden poles using an ultrasonic detector. This device measures the time of an ultrasonic pulse to propagate across the diameter of a pole. The velocity of propagation is then computed and if the reading is above a certain value, the pole is considered good. This test procedure is a very localised test procedure and the quality of the results is highly dependent on the boundary conditions. The inability to ascertain the condition of certain poles prompted ESKOM to carry out further research into the field of non-destructive evaluation of wooden poles and the present project is part of that research.

Our initial approach was to review all the available literature on the non-destructive procedures that could be used for testing wooden transmission line poles. The literature survey details such procedures and techniques, be they scientific or commercial. After consideration of the available and emerging non-destructive techniques, it was decided to pursue the vibration analysis method.

Vibration analysis allows one to quantify the state of the pole with frequent testing as part of a preventative maintenance plan. Other contributing reasons for this choice include the ability to test any structure, the global nature of the test and the speed and ease of testing. Although the actual testing procedure is simple and quick, the analysis of the results is time consuming and complex but this can possibly be automated.

Vibration analysis was investigated in depth and a number of tests were carried out on a sample group of short wooden poles. This thesis will discuss the testing procedure, the analysis of the results obtained and how this testing procedure may be of benefit to ESKOM and other users of wooden poles.

2 LITERATURE SURVEY

This chapter attempts to review past research undertaken into the grading and maintaining of wooden transmission line poles world-wide.

The utility industry has long recognised the inherent advantages and disadvantages of using wooden poles as transmission line supports. As a result of increased electrification, the number of wooden poles in service has increased. This growth in the usage of wooden poles has led to a large economic investment on the part of the utilities and hence, the need to maximise the in service life of the poles.

An example of the cost involved is that in 1986, it was estimated that the North American power utilities had 100 million poles in service at a replacement cost of $50 billion. Every year more than 2 million poles were replaced at a cost exceeding $ 500 per pole with excessive decay being the dominant reason for replacement [1]. It is estimated that there are 6 million transmission line poles in service in South Africa at present at a replacement cost exceeding R 600 per pole (Information courtesy of ESKOM).

2.1 EXPERIMENTAL TECHNIQUES USED IN PREVIOUS WOODEN POLE RESEARCH

A great deal of effort has been directed towards improving in-service pole inspection methods. Species identification and visual grading were among the earliest non-destructive methods used for wooden poles but, as for any engineering application, a higher reliability is needed. Following this visual grading and prior to any research or development of testing procedures, the technique employed by experienced line operators was to "prod" or "sound" the pole with a hammer or screwdriver [2]. An experienced line operator would then decide from the sound whether the pole was rotten or not. This inspection method is obviously highly questionable. Another "destructive" test included removing cores from the pole in search of rot pockets. This test has limited accuracy and rot pockets may remain undetected. Further, the detection of rot gives only a general indication of the pole's remaining strength.

The research has progressed using techniques such as mechanical methods, visual inspection, ultrasonic and impedance testing, x-rays, electrical resistance methods and vibration analysis. There are several techniques already in use commercially in the timber industry. In most cases the techniques have been used non-destructively and the results obtained have usually been compared with results obtained using a destructive technique.

The use of non-destructive techniques to determine the properties of wood, which possesses a large inherent variability, can greatly decrease the uncertainty of prediction. Most of the non-destructive techniques for predicting the strength of wood are based on empirical relationships between a given strength property such as modulus of rupture (MOR) and modulus of elasticity (MOE). These empirical MOR - MOE relationships are then used for the prediction of the strength of members evaluated by non-destructive procedures.

2.1.1 MECHANICAL TECHNIQUES

Mechanical techniques have been developed and used in the field by different utilities. This approach, to finding the strength of wooden poles, relies on applying a force to the pole and measuring the deflection of the pole at a specific position. From the values obtained from such a test, one can calculate the maximum bending moment and the Modulus of Elasticity (MOE). This type of test is limited to the testing of single poles and the testing equipment is usually very cumbersome to manoeuvre and time consuming to use. Another concern that has been raised when using a mechanical method has been whether the bending of the pole results in any permanent deformation of the weaker fibres or in the hardware connections at the top of the pole due to the increased tension in the lines. Neither of these occurrences have been quantified.

The Electricity Council Research Centre [3] based in Chester, England developed two mechanical devices to test for bending strength prior to ultimate destruction. They claimed that by subjecting a portion of a pole to a constant bending moment most accurately interpreted the elastic properties of the pole and that timber research had shown that the relationship between the moduli of rupture and elasticity were reasonably constant for a given wood species. Hence if one can measure elasticity, the rupture modulus can be predicted.

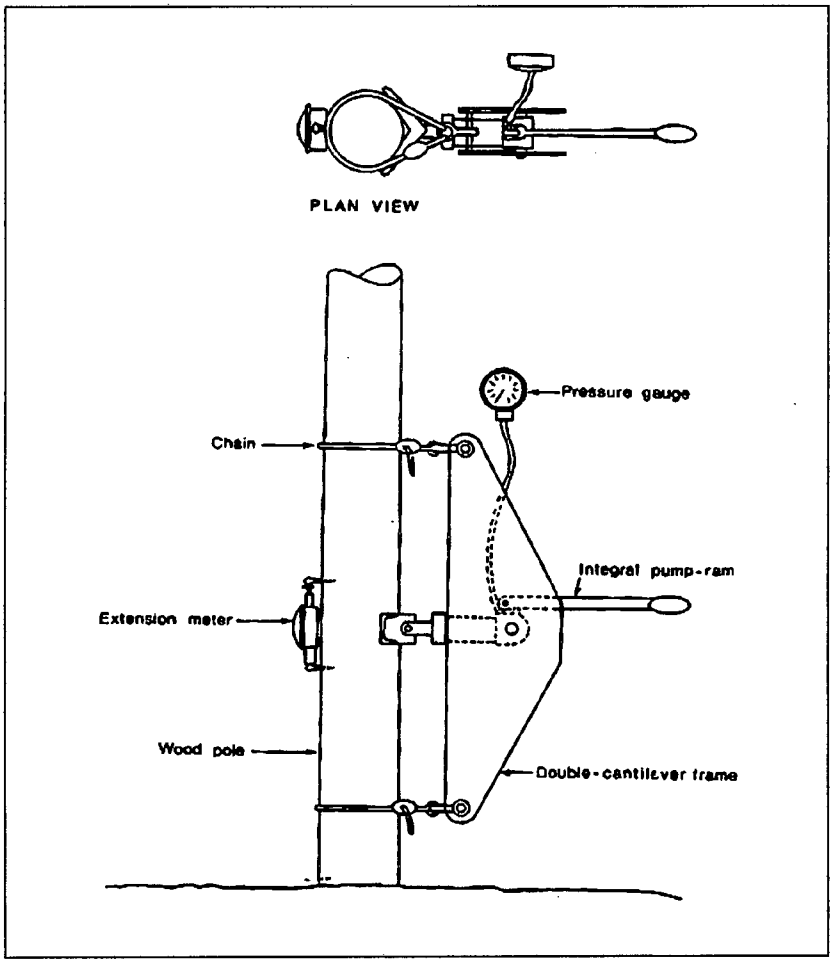

Figure 1: The Three Point Loading Device.

The two devices included the PEST (acronym for pole elasticity strength tester) and a three point loading device. The more portable three point loading device was found to be less successful that the PEST. The diagrams in Figure 1 and Figure 2 show the two devices.

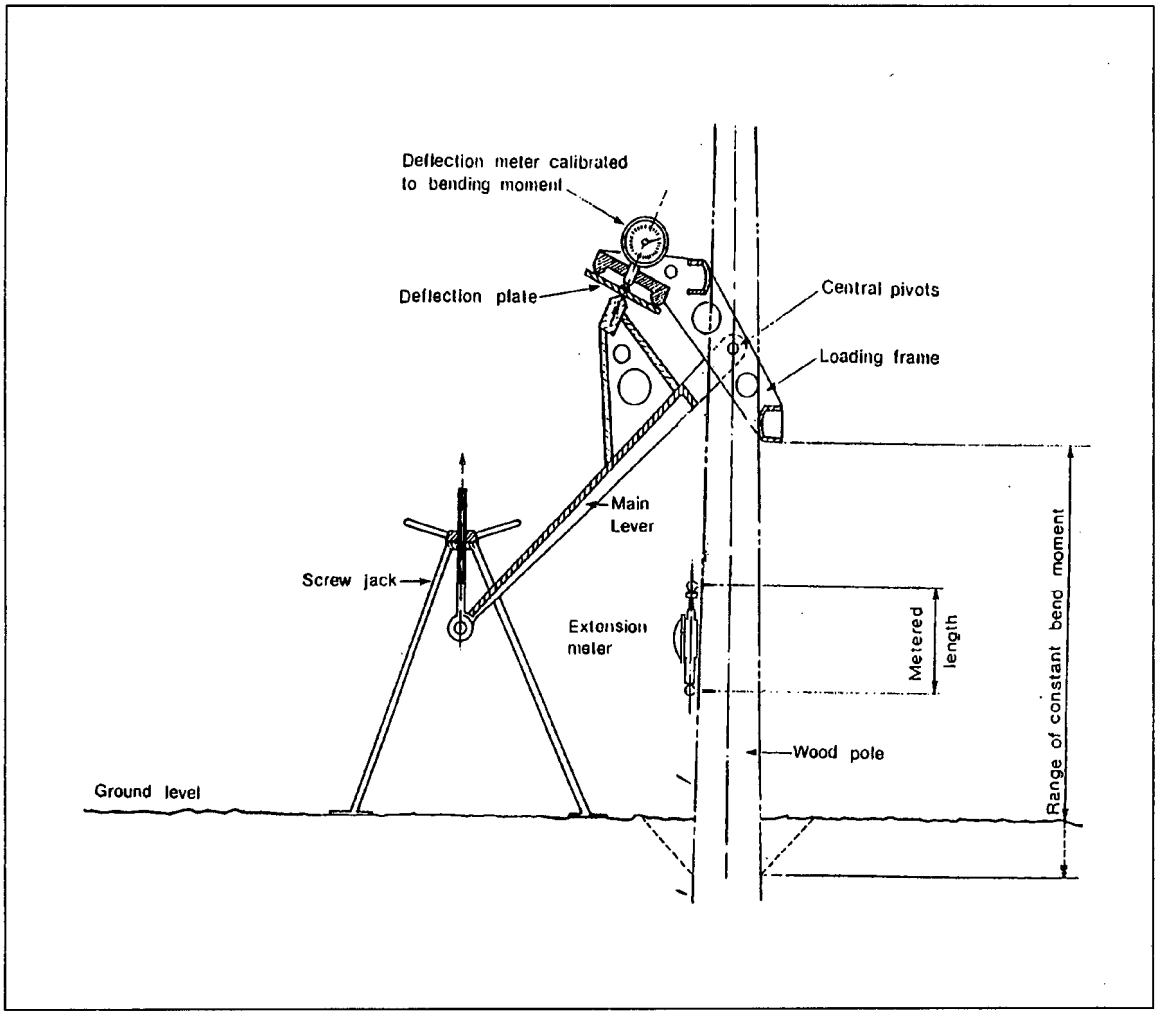

Figure 2: The PEST Device.

In tests carried out on a sample set of 30 poles removed from service, the results showed that of the poles that were rejected by ESI (English Standards Institute) Standard 43-10, 79% were rejected by the PEST test. These tests

highlighted the advantage of the PEST test; namely the ability to indicate where strengths in excess of the minimum requirements exist. This offers the opportunity to defer the replacement of some of poles, which leads to the desired economic saving.

Electrical Power Research Institute (EPRI) Report No. RP1352-1 [4] details in three volumes the probability-based design of wooden transmission structures. The objectives of this project were to develop improved design procedures for wooden transmission line structures that would result in a consistent level of safety and reliability and to assess wooden pole strength and variability for both new and in-service poles.

The first volume deals with the research on the strength and stiffness of wooden utility poles. The research started with an analysis of pre-existing data on wooden pole properties and the major variables influencing the pole's strength. This analysis was followed by a series of non-destructive and destructive tests on full size poles that had been removed from service. The purpose for testing poles that had been removed from service while still structurally sound was to show whether or not time in-service effects can be quantified for use in the initial design of transmission line structures and to study methods of testing so that a procedure for large scale in-service testing can be incorporated.

The destructive testing procedure was designed to the American Society for Testing and Materials (ASTM) D 1036: "Static Tests of Wood Poles" [5],

which allows for both the universal three point loading machine method or the cantilever method. The use of the universal method is impractical for larger poles and hence, the cantilever method was used. Figure 3 below shows the method used to destructively test the poles.

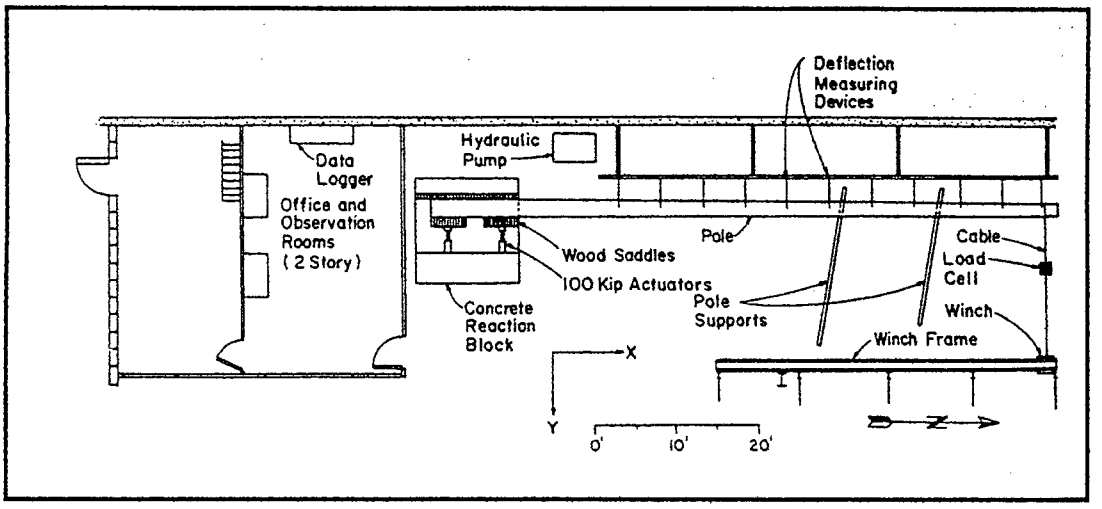

Figure 3: The EPRI Destructive Pole Tester

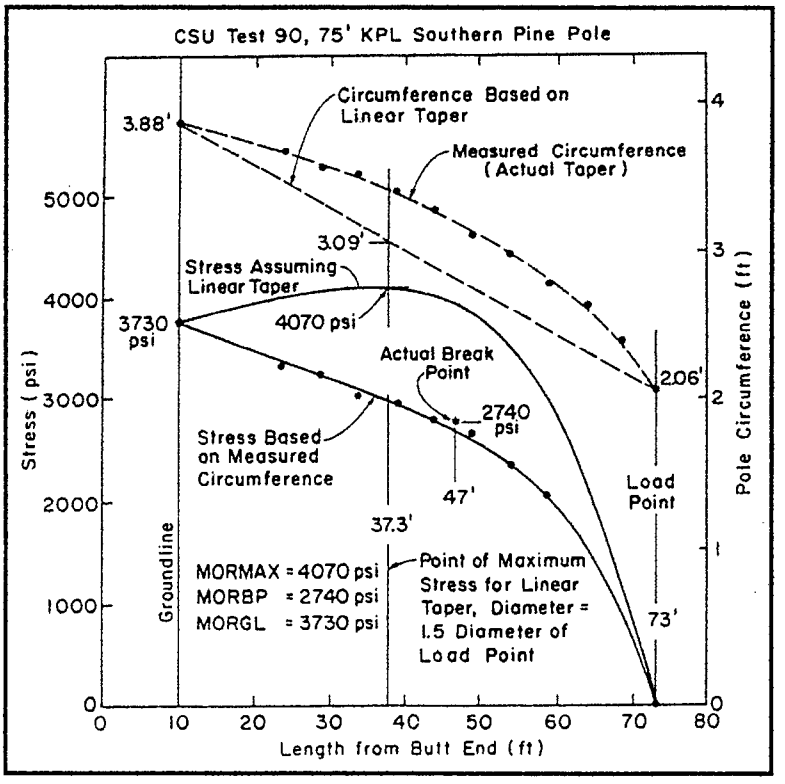

Figure 4: Examples of Effects of Actual Taper on Stress Calculations for Test Poles.

Two fundamental assumptions that are made in the design of wooden pole structures are that every cross section is round and that the pole tapers uniformly from the ground line to the tip. For the calculation of the modulus of rupture at ground line (MORGL) and modulus of rupture at breaking point (MORBP), the poles were assumed to be round but the circumferences at the particular points were measured. The Modulus of Rupture is the computed maximum fibre stress in the extreme fibres at the point of maximum load. Figure 4 above illustrates the effects of actual taper on results of modulus of rupture.

The test results for both the MORGL and MOE show that the strength of the pole decreases with service time which supports the original hypothesis. In some species this reduction is less than with others and this is due to their natural resistance to decay (Western Redcedar is considered to have a higher resistance than the other tested species). The MOE values for new poles of certain species were found to be lower than those obtained in the testing procedure and this raised questions about the original data. The measurements of MOE were crude in many of the previous tests of new poles.

The results for the MORGL were compared with the values specified for design by American National Standards Institution (ANSI) and the MOE with those specified by the American Society for Testing and Materials (ASTM) and these graphs are shown below in Figure 5 and Figure 6.

The ASTM "green" values are the values obtained from laboratory tests on green samples and those shown in the graphs are considered to be conservative and will lead to over design, while the dry (12 % moisture content) values appear to be nearer the measured pole stiffnesses.

This test procedure has also highlighted the fact that the variability of MOE is an important feature of the proposed design procedure since the influence of stiffness in the design of a free standing pole is significant. Proper evaluation of this variable and its correlation with strength is increasingly important and this was further researched in the non-destructive procedure.

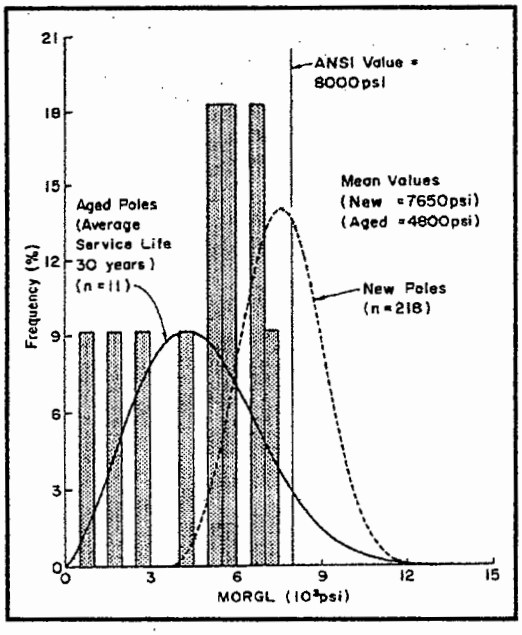

Figure 5: Distribution of Pole Strength (MORGL) for New and In-service Poles

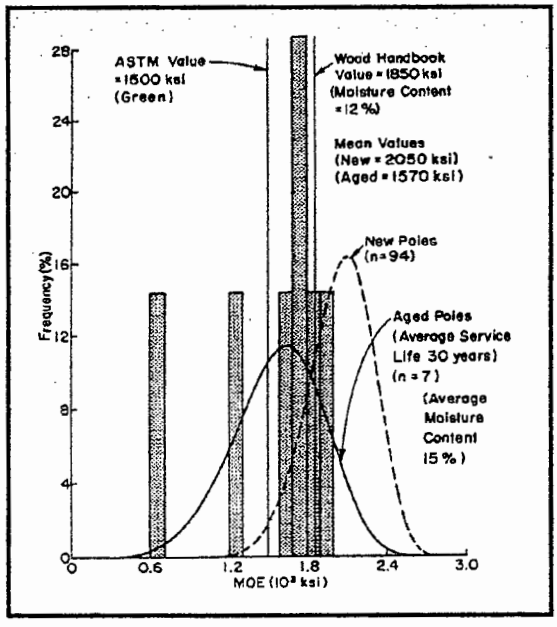

Figure 6: Distribution of Stiffness (MOE) Values for New and In-service Poles

The existing ESKOM pole tester operates in a similar way to both the above mentioned test procedures. The tester applies a bending moment to the pole and the deflection at ground line and the force are measured. The maximum force applied is 10.4 kN and the maximum deflection that is permitted is 10 % of the Ultimate Strain, as calculated from the properties of the wood (For ESKOM poles, see Table 1). The deflection is measured at ground line and the top attachment point of deflection meter is below the level of the "shoe" of the tester.

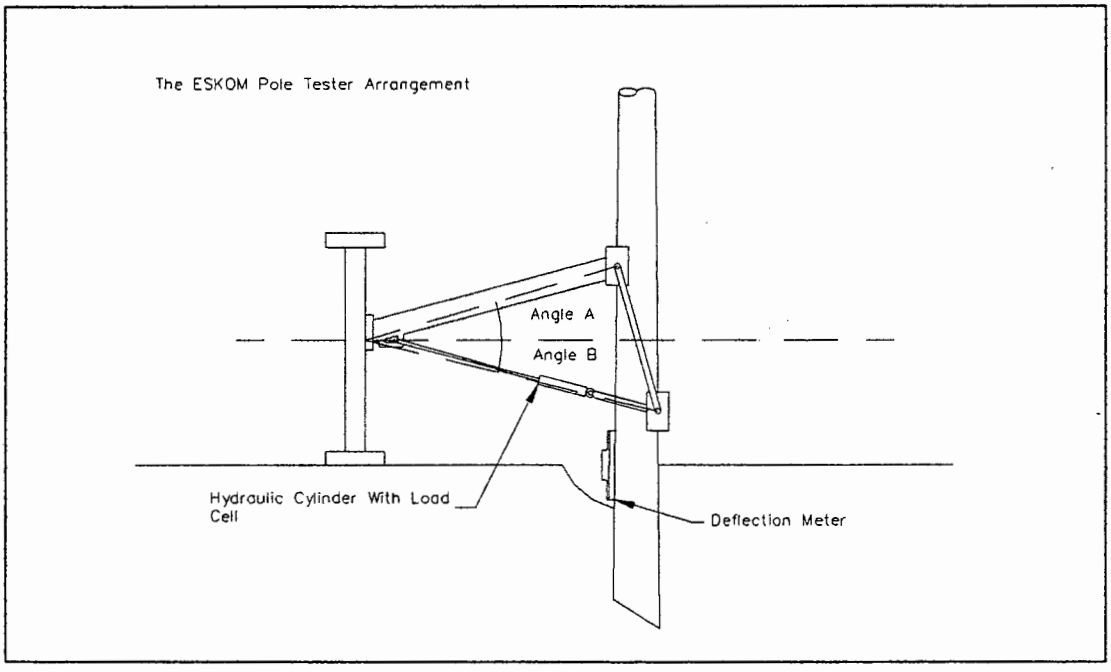

Figure 7: The ESKOM Pole Tester Setup.

As can be seen from Figure 7, the tester applies a moment to the pole in such a way that the forces are equal (Angle A is equal to Angle B). This in turn applies a bending moment to the base of the pole. The free body and bending moment diagrams due to this loading are of the following form.

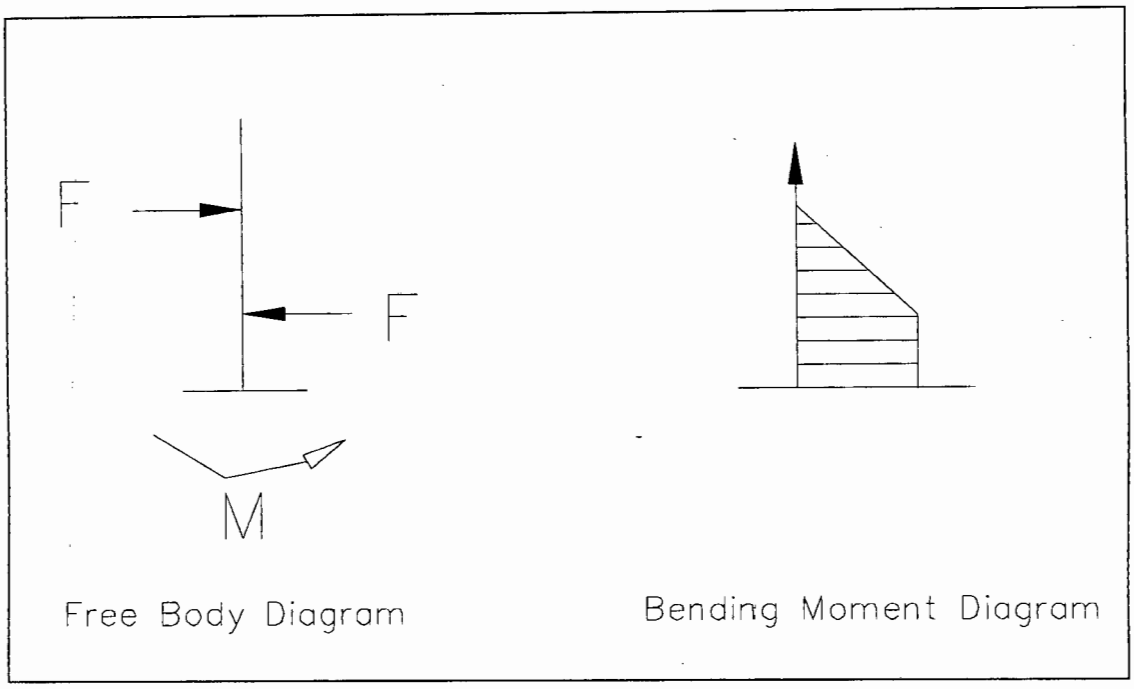

Figure 8: The Free Body And Bending Moment Diagrams for the ESKOM Pole Tester.

The bending moment applied at the base of the pole and in the area that the deflection meter is placed, is constant. The experimental procedure measures the increasing deflection and increasing moment as the force is increased. This measurement continues until either the force or the deflection reaches a predetermined maximum value. The values are then plotted on a change in deflection versus bending moment. The trend is then extrapolated to the ultimate strain and the maximum bending moment corresponding to this value is recorded. Figure 9 shows the extrapolation of the bending moment following a set of readings.

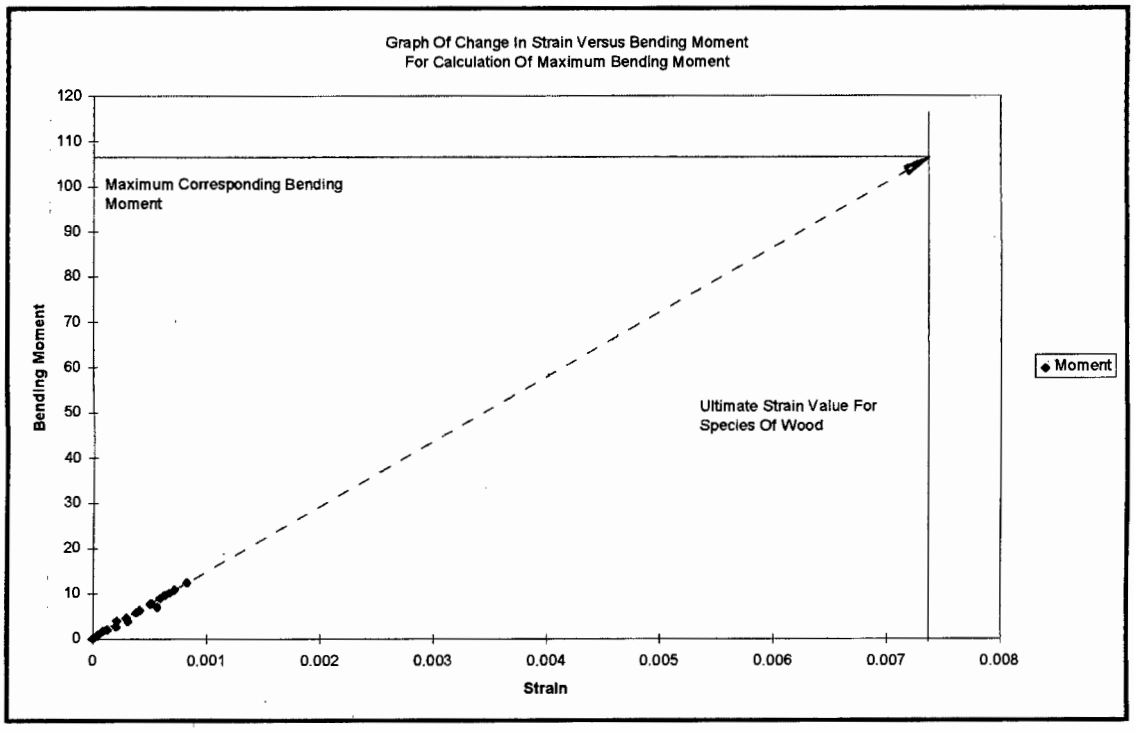

Figure 9: The Extrapolation of the Maximum Bending Moment.

The extrapolated value for the maximum bending moment is then compared with a calculated value. If the extrapolated value is greater than a pre-determined value, the pole is considered to be stable enough for further service. The calculated value is based on a calculation known within ESKOM as the "wind-on-pole" calculation. This involves the calculation of a maximum bending moment taking into account the outside forces the pole might experience and the external properties of the pole. An example of this calculation can be seen in Appendix C.

The Pilodyn Wood Tester [6] is another example of a "non-destructive" mechanical technique. This tester was developed in Sweden and was designed to detect shell rot in poles. The tester is based on the reduced

impact strength of decayed wood. The Pilodyn operates by injecting a spring-loaded blunt steel pin radially into the wood with a controlled amount of energy and measuring the resulting depth of penetration. This depth of penetration is a function of the initial density and the subsequent reduction in density caused by decay. This tool is only effective for detecting decay which is confined to the outer shell of the pole and is unsuitable for inspection of internally decayed poles. This test can, however, be correlated with the actual bending strength of the pole. Fagan [7] evaluated the Pilodyn for EPRI RP-1352 when used in conjunction with sonic NDE techniques.

2.1.2 ELECTRICAL RESISTANCE TECHNIQUES.

A device that was originally developed to detect decay in living trees, is being used to detect internal decay in wooden poles. The *Shigometer* operates on the principle that as wood progressively decays, its resistance to pulsed electric current decreases, This technique only works in wood which has a moisture content above the fibre saturation point (about 27 %). This is usually the moisture condition at the ground line and in decay portions of the pole. According to Graham and Helsing [2], the shigometer is effective in detecting rot but in some cases, it indicated incorrectly that poles were rotten. The authors suggest that this testing technique should be combined with drilling and coring suspect poles.

2.1.3 VIBRATION TECHNIQUES

Several studies have considered the possibility of using sonic vibrations to detect the presence of internal decay. The resonant frequency at which a pole vibrates when excited by an external force is closely related to the condition of the pole: including whether or not it contains decay. In 1963, a device known as the POL-TEK was developed by the Detroit Edison Company [8]. This test procedure cannot detect early stages of decay in which fibre breakdown has not begun. Heath Incorporated [9] applied for a patent for a similar device to that of the Detroit Edison Company in 1967.

EPRI [4] decided to investigate the use of sonic vibrations as a non-destructive tool as opposed to deflection methods due to the impracticality of field measurements. The desired approach was to evaluate the MOE of a pole using sonic stress waves. This method is based on the relationship between the speed of sound in the material (v) and its dynamic modulus of elasticity (E_d). This relationship is given by: $E_d = \frac{v^2 . \rho}{g}$ where g is the gravitational acceleration constant and ρ is the density of wood.

The stress-waves were induced by a single impact using a hammer. The time taken for the induced stress-wave to reach three alternate points, were measured. The three positions measured included a longitudinal evaluation along the surface and parallel to the longitudinal axis of the pole. This position was chosen as to account for the fact that the bending stress is maximum at the surface of the pole and the strength of the pole is dependant on the condition of the outer fibres. A transverse position was chosen along the diameter of the pole to ascertain the extent of internal decay. Finally a diagonal measurement was made in order to evaluate a combination of longitudinal and transverse velocities. Figure 10 shows the three different evaluation procedures. This test also incorporated the Pilodyn test technique to measure the density of the poles that were tested, although this method had been found to be unsatisfactory for an evaluation of density "Fagan [7]".

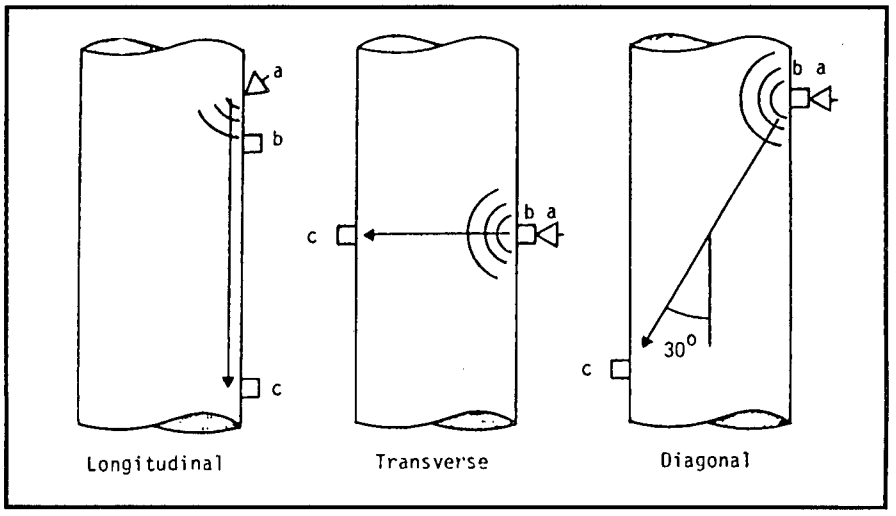

Figure 10: Schematic of Induced Stress-wave Velocity Directions for the NDE of Wood Poles.

EPRI reported that the results obtained using sonic velocity could not accurately predict the strength and stiffness of an individual pole but allowed one to compare a set of poles.

Goodman et al [10] continued research into this field on behalf of EPRI. They continued using the same principle of calculating the dynamic modulus of elasticity by measuring the velocity of stress-wave propagation. The pole length was divided into sections and the NDE data from their test were collected for each section. The poles were subsequently destructively tested and the two methods correlated, which enabled the commercial development of the procedure. They have claimed that their technique can calculate individual pole strengths and is the key to more effective wooden pole management. Thus by measuring and maintaining the condition of the poles, the utility can ensure that the pole can maintain their strength level.

The pole test that Goodman et al discussed was commercialised by Engineering Data Management Incorporated (EDM) and has been used by the Idaho Power Company, Ontario Hydro and Tampa Electric Company [11, 12].

Murphy et al [13] developed a test method that used measurable natural frequencies. By impacting the pole, the researchers were able to measure the vibration response of the pole and hence obtain the structure's modal frequencies. These frequencies were then utilised to determine the stiffness and general condition of the pole through a comparison with mathematically derived frequencies. The major advantage of this method is that the entire pole is examined in contrast to other techniques which only examine a small area of the pole.

They argued that as the stiffness of the ground line portion of a wooden pole is reduced due to rot or some other form of degradation, the structural natural frequencies of the pole decrease. Thus a pole with no rot will vibrate at higher frequencies than one with rot. The obtained natural frequencies were then used to calculate an average modulus of elasticity.

The test procedure was also found to be essentially independent of foundation/soil type, pole shape and variations in wood strength and density. The method is, however, very dependant on an accurate estimation of the conductor effects in the model. This test was commercialised and marketed as the *Vibrante Wood Pole Analyser* [14].

Chandler and Smart [15] carried out research into the use of modal techniques to determine changes in certain physical properties of a structure. The purpose was to determine whether the changes in natural frequencies due to damage could be used to locate flaws. They concluded that it was possible to locate large defects but the method needed some further research until it could reliably be used as a NDT technique.

2.1.4 X-RAY TECHNIQUES

The Mitsubishi Electric Corporation [16] carried out research into detecting the internal decay of wooden poles using radiation. The non-destructive test they developed utilises a radiation computed tomography, a technique that was originally developed for medical use. By using this system, the operator can display sectional images of the pole. The drawbacks involved with this system include the use of radiation and the long periods needed for signal processing and hence, the company suggested that this tool be used solely for laboratory studies. They continued research into the use of ultrasonic wave pulses.

2.1.5 ULTRASONIC TECHNIQUES

The use of ultrasonic testers has led to a number of commercial products available for the non-destructive evaluation of wooden poles. *ANDEC Manufacturing* [17] designed and released a commercial tester known as the CLUE. This tester operates using the time propagation of ultrasonic waves as opposed to impact induced sonic waves.

As mentioned above, the Mitsubishi Electric Company conducted research into the use of ultrasonic wave pulse to generate sectional images of wooden poles. This procedure is based on the time delay of an ultrasonic wave travelling through the centre of a decayed pole compared with a new pole. The transmission method applies ultrasonic waves from a transmitting contactor T and receives the waves at receiving contactor R. Figure 11 below illustrates this technique.

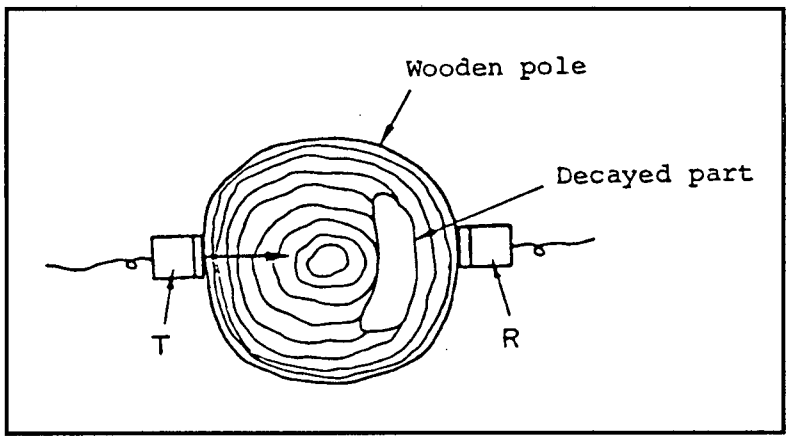

Figure 11: The Transmission Method

In order to detect flaws and their dimensions, the variations in ultrasonic wave propagation time are measured. However, it is necessary to establish a relationship between the ultrasonic wave propagation time and the presence of flaws and their dimensions. Mitsubishi based this relationship on large amounts of measured data. Then by measuring the propagation time through a considered good section and comparing this with a decayed portion, one could correlate the width of the flaw from the relationship. By measuring the pole in different sectors, a plot could be drawn of the section showing the flaws and their position. This procedure is elaborate and time consuming.

Tomikawa et al [18] discussed the use of ultrasonic computed tomography as a means of accomplishing the non-destructive inspection of wooden poles. In using computed tomography, they had to make a certain assumption. Tomography itself depends on linear data. Ultrasound does not propagate in straight lines through wood due to the anisotropy of Young's Modulus in the sap and heart parts of the wood. Additionally, ultrasound is unable to pass through any rotten part that has void areas. The assumption made was to base the technique on delay time: as the technicians at Mitsubishi had done. The results that they obtained reflected the decayed portions of the pole successfully but once again, this procedure was entirely laboratory based and expensive.

2.2 THE STANDARDS OF POLES AND THEIR DESIGN IN SOUTH AFRICA

2.2.1 THE STANDARDS OF WOOD POLES

The standard of timber structures in South Africa is overseen by the South African Bureau of Standards (SABS). This organisation has, following intensive research, provided standards to which wood utility poles must adhere.

The wooden pole in South Africa is specified by either SABS 753-1982 or 754-1982 [19, 20]. These two standards represent the minimum specifications for either pine or eucalyptus poles and cross arms for power transmission, low-voltage reticulation and telephone systems. The specifications cover pine and eucalyptus poles grown in South Africa that have been treated with creosote, a mixture of creosote and waxy oil or a mixture of copper-chromium-arsenic compounds. These treated poles are intended to be used as upright supports for low-voltage reticulation and telephone lines and as upright supports and cross-arms for power transmission lines.

The standards specify certain properties that the poles must have in order to conform to the standard. These properties include species, strength, minimum dimensions, moisture content and freedom from defects. The SABS also has standards for the preservation of poles and methods of treatment. The strength properties are of interest for this thesis as ESKOM utilise SABS

approved poles. Each pole tested as a cantilever must be able to withstand, without showing any sign of failure, a force *F* that is calculated in accordance with the formula below, corresponding to a maximum fibre stress in bending of 55 MPa (or 75 MPa when specified by the purchaser). The pole must exceed the minimum top diameter and have a maximum taper of 5 mm per metre.

For cantilever loading: $$F = \frac{\sigma \times D^3}{10.2 \times L_1}$$

Where: F = force required to cause a fibre stress in cantilever loading of 55 MPa, N

σ = fibre stress. i.e. 55 or 75 MPa

D = diameter of pole at theoretical ground line (TGL). i.e. 1.5 m from the butt end, based on the specified minimum top diameter and a taper of 5 mm per metre of length, mm.

L_1 = distance in mm between TGL and 0.5 m from the top end in the case of poles of length at least 5.7 m and between TGL and 0.1 m from the top in other cases.

For midpoint loading: $$F = \frac{\sigma \times \pi \times D^3}{8 \times L_2}$$

Where: F = force required to cause a fibre stress in cantilever loading of 55 MPa, N

σ = fibre stress. i.e. 55 or 75 MPa

D = diameter of pole at mid-length point based on the specified minimum top diameter and a taper of 5 mm per metre of length, mm.

L_2 = distance in mm between 0.3 m from the top end and 0.3 m from the butt end in the case of poles of length at least 5.7 m and between 0.1 m from the top end and 0.1 m from the butt end in other cases.

The different species that are and have been used by ESKOM can be seen in Table 1. The evaluation of each particular species was carried out by the South African Forestry Research Institute (21). The different species strength properties were evaluated using a three point loading setup.

The modulus of rupture expresses the breaking strength of the beam and is the computed maximum fibre stress, in the extreme fibres of the beam, at the point of maximum load. The fibre stress at proportional limit (P.L.) is the stress that exists in the extreme fibres of the beam when loaded at the proportional limit load and denotes the maximum load a beam will support for a short time without acquiring permanent deformation. Although this reading is indicative of the safe load that clear wood will support for a short time, fibre stress at proportional limit is subject to uncertainty because it is dependent on the increments of loading and deflection used in testing. The modulus of elasticity is a measure of the ability of wood to resist deformation or bending and applies only within the proportional limit. The top values shown in Table 1 are the arithmetic mean values with the standard deviation shown below.

Species	Density ρ	Static Bending (Centre-point)		
		Modulus of Rupture	Fibre Stress at P.L.	Modulus of Elasticity
	kg/m^3	MPa	MPa	MPa
Pinus canariensis	675 64.0	104 15.0	60 9.3	12551 2729
Pinus pinaster	637 70.0	107 15.7	54 8.6	13806 2407
Pinus radiata	611 68.0	101 13.9	55 8.1	13721 2160
Pinus taeda	578 94.0	91 20.1	50 11.1	11225 2997
Eucalyptus cloeziana	875 79.0	141 16.9	94 19.0	19521 3294
Eucalyptus grandis	695 83.5	108 18.5	70 10.3	15772 2346
Eucalyptus grandis/saligna Hybrids	719 151.0	111 25.4	70 13.7	16819 3798
Eucalyptus maculata	800 107.7	127 17.2	81 16.8	17786 2903
Eucalyptus maidenii	936 43.5	105 20.8	61 14.9	12259 3400
Eucalyptus microcorys	924 87.2	139 24.2	95 26.3	19335 3501
Eucalyptus paniculata	1076 51.9	178 20.1	107 22.6	27091 3583
Eucalyptus saligna	850 85.1	128 17.6	80 13.3	16249 2690

Table 1:The Structural Properties of Wood Species Used By ESKOM for Transmission Line Support.

2.2.2 THE DESIGN OF TRANSMISSION LINE STRUCTURES.

The actual design of wood structures in South Africa is governed by certain criteria. These criteria are based on the statutory requirements for design loads and safety factors as laid down by the Machinery and Occupational Safety Act (Chapter IV Section c.63.) Other guidelines are given in the "Code

of Practice for Overhead Power Lines for Conditions Prevailing in South Africa".

For wooden pole design based on the rupture modulus of the species in question, the following safety factors are required:

- A safety factor of 4.5 is required for members continually loaded, e.g. load conditions due to the own weight of the structure and weight of the conductor.
- a safety factor of 2.7 for members that are not continually loaded, e.g. load conditions due to wind loads on the structure and the conductors.

Using the above as guidelines, one can calculate the design safety factors and compare them with those stipulated. It shall be assumed that:

1. Conductors and structure shall be subjected to a 700 kPa wind.
2. Conductors shall be at -5 °C temperature.
3. All conductors are intact

The wind loads on the conductors are calculated by using the design wind pressure (700 kPa) multiplied by the design wind span and a factor of 0.6, which is in effect a span reduction factor.

The material properties of the poles used in the design process are covered by the SABS Standards 753 and 754. These specifications have been discussed in the previous section.

Typical pole design involves the calculation of the external forces exerted on the pole and comparing these values with the value specified by the SABS

Standard and confirming the safety factor. The external forces are made up by the forces exerted on the pole by the wind on the conductor and the pole. The weight of the conductor span lengths is assumed to have no influence on this calculation due to negligible difference between the forces exerted by adjacent spans.

The external forces of the "wind on the conductor" and the "wind on the pole" are calculated using the stated 700 kPa wind. These forces are used to calculate the maximum bending moment of the pole, which occurs at a point below the ground level. A rule of thumb is to assume that this point is a quarter of the pole depth below the ground. A more exact method to calculate the point of maximum bending moment is by calculating the depth of soil required to resist the applied horizontal load and the total depth must furthermore not be less than 1.5 times the distance to the point of maximum bending. An example of both methods can be found in Appendix C. The force at the point of maximum bending moment is calculated and using the SABS Standard, the relevant safety factor is compared.

The design of the cross arm members is governed by the weight of the conductors and the hardware. As above, the maximum bending moment in the cross arm is calculated and compared with the SABS Standard and the safety factor computed. An example of this calculation can be found in Appendix C.

3 THEORETICAL APPROACH

Any motion that repeats itself after a period or interval of time is called a vibration or oscillation. The swinging of a pendulum, the motion of a plucked string or the resultant motion after striking a wooden transmission line pole are all examples of vibration. Hence the theory of vibration deals with the study of oscillatory motions of bodies and the forces associated with them. The use of vibration analysis for the non-destructive analysis of wooden transmission line poles is not a new approach as can be seen from the reviewed literature. This project utilised the approach of measuring and quantifying the response vibrations similar to the approach proposed by Murphy et al [13]. Whereas Murphy et al compared the poles to other data, it is hoped that this principle can grade a pole during in-service performance over a period of time. This allows for a record of the pole's vibration characteristics. The vibration properties of the pole are measured following a modal testing procedure.

Modal testing is "the process involved in testing components or structures with the objective of obtaining a mathematical description of their dynamic or vibration behaviour" [22]. The form of the mathematical model varies considerably from one application to another and may either be an estimate of the natural frequency or a full mass - spring - dashpot model.

Before embarking on a detailed analysis, it is appropriate to put the different stages of vibration analysis/modal analysis into context. The "theoretical"

approach to vibration analysis consists of three phases through which a typical vibration analysis progresses. The first phase describes the structure's physical characteristics, usually in terms of its mass, stiffness and damping properties and is known as the *Spatial Model*. The next phase is to perform an analytical modal analysis of the spatial model which leads to a description of the structure's behaviour as a set of vibration modes; the *Modal Model*. The last phase deals with the analysis of exactly how the structure will vibrate under given excitation conditions and is described as the *Response Model*. The "experimental" approach to vibration analysis happens in reverse order. From measured frequency response functions we can deduce the properties of the structure. Figure 12 and Figure 13 illustrate these two approaches. As can be seen, an essential part of vibration analysis is correlating the analytical with the experimental results/data. Many cases of experiment - theory comparison stop at the stage of obtaining a set of results for each route and simply comparing them. The theoretical method can then be optimised to bring its results in line with those obtained experimentally.

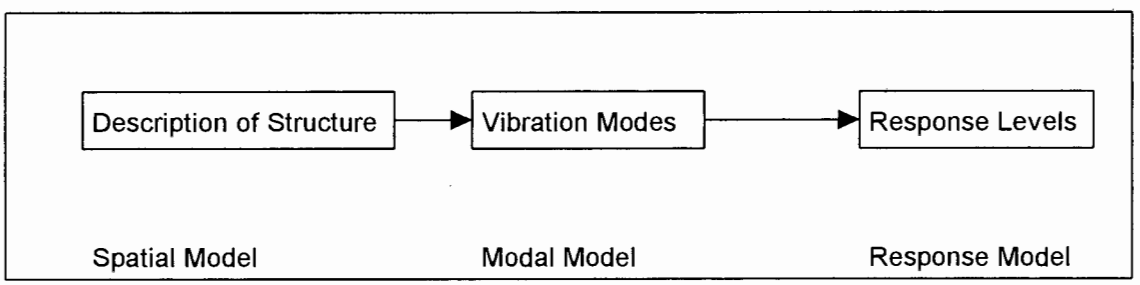

Figure 12: Theoretical Route to Vibration Analysis

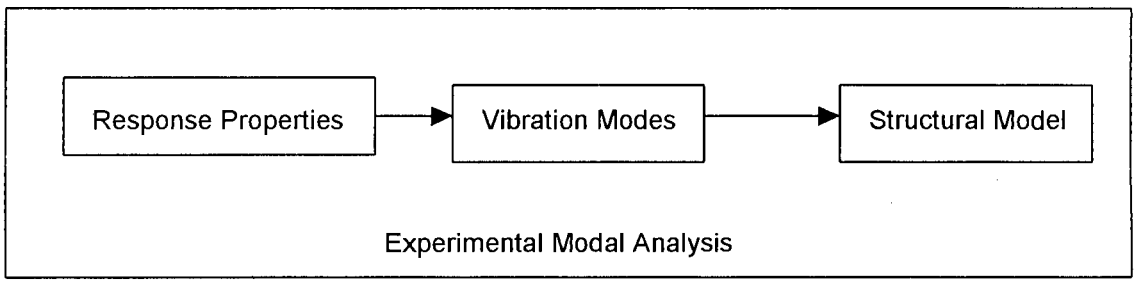

Figure 13: Experimental Route to Vibration Analysis

In order to construct a mathematical model of the pole sample, one must consider the system. The boundary conditions of the pole are considered to be the same as a fixed - free cantilever beam. The vibration will be due to a single impact and this excitation is known as a transient excitation.

Following the definition in Rao [23], the vibration due to this type of excitation shall be considered free. Free vibration is "....if a system, after an initial disturbance, is left to vibrate on its own, the ensuing vibration is known as free vibration....". Hence, assuming free vibration, a shape function was derived for the case of a fixed - free cantilever beam undergoing transverse vibrations.

Consider the free body diagram of the element of beam shown in Figure 14 where M(x,t) is the bending moment, V(x,t) is the shear force and f(x,t) is the external force per unit length of the beam.

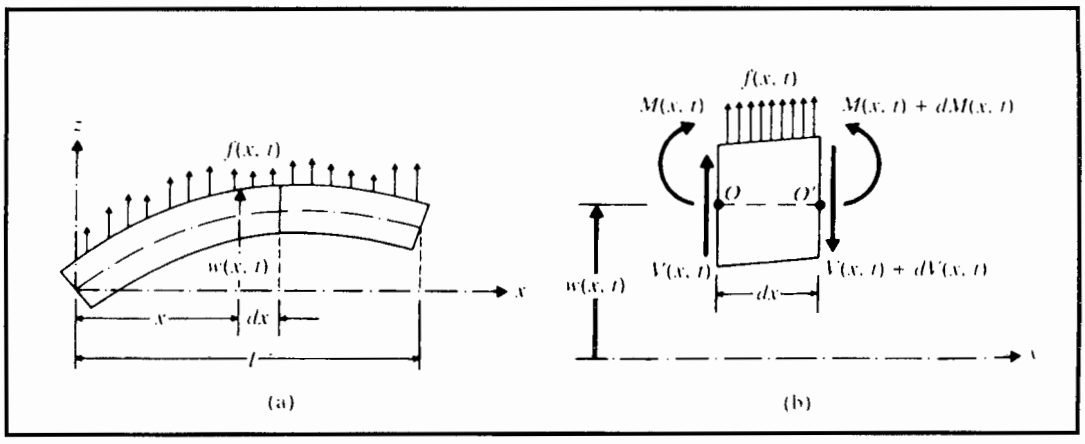

Figure 14: A Beam In Bending

Since the inertia force acting on the element is

$$\rho A(x)dx\frac{\partial^2 w}{\partial t^2}(x,t)$$

the force equation of motion in the z direction gives

$$-(V+dV)+f(x,t)dx+V=\rho A(x)dx\frac{\partial^2 w}{\partial t^2}(x,t) \qquad (1)$$

where ρ is the mass density and A(x) is the cross-sectional area through the beam. The moment equation of motion about the y axis passing through the point 0 in Figure 1 leads to

$$(M+dM)-(V+dV)dx+f(x,t)dx\frac{dx}{2}-M=0 \qquad (2)$$

By writing

$$dV=\frac{\partial V}{\partial x}dx \qquad \text{and} \qquad dM=\frac{\partial M}{\partial x}dx$$

and disregarding terms involving second powers in dx, Equations 1 and 2 can be written as

$$-\frac{\partial V}{\partial x}(x,t)+f(x,t)=\rho A(x)\frac{\partial^2 w}{\partial t^2}(x,t) \qquad (3)$$

$$\frac{\partial M}{\partial x}(x,t) - V(x,t) = 0 \tag{4}$$

By using the relation V=∂M/∂x from Equation 4, Equation 3 becomes

$$-\frac{\partial^2 M}{\partial x^2}(x,t) + f(x,t) = \rho A(x)\frac{\partial^2 w}{\partial t^2}(x,t) \tag{5}$$

From the elementary theory of bending beams, the relationship between bending moment and deflection can be expressed as

$$M(x,t) = EI(x)\frac{\partial^2 w}{\partial t^2}(x,t) \tag{6}$$

where E is Young's Modulus and I(x) is the moment of inertia of the beam cross section about the y-axis. Inserting Equation 6 into Equation 5, we obtain the equation of motion for the forced lateral vibration of a non-uniform beam.

$$\frac{\partial^2}{\partial x^2}\left[EI(x)\frac{\partial^2 w}{\partial x^2}(x,t)\right] + \rho A(x)\frac{\partial^2 w}{\partial t^2}(x,t) = f(x,t) \tag{7}$$

For a uniform beam, Equation 7 reduces to

$$\left[EI\frac{\partial^4 w}{\partial x^4}(x,t)\right] + \rho A(x)\frac{\partial^2 w}{\partial t^2}(x,t) = f(x,t) \tag{8}$$

For free vibration, f(x,t)=0 and Equation 8 becomes

$$c^2\left[\frac{\partial^4 w}{\partial x^4}(x,t)\right] + \frac{\partial^2 w}{\partial t^2}(x,t) = 0 \tag{9}$$

where $$c = \sqrt{\frac{EI}{\rho A}} \quad (10)$$

Since the equation of motion involves a second order derivative with respect to time and a fourth order derivative with respect to x, two initial conditions and four boundary conditions are needed for finding a unique solution for w(x,t). Usually, the values of lateral displacement and velocity are specified as $w_o(x)$ and $w'_o(x)$ at t=0, so that the lateral conditions become

$$w(x, t = 0) = w_o(x)$$

$$\frac{\partial w}{\partial t}(x, t = 0) = \dot{w}_o(x) \quad (11)$$

The free vibration solution can be found using the method of separation of variables as

$$w(x,t) = W(x)T(t) \quad (12)$$

Substituting Equation 12 into Equation 9 and rearranging leads to

$$\frac{c^2}{W(x)}\frac{d^4W(x)}{dx^4} = -\frac{1}{T(t)}\frac{d^2T(t)}{dt^2} = a = \omega^2 \quad (13)$$

where $a=\omega^2$ is a positive constant. Equation 13 can be written as two equations.

$$\frac{d^4W(x)}{dx^4} - \beta^4 W(x) = 0 \quad (14)$$

$$\frac{d^2T(t)}{dt^2} + \omega^2 T(t) = 0 \tag{15}$$

where $$\beta^4 = \frac{\omega^2}{c^2} = \frac{\rho A \omega^2}{EI} \tag{16}$$

The solution of Equation 15 can be expressed as

$$T(t) = A\cos\omega t + B\sin\omega t \tag{17}$$

Where A and B are constants that can be found from the initial conditions.

For the solution of Equation 14, we assume

$$W(x) = Ce^{st} \tag{18}$$

Where C and s are constants and derive the auxiliary equation as

$$s^4 - \beta^4 = 0 \tag{19}$$

The roots of this equation are

$$\begin{aligned} s_{1,2} &= \pm\beta \\ s_{3,4} &= \pm i\beta \end{aligned} \tag{20}$$

Hence the solution of Equation 14 becomes

$$W(x) = C_1 e^{\beta x} + C_2 e^{-\beta x} + C_3 e^{i\beta x} + C_4 e^{-i\beta x} \tag{21}$$

where C_1, C_2, C_3, and C_4 are constants. Equation 21 can also be expressed as

$$W(x) = C_1 \cos\beta x + C_2 \sin\beta x + C_3 \cosh\beta x + C_4 \sinh\beta x \quad (22)$$

where C_1, C_2, C_3, and C_4 are different constants that can be determined by the boundary conditions. The natural frequencies of the beam are computed from Equation 16 as

$$\omega = \beta^2 \sqrt{\frac{EI}{\rho A}} = (\beta l)^2 \sqrt{\frac{EI}{\rho A l^4}} \quad (23)$$

To determine the analytical equation for a fixed-free beam, we use the boundary conditions and substitute these into Equation 22. For the case that we are considering, the boundary conditions at the free and fixed ends are as follows:

At the free end, the bending moment and the shear force are zero

$$\text{Bending Moment} = EI \frac{\partial^2 w}{\partial x^2} = 0 \quad (24)$$

$$\text{Shear Force} = \frac{\partial}{\partial x}\left[EI \frac{\partial^2 w}{\partial x^2} \right] = 0 \quad (25)$$

At the fixed (clamped) end, the deflection and the gradient is zero

$$\text{Deflection} = w = 0 \quad (26)$$

$$\text{Slope} = \frac{\partial w}{\partial x} = 0 \qquad (27)$$

Substitution of Equation 23 into Equation 22 leads to

$$C_1 + C_3 = 0$$

Equation 24 and Equation 22 gives

$$\left.\frac{dW}{dx}\right|_{x=0} = \beta\left[-C_1 \sin\beta x + C_2 \cos\beta x + C_3 \sinh\beta x + C_4 \cosh\beta x\right]_{x=0} = 0$$

or $$\beta[C_2 + C_4]$$

Thus the solution, Equation 22 becomes

$$W(x) = C_1(\cos\beta x - \cosh\beta x) + C_2(\sin\beta x - \sinh\beta x) \qquad (28)$$

Applying Equations 25 and 26 to 27 yields

$$-C_1(\cos\beta l + \cosh\beta l) - C_2(\sin\beta l + \sinh\beta l) = 0$$
$$C_1(\sin\beta l - \sinh\beta l) - C_2(\cos\beta l + \cosh\beta l) = 0$$

For a nontrivial solution of C_1 and C_2, the determinant of their coefficients must be zero

$$\begin{vmatrix} -(\cos\beta l + \cosh\beta l) & -(\sin\beta l + \sinh\beta l) \\ \sin\beta l - \sinh\beta l & -(\cos\beta l + \cosh\beta l) \end{vmatrix} = 0$$

Expanding the determinant gives the frequency equation

$$2\cos(\beta l).\cosh(\beta l) + 2 = 0 \qquad (29)$$

The roots of this equation, $\beta_n l$, give the natural frequencies of vibration

$$\omega_n = (\beta_n l)^2 \sqrt{\frac{EI}{\rho A l^4}} \qquad n=1, 2,\ldots\ldots$$

where the values of $\beta_n l$, n=1, 2,.....satisfying Equation 28 are given by the roots.

C_2 can be expressed in terms of C_1 and hence Equation 27 can be written as

$$W(x) = C\left[(\sin\beta_n x - \sinh\beta_n x) - \left[\frac{\sin\beta_n l + \sinh\beta_n l}{\cos\beta_n l + \cosh\beta_n l}\right](\cos\beta_n x - \cosh\beta_n x)\right] \qquad (30)$$

The above equation, called the mode shape function, can now be used to establish what differences one can expect by varying the properties of the wood sample in particular regions over the length. The mode shapes can be plotted from this function.

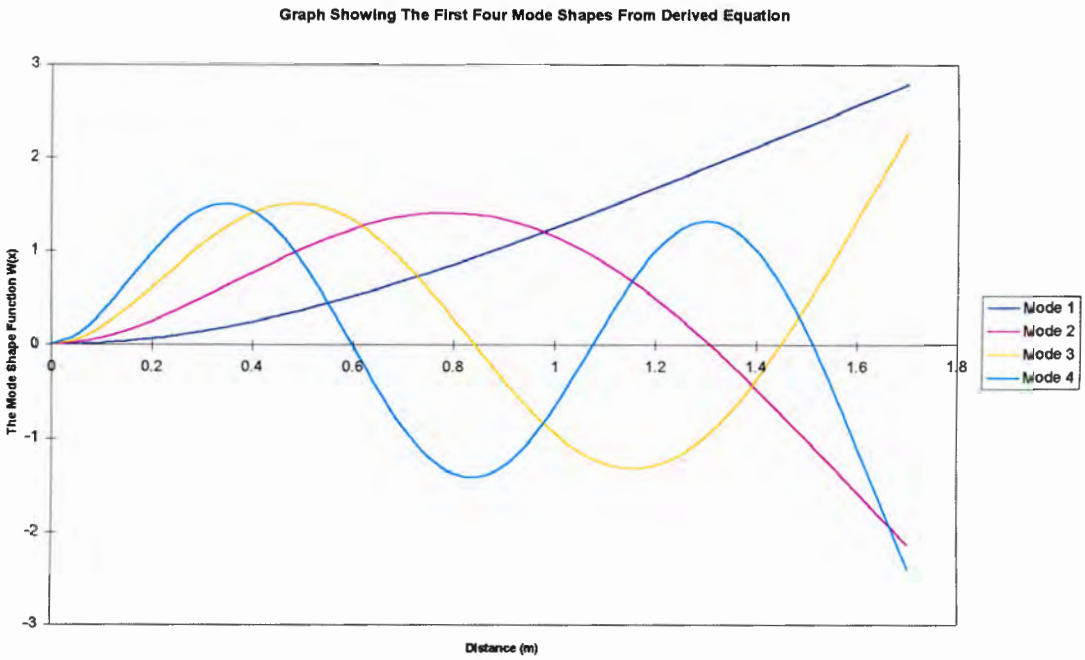

Figure 15: The First Four Mode Shapes for a Pole Sample.

Rayleigh's Method can be applied to find the fundamental frequencies of a continuous system. This method is an integral over the length of the sample but requires an assumed mode shape function (Equation 29). The equation for determining the natural frequencies of a continuous fixed-free vibration system is thus

$$\omega^2 = \frac{E_1 I_1 \int_0^{l1}\left[\frac{d^2W}{dx^2}\right]^2 dx + E_2 I_2 \int_{l1}^{l2}\left[\frac{d^2W}{dx^2}\right]^2 dx + \ldots\ldots}{\rho_1 A_1 \int_0^{l1}(W)^2 dx + \rho_2 A_2 \int_{l1}^{l2}(W)^2 dx + \ldots\ldots} \qquad (31)$$

This can then be compared with the exact solution for the same system (Given by Equation 23 and the calculations can be seen in Appendix D). The

values for the first four modes compare exactly. Thus the derived shape function is considered to be a good representation of the exact solution.

4 EXPERIMENTAL METHOD

The experimental method employed during this project followed research into previous vibration analysis techniques. The experimental procedure is essentially simple. The pole is impacted and the impact force and the vibration response are measured using piezoelectric transducers. This measurements are sampled at a predetermined rate by a spectrum analyser. The time domain data can then be converted to the frequency domain by the analyser or the time data can be transferred to a computer where the data analysis can be done using a computer software package.

The seven sample poles obtained form ESKOM were buried in concrete in paint drums in order to simulate a fixed boundary condition. The photographs of the seven pole samples can be seen in Appendix F. For the purposes of the experiment, the drums were tied to a steel frame with tension cables The frame was rested on bags of sand with two more bags weighting the frame down. This was done in an effort to isolate the vibrating system from any external effects. Photograph 1 shows the steel frame, sand bags, tension cables and pole in a drum of concrete.

The impact on the pole is applied by a spring loaded projectile. This "impactor" consisted of a body, a helical spring (Spring Constant ±7200 N.m), a slide to which the force transducer is attached and a trigger mechanism. The impactor is strapped to the pole using ratchet lever straps. The impact

slide is then loaded and held in place by the trigger mechanism. Figure 16 illustrates the impactor used in the experimental procedure.

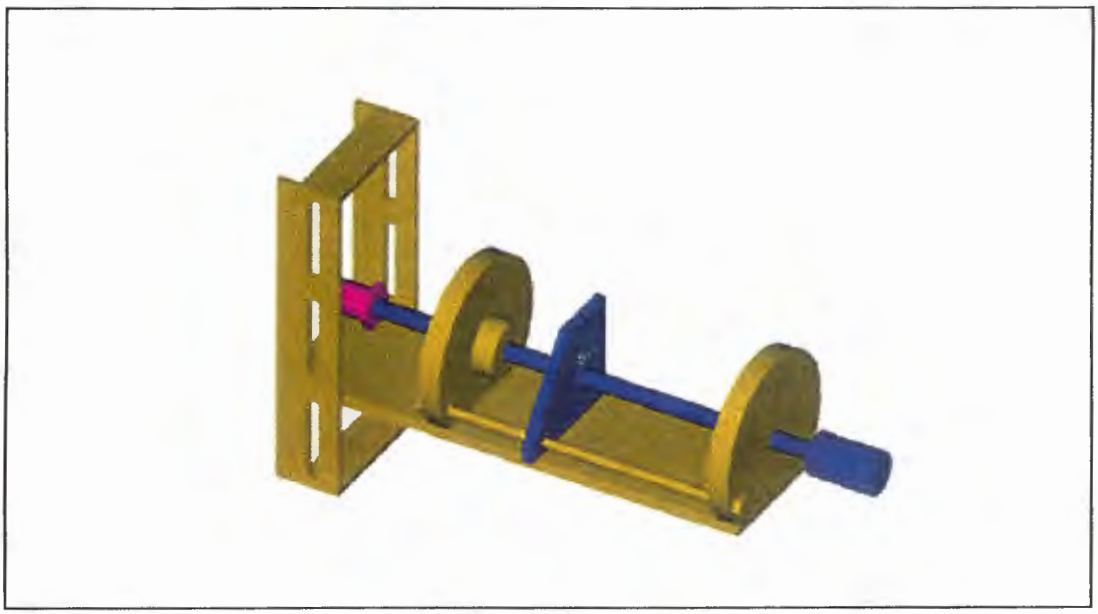

Figure 16: Diagram of Impactor

Photograph 1: The Isolation of the Experiment from External Vibration.

Drawings of the design of the impactor can be seen in Appendix E. When the trigger is released, the slide moves forward and strikes the pole with a considerable force. The magnitude of the impact is determined by the mass of the impact slide and the velocity at which it is moving when it strikes the structure. The frequency range that is effectively excited by this type of device is controlled by the stiffness of the contacting surfaces and the mass of the slide. When the slide impacts the test structure, the structure experiences a force pulse similar to a half sine wave similar to what is shown in Figure 17. The frequency content of a pulse such as this is also shown in Figure 17 and is essentially flat up to a certain frequency (f_c). Clearly, a pulse of this type would be relatively ineffective at exciting vibrations in the frequency range above f_c. There is a relationship between this cut-off frequency f_c and the duration of the pulse T_c. In order to raise the frequency range, the pulse duration must be as short as possible. This is achieved by ensuring that the impact materials are as stiff as possible.

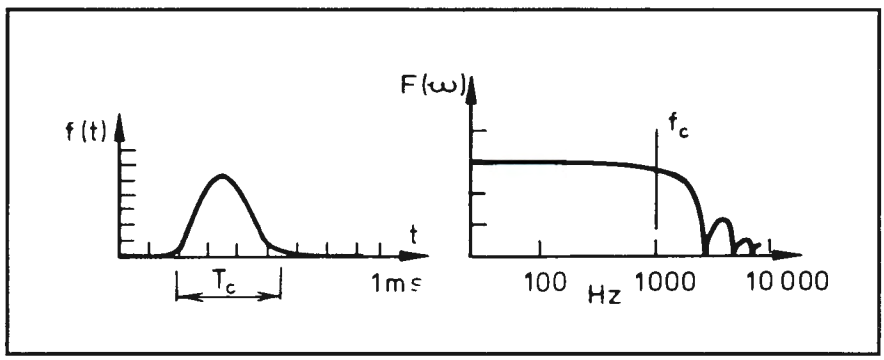

Figure 17: Typical Force Pulse and Spectrum

Photograph 2 shows the impactor strapped to the pole with the force transducer attached to the slide and the accelerometer attached diametrically

opposite. The force of impact is measured using a PCB Force Transducer(Model 208 B03) that is mounted on the front of the slide. This piezoelectric force transducer and the accelerometer have their own built-in amplifiers and are powered by current limiting power supplies. The impact of the transducer also acts as a level trigger for the spectrum analyser to start registering the two input channels. The analyser reads the two channels and stores the time domain data for the impact and the response. The response is measured diametrically opposite to the impact using a Wilcoxon accelerometer. The experimental setup can be seen in Photograph 3. The specifications of the transducers, the calculation of the spring's spring constant from compression tests and the photographs of the spectrum analyser and current limiting power supplies can be found in Appendix B.

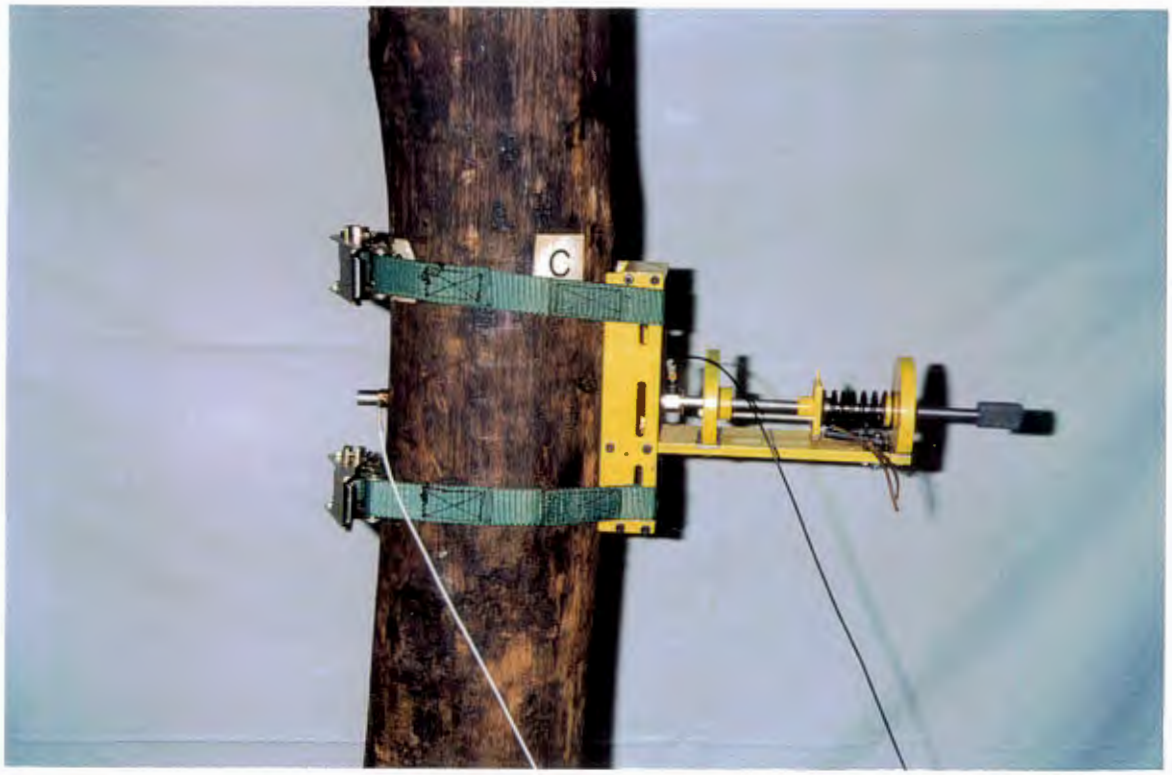

Photograph 2: The Impactor Showing the Force Transducer and the Accelerometer.

Photograph 3: The Experimental Setup

The spectrum analyser displays the time domain data of each test. An example of the measured time data for an impact and response can be seen in Figure 18.

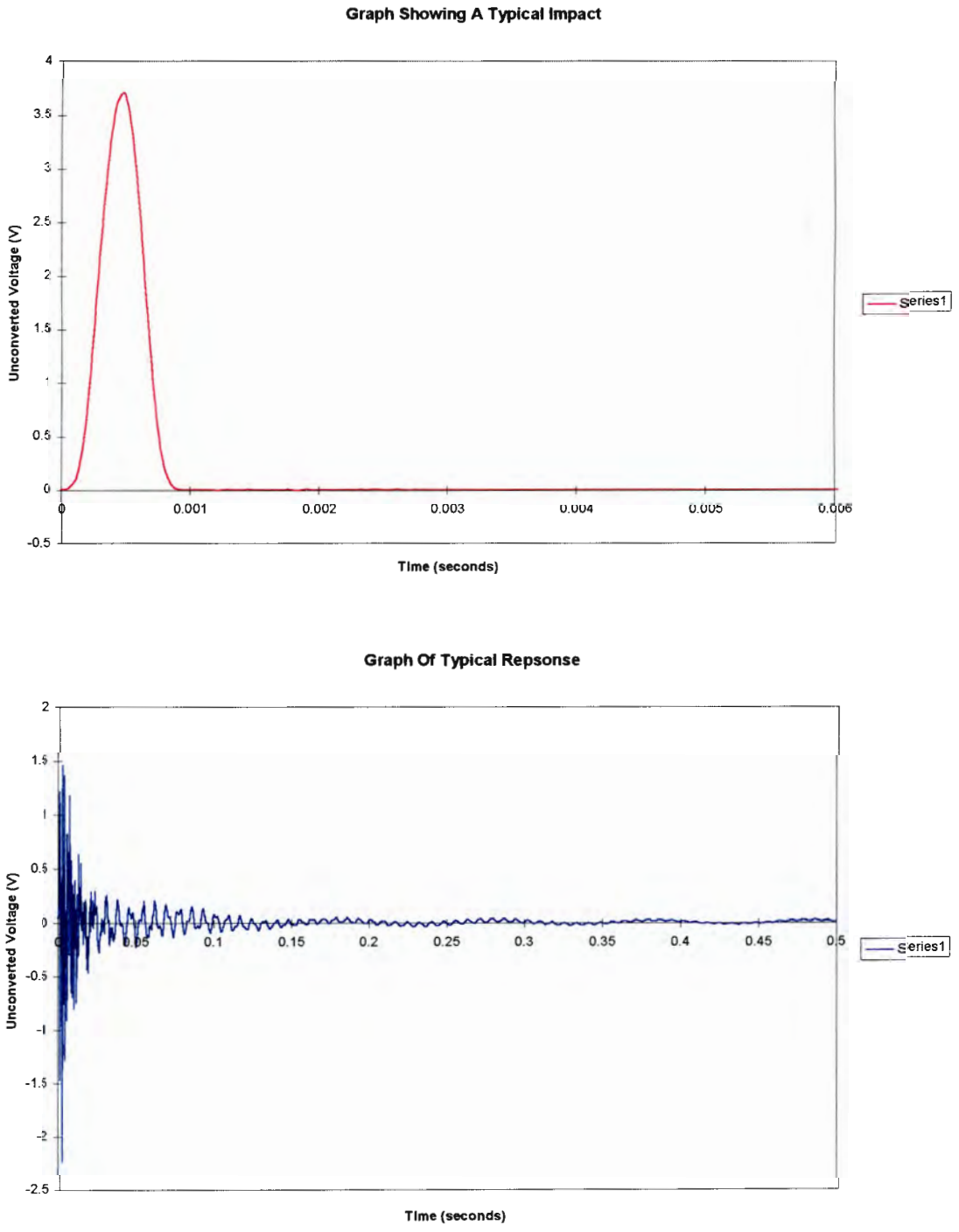

Figure 18: An Example of a Measured Impact and Response.

As mentioned before, the data can either be analysed using the built in functions of the analyser or exported to a desktop computer were they can be analysed using a suitable software package. The analysis of the data using

Mathcad™ [24] is carried out in the following format. The measured time data for the impact and the response are read into a sheet. The data is converted into the correct units (Newton and $m.s^{-2}$) and transformed using a Discrete Fourier Transform. The Frequency Response Function (FRF) is calculated using the following relationship:

$$FRF = \frac{FFT(\text{Response}) \times \overline{FFT(\text{Impact})}}{FFT(\text{Impact}) \times \overline{FFT(\text{Impact})}}$$

The FRF parameter for this experiment is known as *Inertance* or *Accelerance*. This is due to the fact that the response parameter is acceleration. The modulus of this FRF is then plotted against frequency. Figure 19 shows a plot of a Frequency Response Function and one can clearly see the modes of vibration. It is the frequencies of these modes that tell us more about the properties of the pole and that can also be compared with the results obtained theoretically using the derived equation.

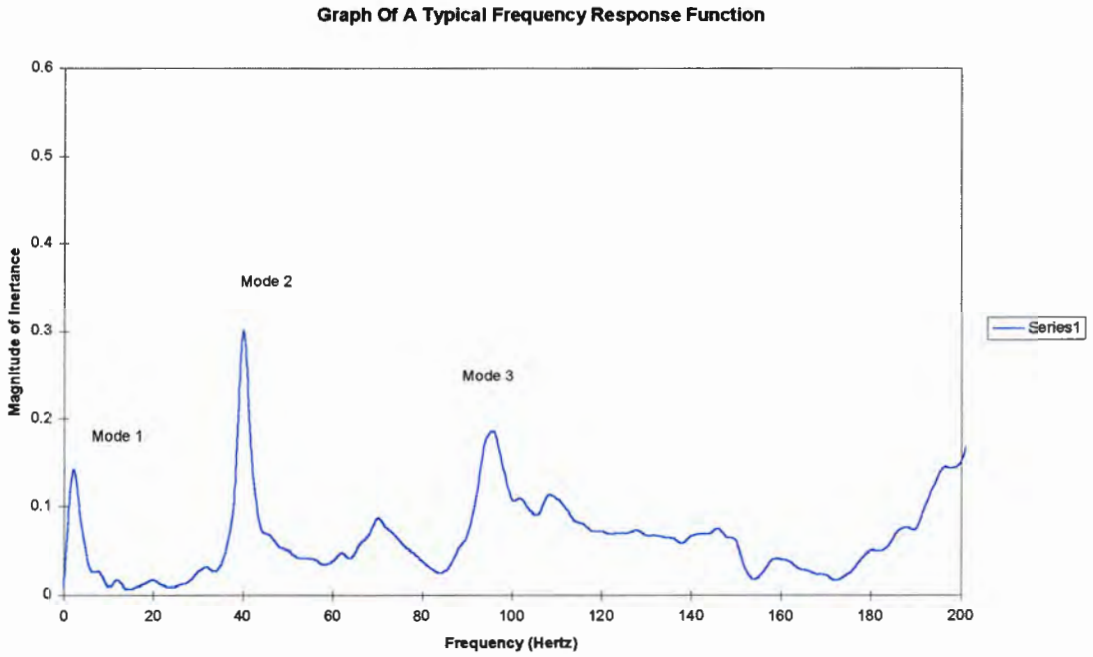

Figure 19: An Example of a Frequency Response Function

This is the procedure that was used on all the seven wooden poles and the results will be analysed in the following chapter.

The experimental procedure continued by including the infliction of a certain amount of ground line degradation on three pole samples. This degradation was inflicted by drilling radial holes into the pole in two cases and cutting a circular groove in the other case. The degradation was quantifiable by calculating the volume removed. Tests were carried out as more material was removed. The "degradation" was continued until an appreciable percentage was removed from the ground line area. The data collected during this procedure allowed the comparison of the effects of degradation on the properties of a single pole and will be discussed in the next chapter.

The laboratory experiments were complemented by the testing in the field of a free standing pine pole. The testing procedure for this pole was the same as the laboratory tests except that the impactor was replaced by a larger impact hammer. This was due to the size of the pole and the inability of the designed impactor to excite the pole sufficiently. The impact response in this case, was measured at 4 different positions on the pole. These points were at 1, 2, 3 and 4 metres respectively from ground level. The reason for this was to ensure that all the relevant data was recorded and to minimise the possibility of not recording data due to the fact that an accelerometer may fall on a node of vibration. This pole was also degraded by drilling holes at

ground line in order to see what effects this would have on the modal frequencies.

Another part of this field work was to compare the results obtained using the ESKOM Pole Tester before and after the pole was degraded. This allows for a direct comparison between the change in maximum bending moment and the change in mode frequency. The results of these tests will be covered in the next chapter.

5 RESULTS AND ANALYSIS

The experiments undertaken on the sample wooden poles have provided large amounts of data. The results will be presented and discussed in three parts. The first comparison shall be drawn between the seven sample poles. The next step will entail a comparison covering the three samples that were "degraded". The final section will present the results from the field testing of the free standing full length pole and compare these with the results obtained using the ESKOM mechanical pole tester.

5.1 SEVEN SAMPLE POLES.

The seven pole samples (See Appendix F) obtained from ESKOM covered the whole spectrum of pole quality. The poles were assigned labels to distinguish their state. The sample set consisted of one new, four in-service poles and two poles with excessive decay. Hence they were labelled from A to G with A being the new pole. All the samples were approximately 2 metres long and stood between 1.67 and 1.71 metres once planted in the concrete. The table below shows their dimensions and a brief description of the pole.

Pole Name	Length	Diameter at Ground Line (Both axes)	Diameter at Top	Description
	cm	mm	mm	
Pole A	169	185	170	New pole with no service.
Pole B	167	190	188	Pole with very short service time. The length is to the middle of the snap. This pole failed in the field.

Pole C	168	175	175	Pole with medium service time.
Pole D	171	131/142	131/141	Pole with medium service time.
Pole E	168	131	133	Pole with medium service time.
Pole F	169	161	160	Pole with excessive rot and a longitudinal crack running the length of the pole.
Pole G	169	168/148	131/148	Pole with excessive rot and considered to be hollow in the centre of the core.

Table 2: The Physical Properties of the Seven Pole Samples

The excessive rotting present in poles F and G can be seen in Appendix F.

As pointed out in Murphy et al [13], the effect of ground line degradation due to rot or some other form does effect the frequency of vibration. The degradation effects the stiffness of the pole and hence the frequencies of vibration will decrease. Hence, the values of the vibration modes of the pole samples should decrease from the pole considered to be in a good condition to that of a pole considered to be in a worst condition.

The following graphs show the differences in frequency of the vibration modes of the seven sample poles. Figure 20 shows the Frequency Response Functions of poles A,C and F, thereby illustrating the FRF's of a good pole, an in-service pole and a rotten pole. Figure 21 and Figure 22 show the FRF's of pole B, F and G.

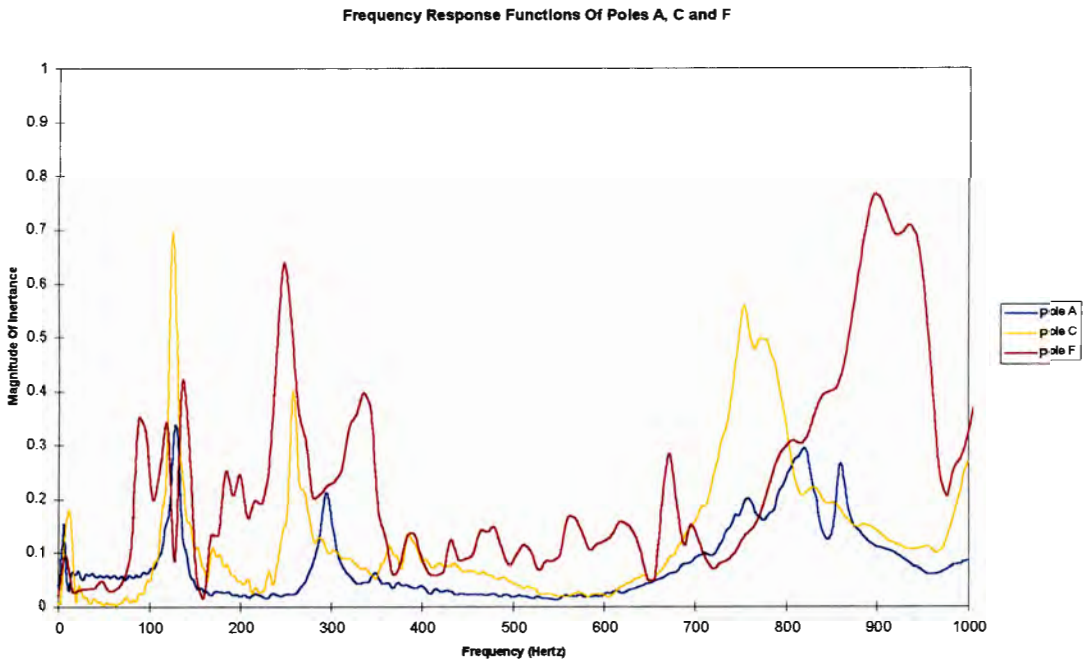

Figure 20: Graph Showing the Frequency Response Function of Poles A,C and F.

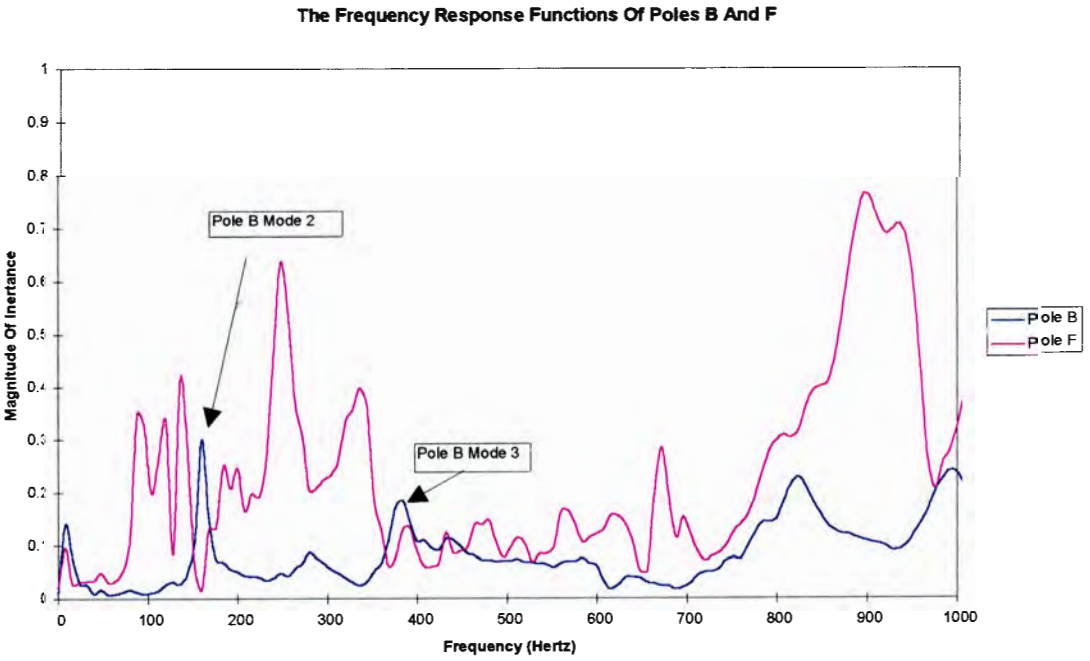

Figure 21: Graph Showing the Frequency Response Functions of the Poles B and F.

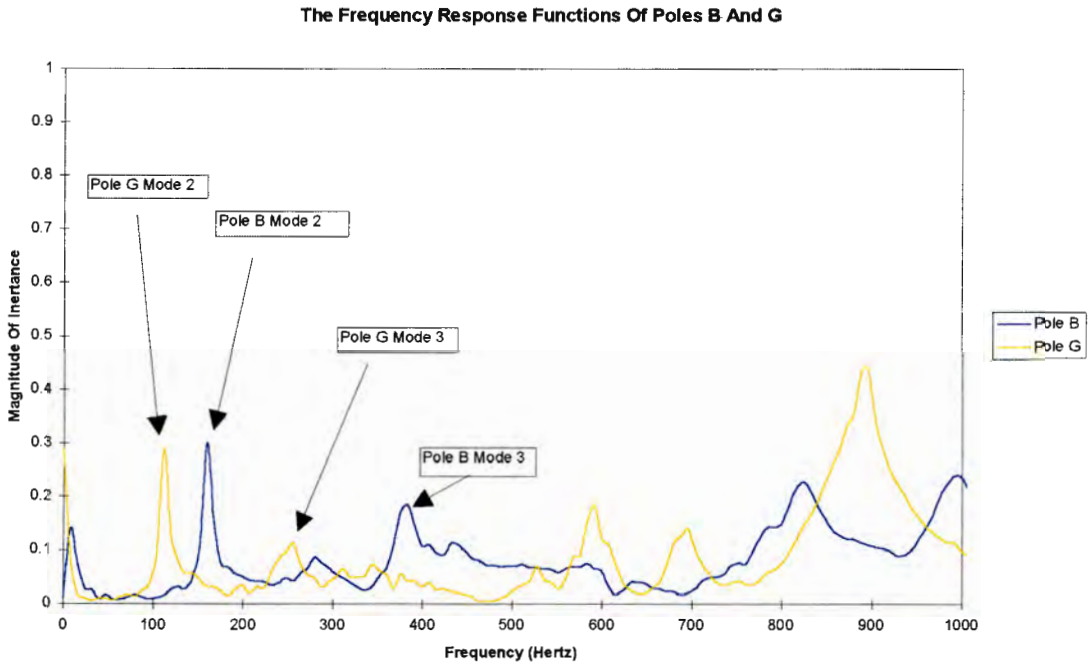

Figure 22: Graph Showing the Frequency Response Functions of the Poles B and G.

Pole B has some of the highest values for vibration modes and poles F and G are known to be decayed. As can be seen, the values for the mode frequencies of pole B are considerably higher than for pole G: hence the assumption that Pole B is stiffer than Pole G is valid. This allows us to categorise the poles according to their stiffness. The FRF of pole F is unsuitable to make a comparison due to the crack that runs the length of it. The FRF's for each pole are plotted separately and are in Appendix A.

Besides the above methods of comparison, difficulty arises since their physical dimensions differ. In most cases the poles are the same length but the cross sectional area and the moment of inertia differ due to the difference in diameter. In order to compare the pole samples, the values for the second

and third modes for each pole were calculated using the mathematical derived formula. The property values used for density and MOE were obtained from Table 1. Table 3 shows the values for both the experimental and theoretically calculated values. As can be seen, the theoretical values for the mode frequency are much larger than those obtained experimentally. This can be attributed to the assumed values for density and Young's Modulus.

In order to ascertain whether the experimental will correlate with the calculated values, one can consider the quotient of the frequency of Mode 3 over Mode 2. In the theoretical case, the quotient should be governed by the factor β_n (In this case the division gives a constant 2.8). Applying this principle to the experimentally obtained results, we can see that the results vary between 16% - 36% from the "required" 2.8, from which it follows that the derived theoretical equation should possibly incorporate a damping factor. Figure 23 below shows the difference between the experimental and the theoretical (The error bars represent 5% of the value). The parallel nature of the trend of the experimental as opposed to that of the theoretical supports the need for a damping factor.

Pole Name	Experimental Values		Calculated Values		Value for Mode 3/Mode2	
	Mode 2	Mode 3	Mode 2	Mode 3	Exp.	Calc.
Pole A	129	295	1471	4119	2.29	2.8
Pole B	160	384	1266	3544	2.4	2.8
Pole C	126	259	1468	4109	2.06	2.8
Pole D	128	292	1105	3094	2.28	2.8
Pole E	218	472	1107	3100	2.17	2.8
Pole F	120	248	1334	3736	2.07	2.8
Pole G	112	256	1233	3452	2.29	2.8

Table 3: Table Showing Comparison Between the Experimentally and Mathematically Derived Frequency Values

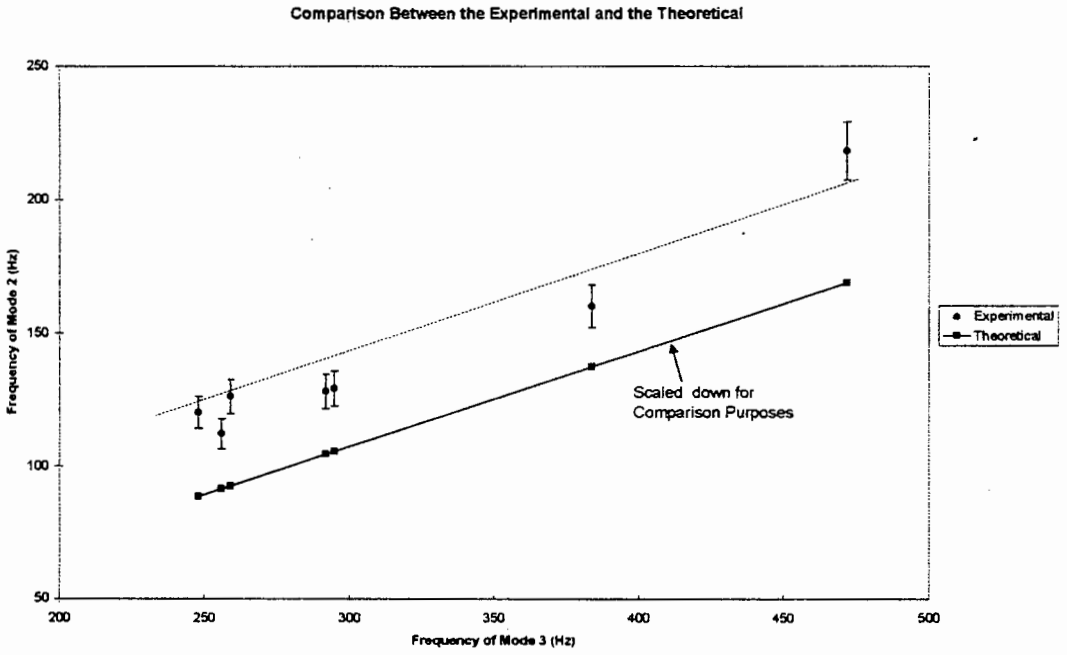

Figure 23: Graph Illustrating the Parallel Nature of the Results Experimentally Obtained and the Mathematically Predicted Frequency Values.

5.2 "DEGRADATION" OF THREE SAMPLE POLES

The degradation of the poles A, C and E was carried out in stages. The extent of the degradation is shown in the three photographs below.

Photograph 4: Material Removal from Pole A.

Photograph 5: Material Removal from Pole C.

Table 4 quantifies the stages in material removal as a percentage of the material removal in the region. Also included in the table are the percentage changes in frequency and volume of the samples. The taper of the sample poles is essentially zero and in calculating the total volume removed from the pole, the cross section was considered uniform.

Photograph 6: Material Removal from Pole E.

Pole A			
Number Of Holes	% Volume Removed	% Mode 2 Change	% Mode 3 Change
No Holes	0.00	0.00	0.00
63 Holes	6.22	1.16	2.03
147 Holes	14.52	1.94	2.71
210 Holes	20.74	2.33	4.07
315 Holes	31.11	3.88	10.17
399 Holes	39.41	5.43	13.56
399 Foam Filled Holes	39.41	3.10	9.83
Pole C			
Number Of Holes	% Volume Removed	% Mode 2 Change	% Mode 3 Change
No Holes	0.00	0.00	0.00
61 Holes	5.36	0.79	3.86
102 Holes	8.97	1.59	5.02
150 Holes	13.19	2.38	6.18
200 Holes	17.58	3.17	7.34
260 Holes	22.86	3.97	9.65
Pole E			
Number Of Holes	% Volume Removed	% Mode 2 Change	% Mode 3 Change
No Holes	0.00	0.00	0.00
110 mm Diameter	35.53	9.17	4.66
93 mm Diameter	53.92	16.51	9.75
75 mm Diameter	70.03	21.10	22.46

Table 4: Table Showing the Percentage of Material Removed

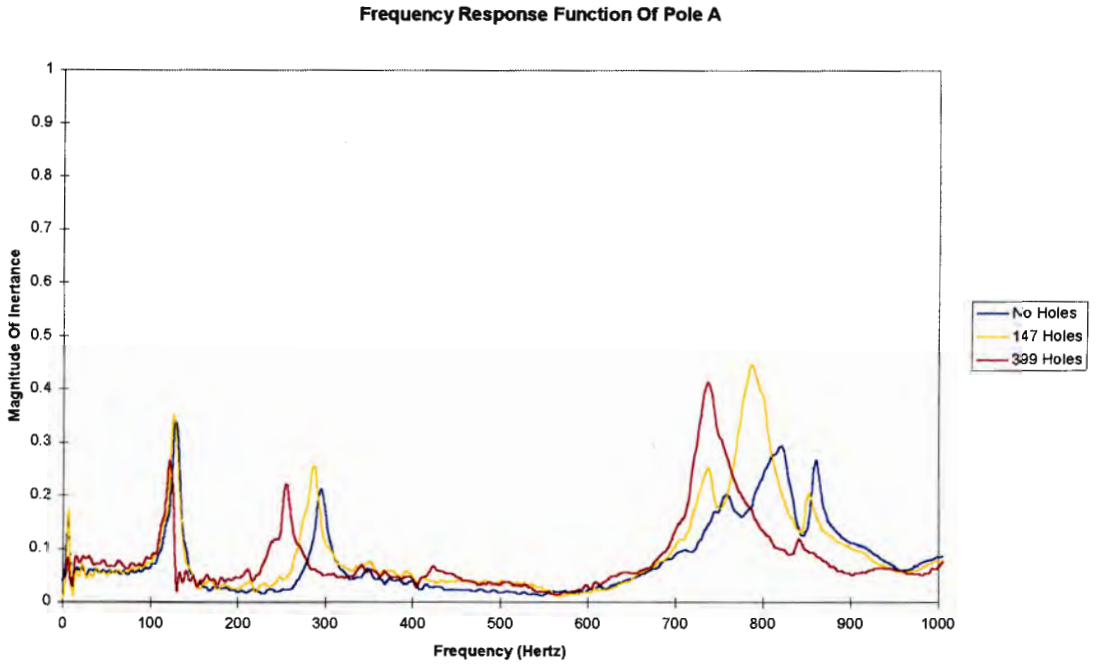

Figure 24: The Frequency Response Functions of Pole A Following Degradation

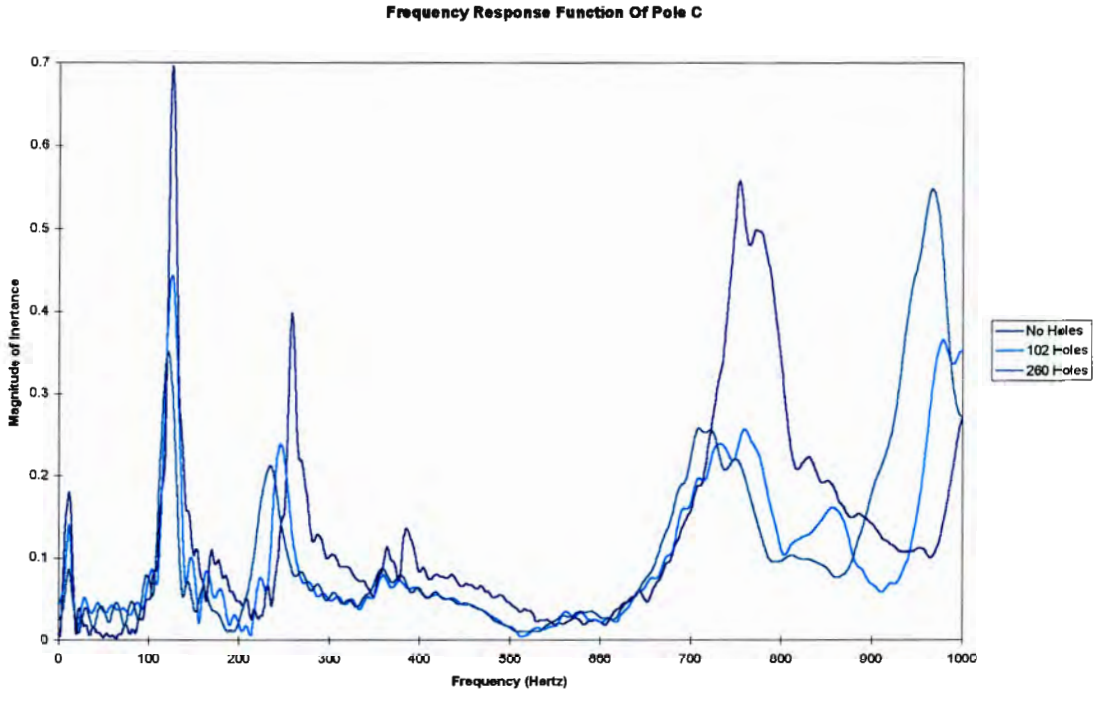

Figure 25: The Frequency Response Functions of Pole C Following Degradation

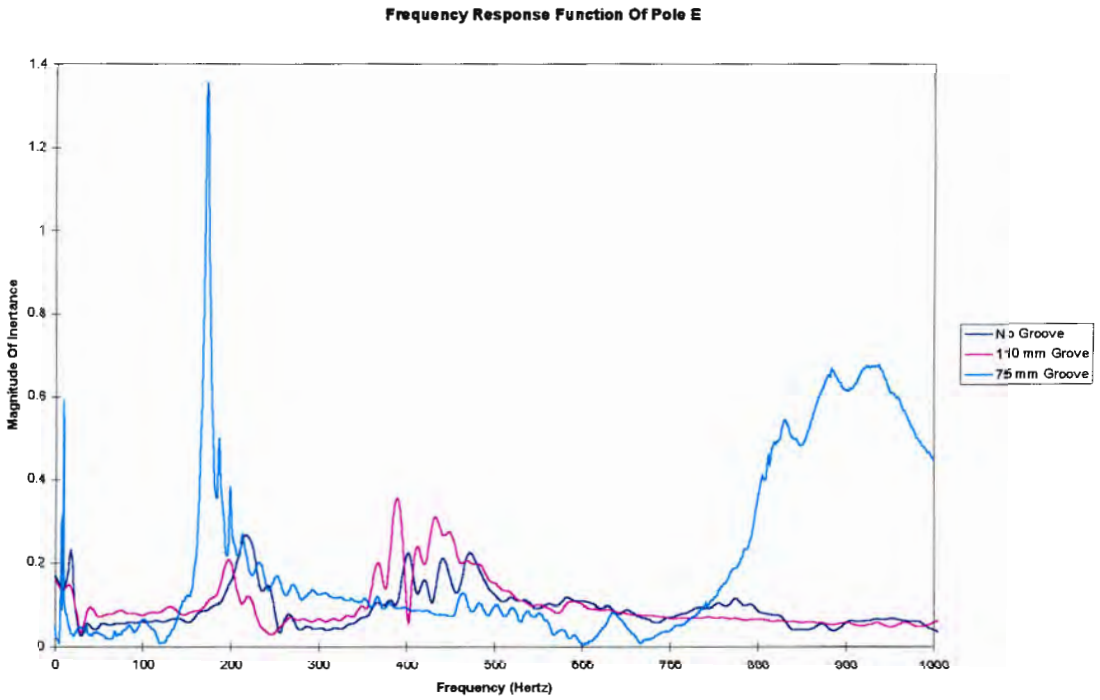

Figure 26: The Frequency Response Functions of Pole E Following Degradation

Figure 27 shows the percentage volume removed from each pole sample versus the percentage change in frequency; included in the graph are the curves of the full length pole.

As can be seen from the graphs there is a definite decrease in frequency corresponding to decrease in volume at groundline. The nature of the curves is also linear which now allows possibly an easier method of comparison. From this degradation process, the following points were noticed.

Pole A was degraded to a point at which the holes were refilled with expanding foam. By replacing the removed material with foam, the percentage change in frequency dropped, which in turn can be characterised

by an increase in stiffness of the pole. This may have some bearing on preventative maintenance.

Pole E was degraded by taking away the outer wall. It was presumed that the change in frequency through such an exercise would lead to a more rapid decrease in frequency since it is assumed that the stiffness of the pole is in its outer wall fibres. The trend for this degradation is also very similar to that of the other poles, which does not support the former theory of outer wall fibres.

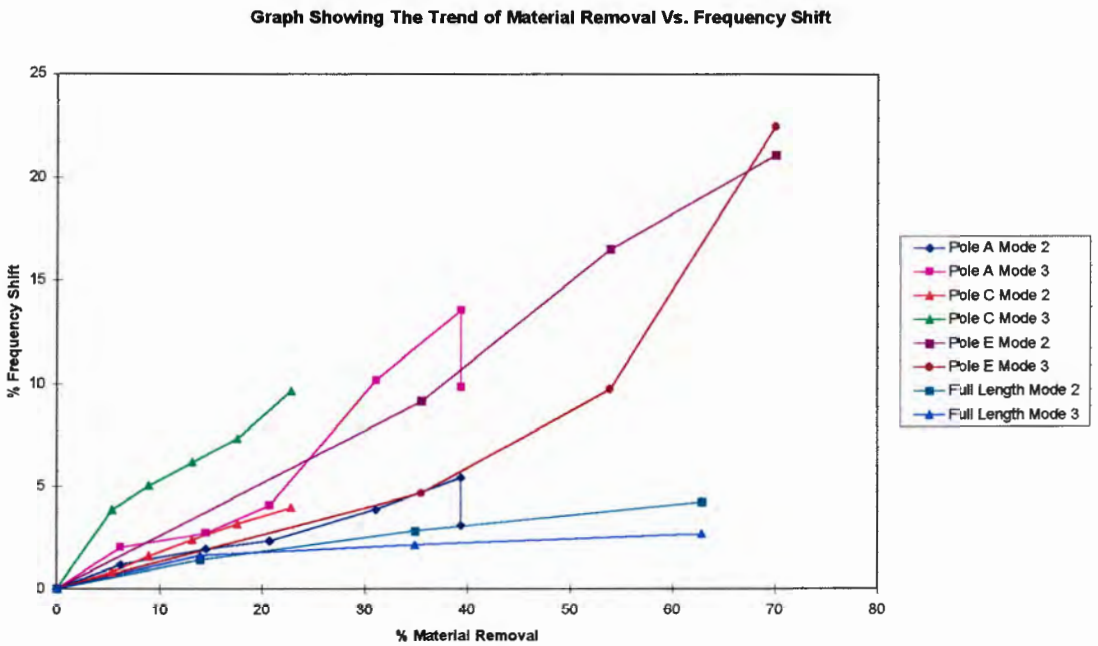

Figure 27: Graph Showing Trend of Material Removal versus Frequency Shift

Following the above, one can reasonably state that in-service decay or material removal does slowly decrease the stiffness of the pole.

5.3 FIELD TESTING OF A FULL LENGTH ESKOM POLE

This section deals with the results obtained using vibration analysis and the ESKOM Pole Tester. The pole in question was tested in situ and allows a comparison between the experimental procedure that is the topic of this thesis and ESKOM's existing testing equipment. The pole had the following dimensions:

Pole Name	Length	Diameter at Ground Line (Both axes)	Diameter at Top	Description
Jhb Pole	7.57	0.273	0.197	Full length pole planted 2 m in ground.

The pole was tested using an impact hammer with the accelerometers placed in 4 different positions in order to minimise the possibility of "missing" a node. The graphic results of the 4 test positions can be seen in Appendix A.

The results obtained using the ESKOM Pole Tester are available in the Table 5. The pole was tested five times and the percentage change of the averages of the test is also shown.

Maximum Bending Moment		
	Initial Value	Following Degradation
Test 1	124.26	89.9
Test 2	135.9	92.05
Test 3	138.74	93.6
Test 4	137.42	94.5
Test 5	139.6	89.7
Average	135.184	91.95
Percentage Difference		47.01903208

Table 5: The Maximum Bending Moment of In-Service Pole Before and After Artificial Degradation

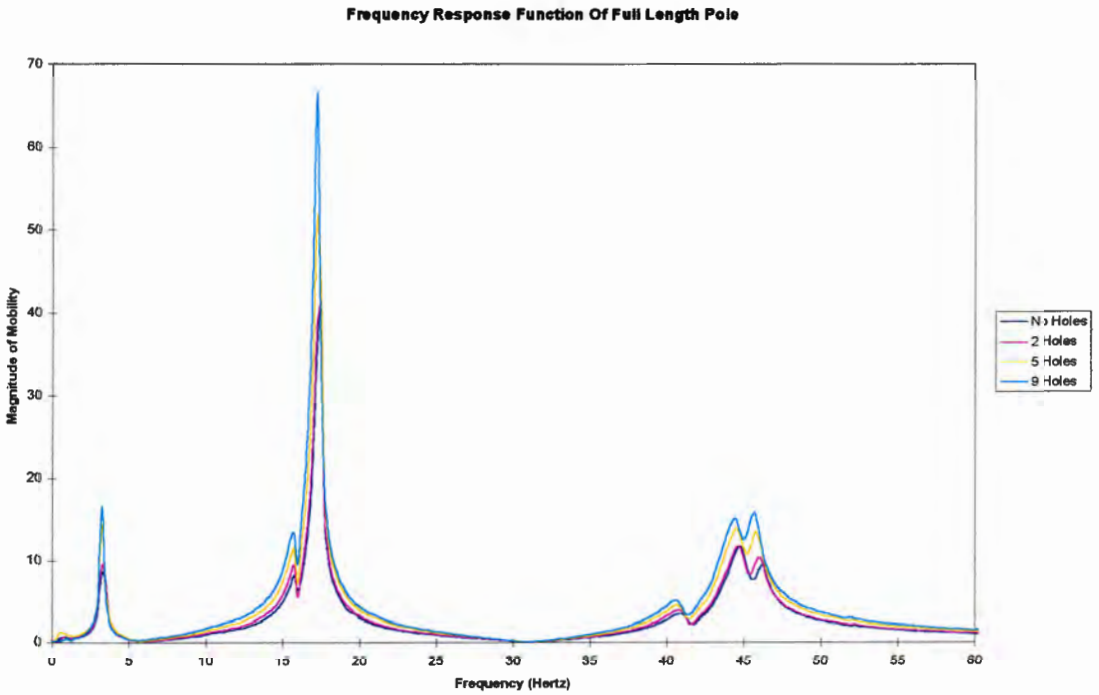

Figure 28: The Frequency Response Function of the Full Length Pole

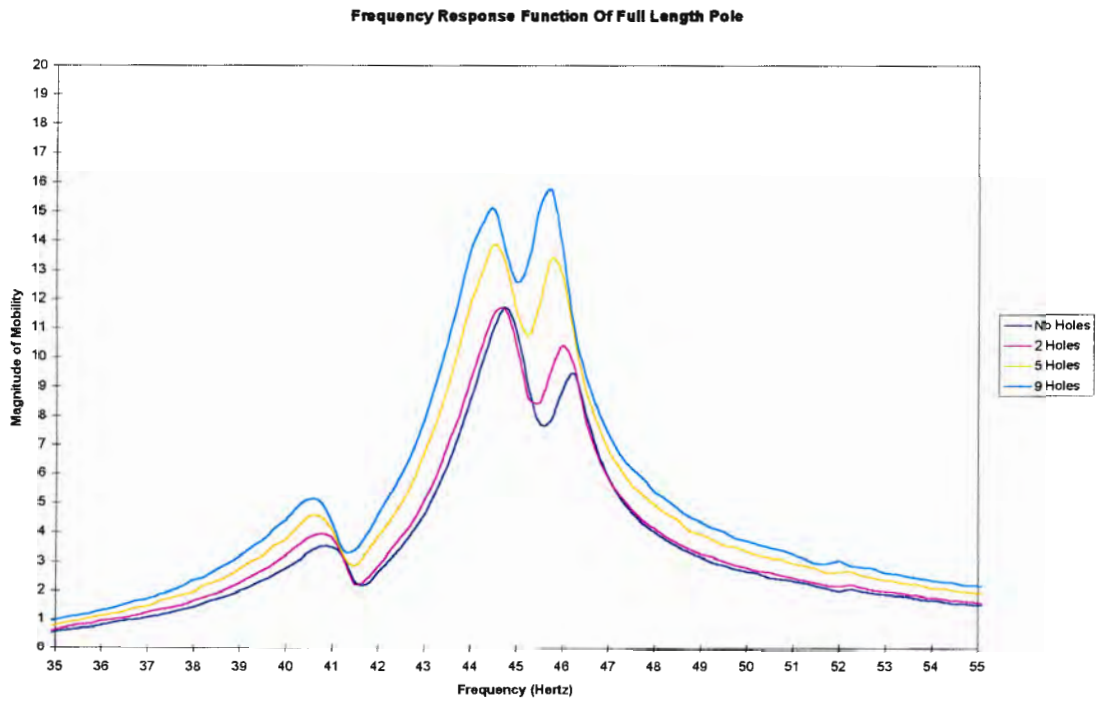

Figure 29: The Frequency Response Function of a Full Length Pole Showing the Third Mode of Vibration

Figure 29 shows clearly the frequency shift due to groundline degradation.

Full Length Pole			
Number Of Holes	% Volume Removed	% Mode 2 Change	% Mode 3 Change
No Holes	0.00	0.00	0.00
2 Holes	13.97	1.41	1.60
5 Holes	34.93	2.82	2.14
9 Holes	62.87	4.23	2.67

Table 6:Table Showing the Percentage of Material Removed and Corresponding Frequency Decrease

Since the full length pole was tested using the ESKOM Pole Tester before and after the vibration tests were undertaken, a comparison can be made.

The removal of 62.86 % of the material of the pole in the groundline area accounted for a decrease of ±47 % in the maximum bending moment that the pole could withstand and a decrease in modal frequency of 4.2% for mode 2 and 2.7% for mode 3.

6 CONCLUSIONS

From the tests that were carried out , the following conclusions can be drawn:

- The use of vibration analysis as a tool for the determination of the strength of a wooden pole has been shown in the laboratory to allow comparisons to be drawn between samples. The method has clearly shown that a pole with a weaker "hinge" has different frequency characteristics in comparison with a pole considered to have a stronger "hinge".
- The correlation between the experimental and the theoretical approach has shown that the frequency values obtained experimentally for the modal frequencies of each pole sample differ from those calculated by a damping factor. The correlation does not allow for a direct representation of the strength of the pole.
- The experimental method has also shown that by removal of material the vibration characteristics of a single pole change and that this can in turn be monitored.
- The progressively artificially degraded poles show a linear trend with respect to the change in frequency versus the percentage material removal. This trend allows for the comparison of a certain pole sample at different times and for the incorporation of a testing procedure that will monitor the history of a pole. By periodically testing the in-service poles, the power utility can formulate a preventative maintenance plan and determine the time at which the pole must be removed.

- The tests carried out on a full length pole revealed that for small shifts in modal frequency, the decrease in the maximum bending moment of the pole obtained using the existing ESKOM Pole Tester, was significant.

7 RECOMMENDATIONS

From the above information and conclusions, the following recommendations can be made.

- It is recommended that the procedure discussed in this thesis be further investigated for use as a tool for the determination of the history of an in-service transmission line pole or the determination of the strength of the pole.
- The two aspects that must be investigated further include:
    - The formulation of a better mathematical model so that the experimental results can be more accurately modelled, in order to provide a comparison between two poles or a single pole over a period time or for the determination of the strength of a pole
    - The incorporation of a more sensitive measuring technique to ensure that the error in determining the modal frequency is minimal due to the fact that small frequency shifts have been shown to account for large changes in the maximum bending moment of a pole.
- It is also recommended that a preventative maintenance procedure be combined with the discussed vibration analysis technique in order to ensure uninterrupted power supply.

8 REFERENCES

1 Breeze, J.E., 1981, "Devices to Measure Strength of Wood Poles", Contract No. 058 D141, Report for the Canadian Electrical Association.

2 Graham, R.D. and Helsing, G.G., 1979, "Wood Pole Maintenance Manual: Inspection and Supplemental Treatment of Douglas-fir and Western Redcedar Poles", Forest Research Laboratory, Oregon State University, Research Bulletin 24.

3 Elcock, G., 1986, "Pole Breaking Proving Test of the PEST Pole Strength Predictor", ECRC/R2112, The Electricity Council Research Centre, Chester.

4 Electric Power Research Institute (EPRI), Editor Landers, P., 1981, "Probability-based Design of Wood Transmission Structures, Volume 1, 2, 3: Strength and Stiffness of Wood Utility Poles", EPRI EL-2040, Volume 1, 2, 3, Project 1352-1.

5 American Society for Testing and Materials, 1979, "Annual Book of ASTM Standards, Part 22 - Wood, Adhesives" D 1036 , Philadelphia, pp 267-284.

6 Hoffmeyer, P., 1978, "The Pilodyn Instrument as a Non-destructive tester of the Shock Resistance of Wood", Paper Presented at the Non-destructive testing Meeting in Vancouver, Washington, August 1978

7 Fagan, G.B., 1980, "Non-destructive Specific Gravity Determination of Utility Poles Using the Pilodyn Wood Testing Instrument", Dept. of Forest and Wood Sciences, Colorado State University, 1980

8 Collins, R.V., 1972, "The Role Of NDT in an Electric Utility", Paper Presented at the National Conference of the American Society for Non-destructive Testing, October 1972.

9 Heath Incorporated, Patent office

10 Goodman, J.R., Bodig, J. and Stewart, A.H., 1986, "Reliability of In-Service Wood Pole Utility Structures", 14 th Inter-Ram Conference for Electric Power Industry.

11 Hasenoerhi, P.J., 1987, "Nondestructive Evaluation in Wood Pole Management", Transmission and Distribution, December 1987, pp 38 - 43.

12 Editor, 1987, "Innovative Wood Pole Management Program Uses NDE Technique", Electrical World, March 1987, pp 39 - 42.

13 Murphy, M.W., Franklin, D.E. and Palylyk, R.A., 1986, "A Non-destructive Testing Technique for Wood Poles", Contract No. 199 D376 Part 2, Report for the Canadian Electrical Association.

14 Hird, E.V., 1989, "Field Test Your Wood Poles - Electronically", Telephone Engineer and Management, 15 April 1989.

15 Smart, M. and Chandler, H.D., 1995, "Modal Testing for NDT of Structures", R & D Journal, 1995, 11(3), pp 79 - 85.

16 Technical Brochure, 1983, "Wooden Pole Decay Detector", The Mitsubishi Electric Corporation, November 1983

17 ANDEC Manufacturing, "CLUE Wooden Utility Pole Tester", Sales Brochure, ANDEC Manufacturing.

18 Tomikawa, Y., Iwase, Y., Arita, K., Yamada, H., 1986, "Non-destructive Inspection of a Wooden Pole Using Ultrasonic Computed Tomography", IEEE Transactions on Ultrasonics, Ferroelectrics, and Frequency Control, Volume UFFC-33 No. 4, July 1986.

19 SABS 753-1982, 1982, "Standard Specification for Pine Poles and Cross-arms for Power Transmission, Low-voltage Reticulation and Telephone Systems", SABS 753-1982, Published by the Council of the South African Bureau Of Standards

20 SABS 754-1982, 1982, "Standard Specification for Pine Poles and Cross-arms for Power Transmission, Low-voltage Reticulation and Telephone Systems", SABS 753-1982, Published by the Council of the South African Bureau Of Standards

21 The Department of Forestry, 1977

22 Ewins, D.J.,1984, "Modal Testing: Theory and Practice", Published by Research Studies Press Ltd., Hertfordshire England, 1984

23 Rao, S.S., 1990, "Mechanical Vibrations", Second Edition, Published by Addison-Wesley Publishing Company, 1990

24 Mathcad, Mathsoft Incorporated, 1995

9 BIBLIOGRAPHY

1. Krishnasamy, S., Shehata, A., 1992, "non-destructive Assessment of Wood Poles", Published by the Canadian Electrical Association Engineering and Operating Division.
2. Wang, Y. And Bodig, J, 1990, "Strength Grading method for Wood Poles", Journal for Structural Engineering, Vol. 116, No. 11, November 1990.
3. Wang, H-C., 1967, "Generalised Hypergeometric Function Solutions on the Transverse Vibration of a Class of Non-uniform Beams", Journal of Applied Mechanics, September 1967.
4. Craver, W. And Egle, D., "A Method for Selection of Significant terms in the Assumed Solution in a Rayleigh-Ritz Analysis", The Journal for Sound and Vibration, pp 133 - 142, 1972.
5. Hutchinson, J., 1980, "Vibrations of Solid Cylinders", Journal of Applied Mechanics, Vol. 47, December 1980.
6. Penny, J. and Reed, J., 1971, "An Integral Equation Approach to the Fundamental Frequency of Vibrating Beams", The Journal of Sound and Vibration, pp 393 - 400, 1971.
7. Sinclair, A. And Farshad, M., 1987, "A Comparison of Three Methods for Determining Elastic Constants of Wood", Journal of Testing and Evaluation, pp 77-86, March 1987.

8. Hutchinson, J., 1981, "Transverse Vibrations of Beams, Exact Versus Approximate Solutions", Journal of Applied Mechanics, Vol. 48, December 1981.
9. Klein, L., 1974, "transverse Vibrations of Non-uniform Beams", The Journal of Sound and Vibration, pp 491 - 505, 1974.
10. SABS 0163 Part I -1980, 1980, "The Design of Timber Structures", Published by the Council of the South African Bureau of Standards.
11. SABS 539-1980,1980, "Wood Preserving Creosote (Lurgi-gasification Process)", Published by the Council of the South African Bureau of Standards.
12. SABS 457-1982, 1982, "Wooden Poles, Droppers, Guard Rail Posts, and Spacer Blocks", Published by the Council of the South African Bureau of Standards.
13. SABS Method 987 - 1994, 1994, "Depth of Penetration of Preservation and Detection and Depth of Sapwood in Timber", Published by the Council of the South African Bureau of Standards.
14. SABS 538-1980,1980, "High Temperature Wood Preserving Creosote", Published by the Council of the South African Bureau of Standards.
15. Balfour, I. And MacDowell, T., 1985, "Refurbishment of Wood Pole Distribution Lines in North Scotland", North of Scotland Hydro-Electric Board, 1985.
16. The Subcommittee on Wood Research of the ASCE Committee on Wood, 1986, "Structural Wood Research Needs", The Journal of Structural Engineering, Vol. 112, No. 9, September 1986.

17. Bucur, V. and Chivers, R., 1991, "Acoustic Properties and Anisotropy of Some Australian Wood Species", Acustica, Vol. 75, 1991.

18. McCracken, F. And Vann, S., 1983, "Sound Can Detect Decay in Standing Hardwood Trees", Res.Pap. SO-195, Published by the U.S. Department of Agriculture Forest Service, 1983.

19. Bucur, V and Rocaboy, F., 1988, "Surface Wav Propagation in Wood: Prospective Method for the Determination of Wood Off-Diagonal Terms in Stiffness Matrix", Ultrasonics, Vol. 26 November 1988.

20. Bucur, V. And Feeney, F., 1992, "Attenuation of Ultrasound in Solid Wood", Ultrasonics, Vol. 30, No. 2, 1992.

21. McCuen, R., Aggour, M. and Ayyub, B., 1988, "Spacing for Accuracy in Ultrasonic Testing of bridge Timber Piles", The Journal of Structural Engineering, Vol. 114, No. 12, December 1988.

22. de Silva, C. and Palusamy, S., 1984, "Experimental Modal Analysis - A Modelling and Design Tool", Mechanical Engineering, June 1984.

Appendix A

Appendix A

The Frequency Response Functions Of The Seven Pole Samples

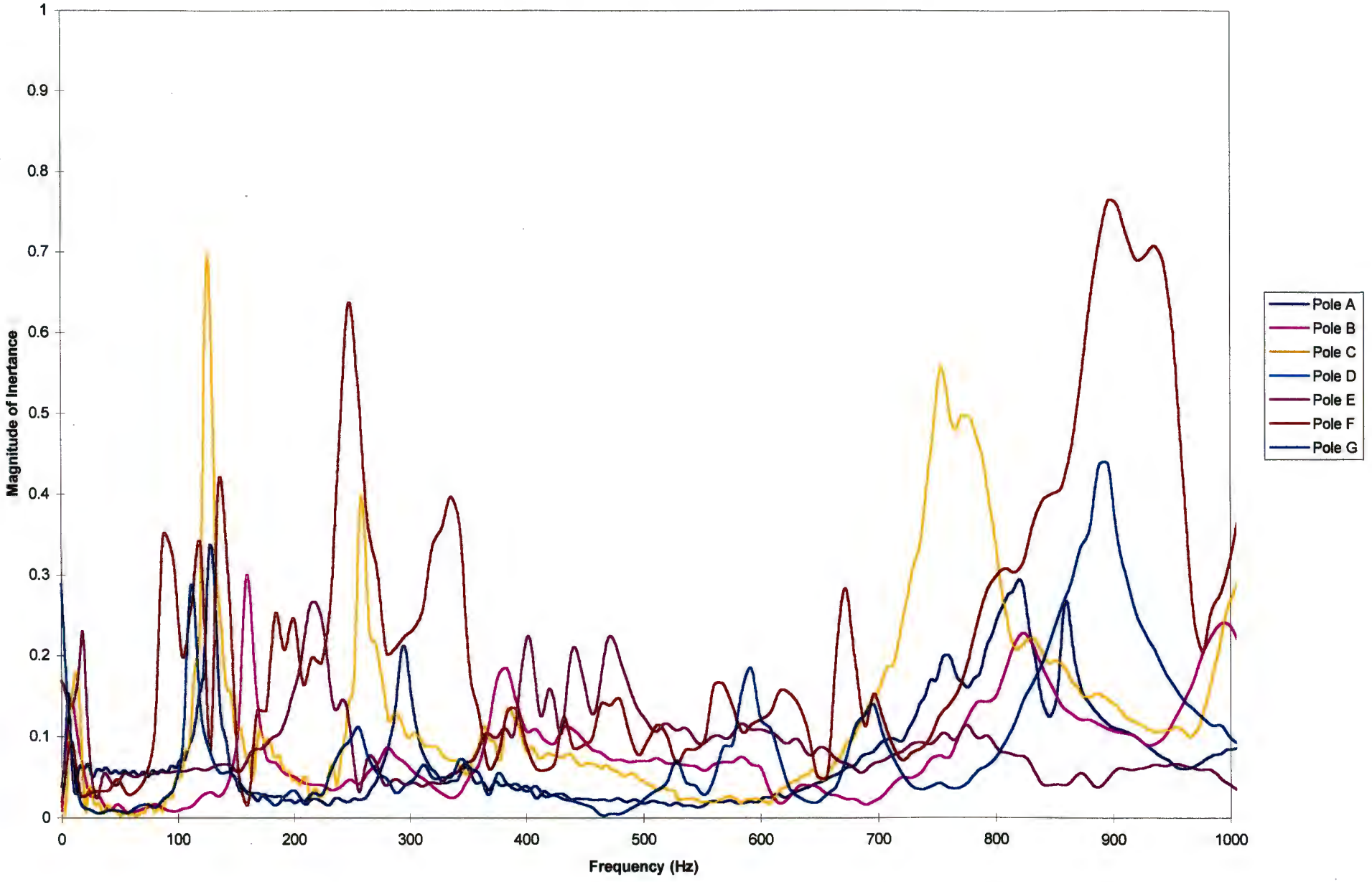

The Frequency Response Function of Pole B

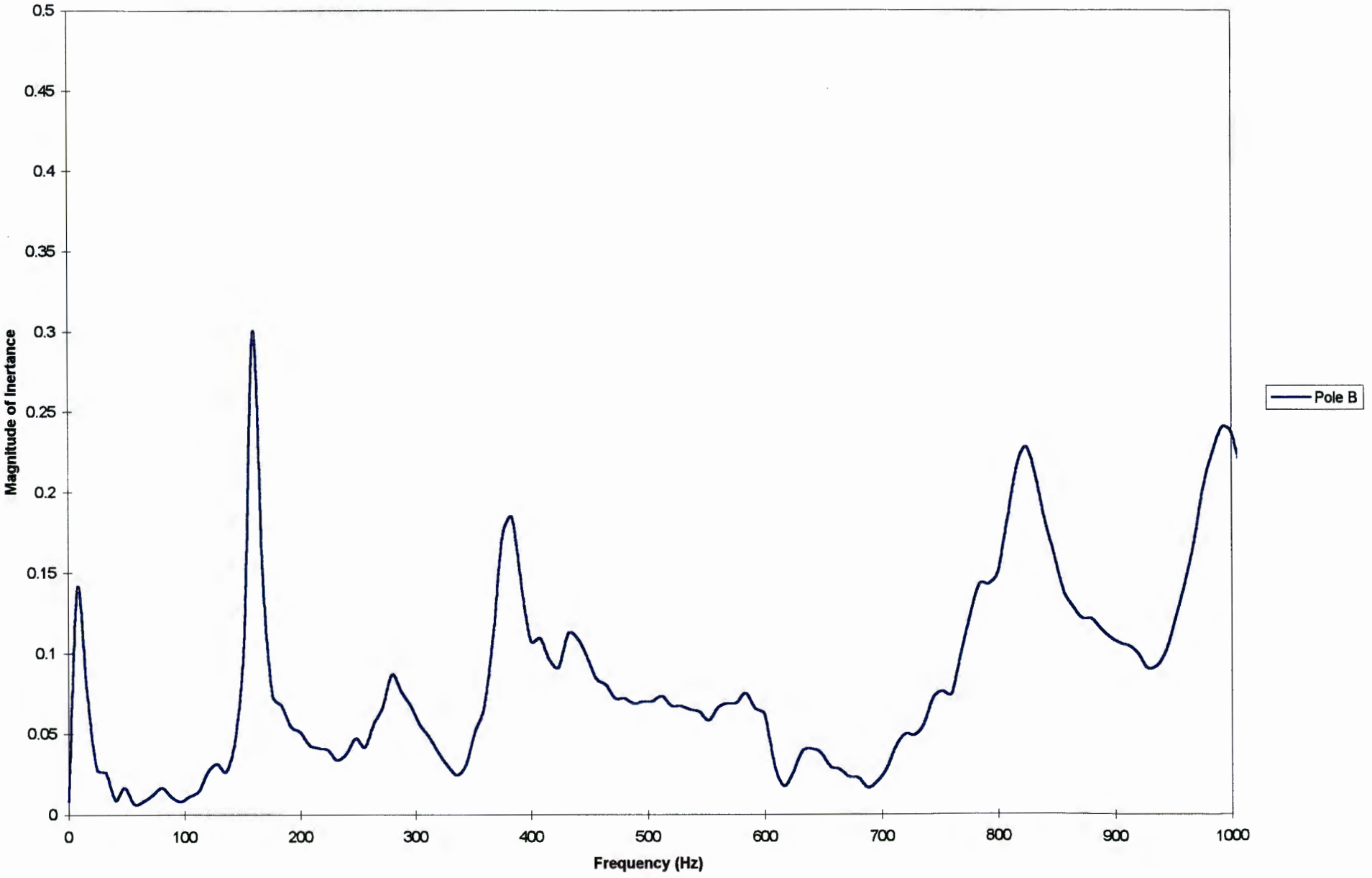

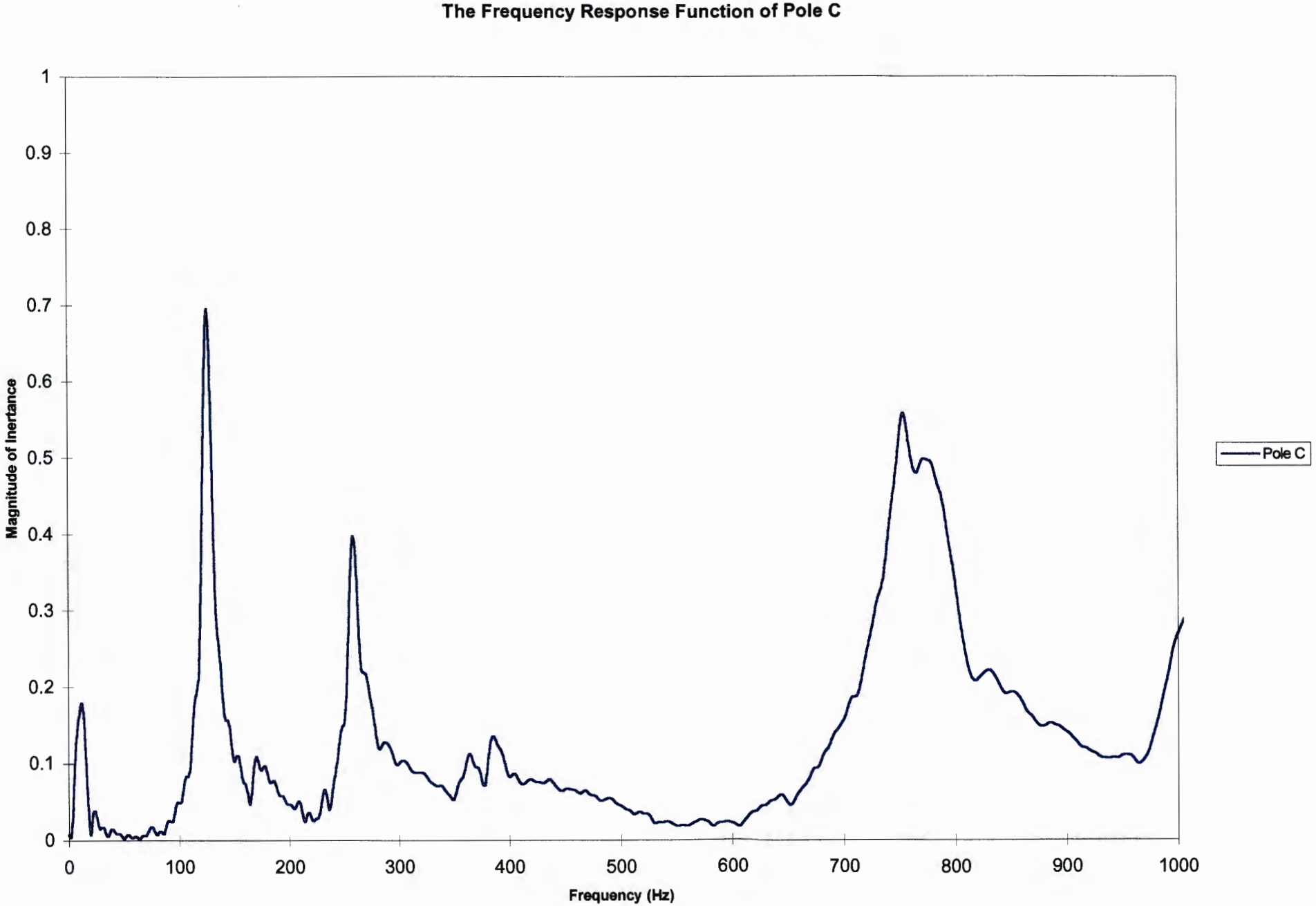
The Frequency Response Function of Pole C
Magnitude of Inertance
Frequency (Hz)
Pole C
0
0.1
0.2
0.3
0.4
0.5
0.6
0.7
0.8
0.9
1
0
100
200
300
400
500
600
700
800
900
1000

The Frequency Response Function of Pole D

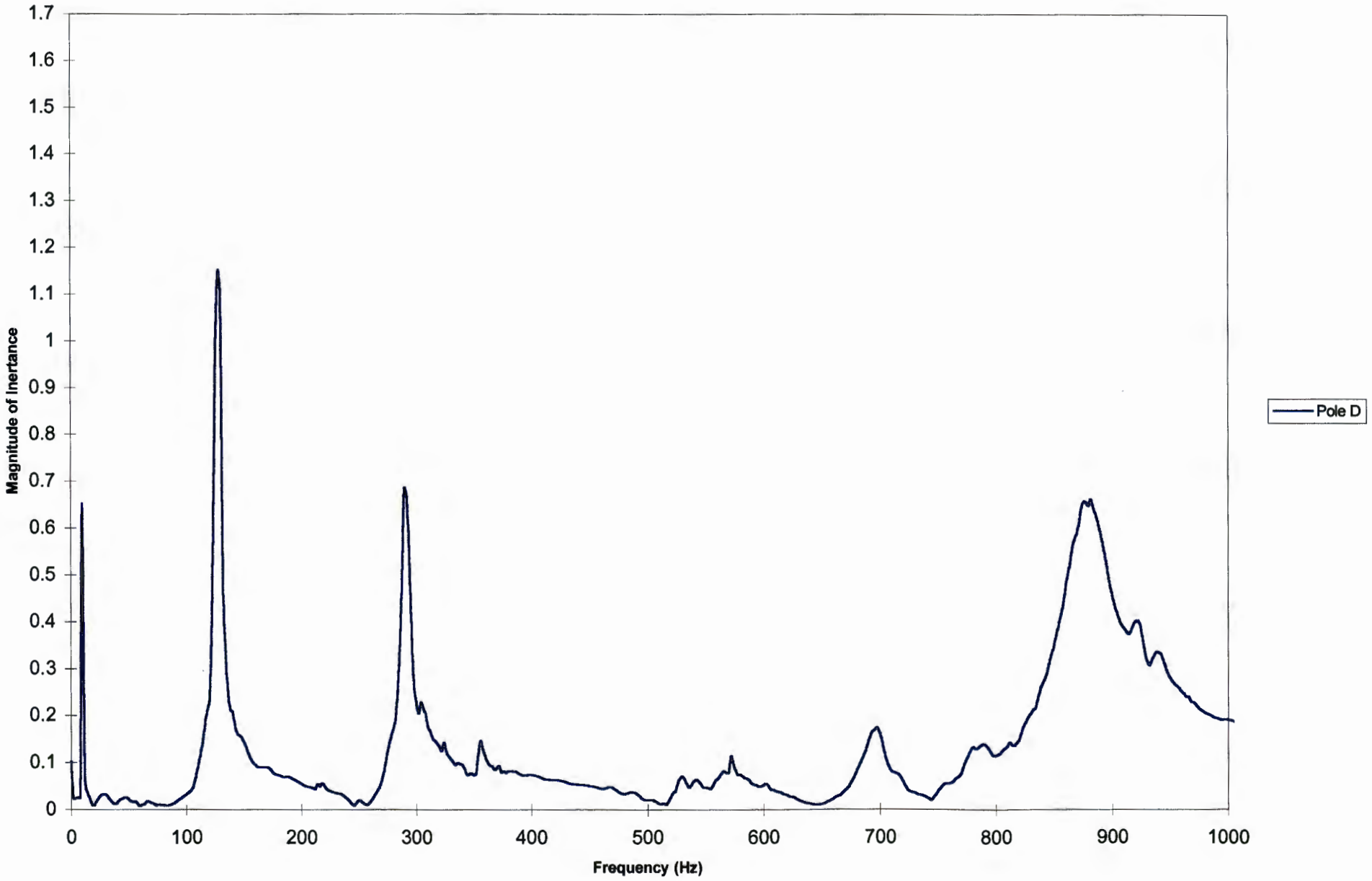

The Frequency response Function of Pole E

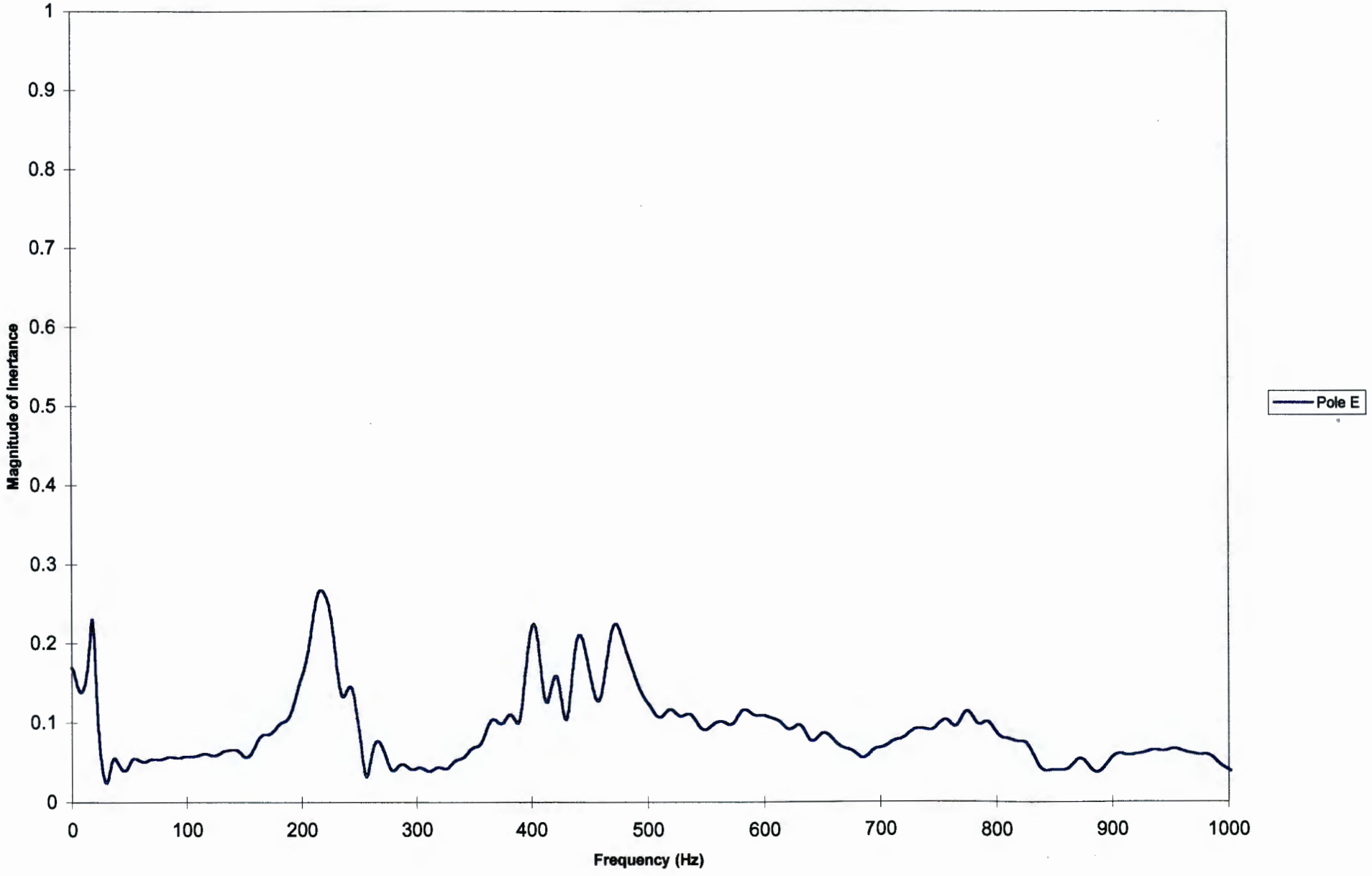

The Frequency Response function of Pole F

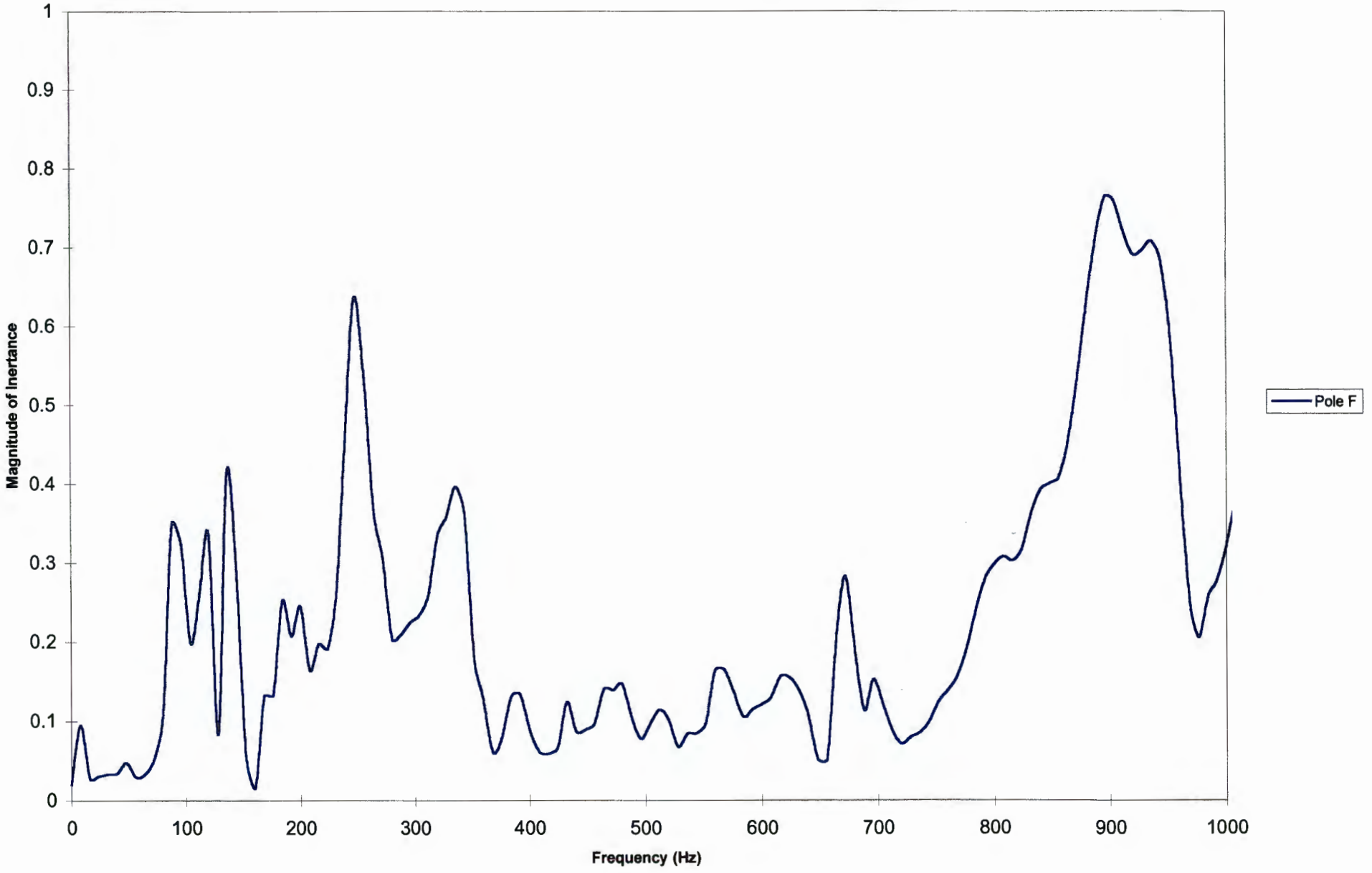

The Frequency Response Function of Pole G

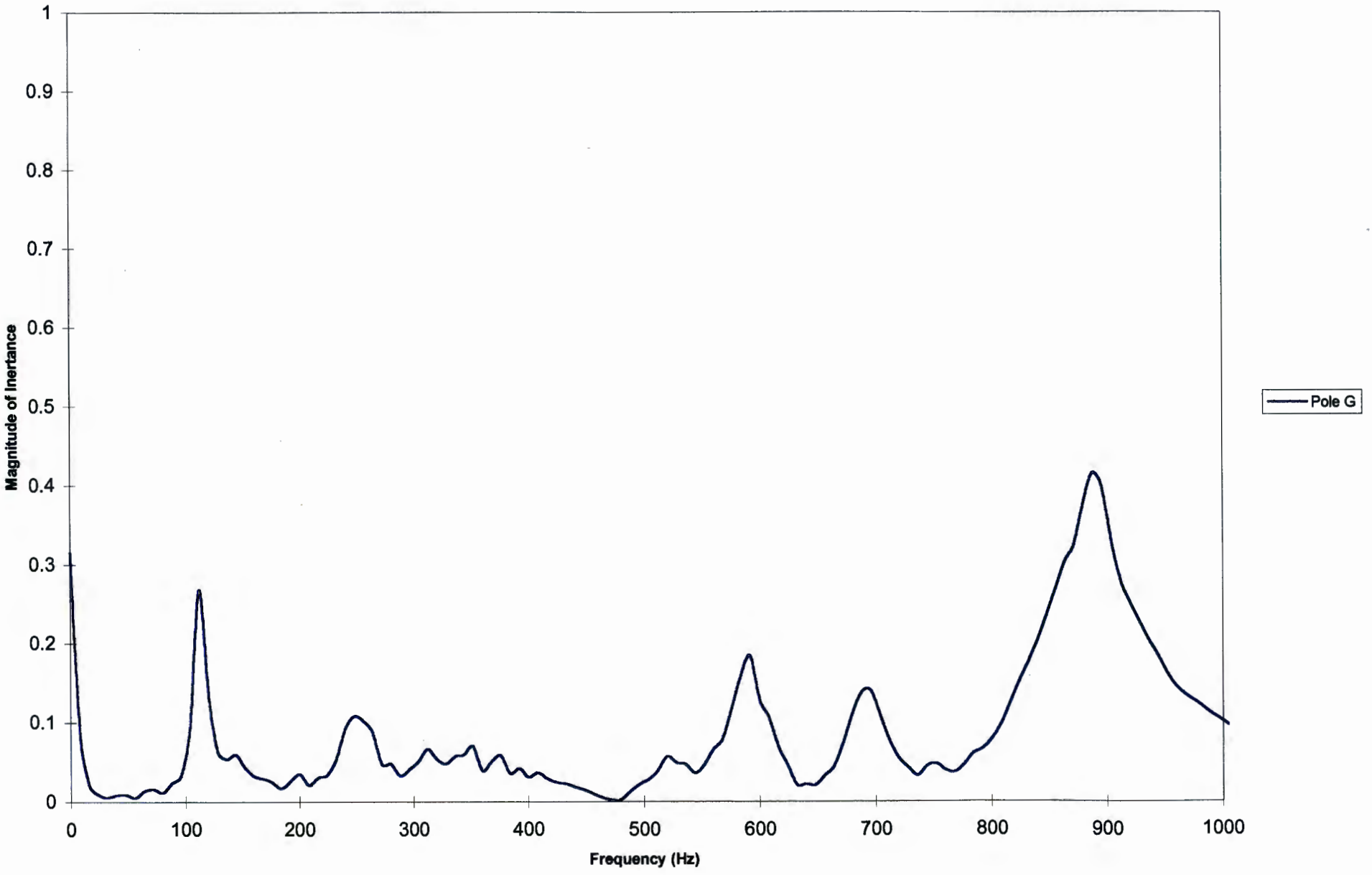

Frequency Response Function Of Degraded Pole A

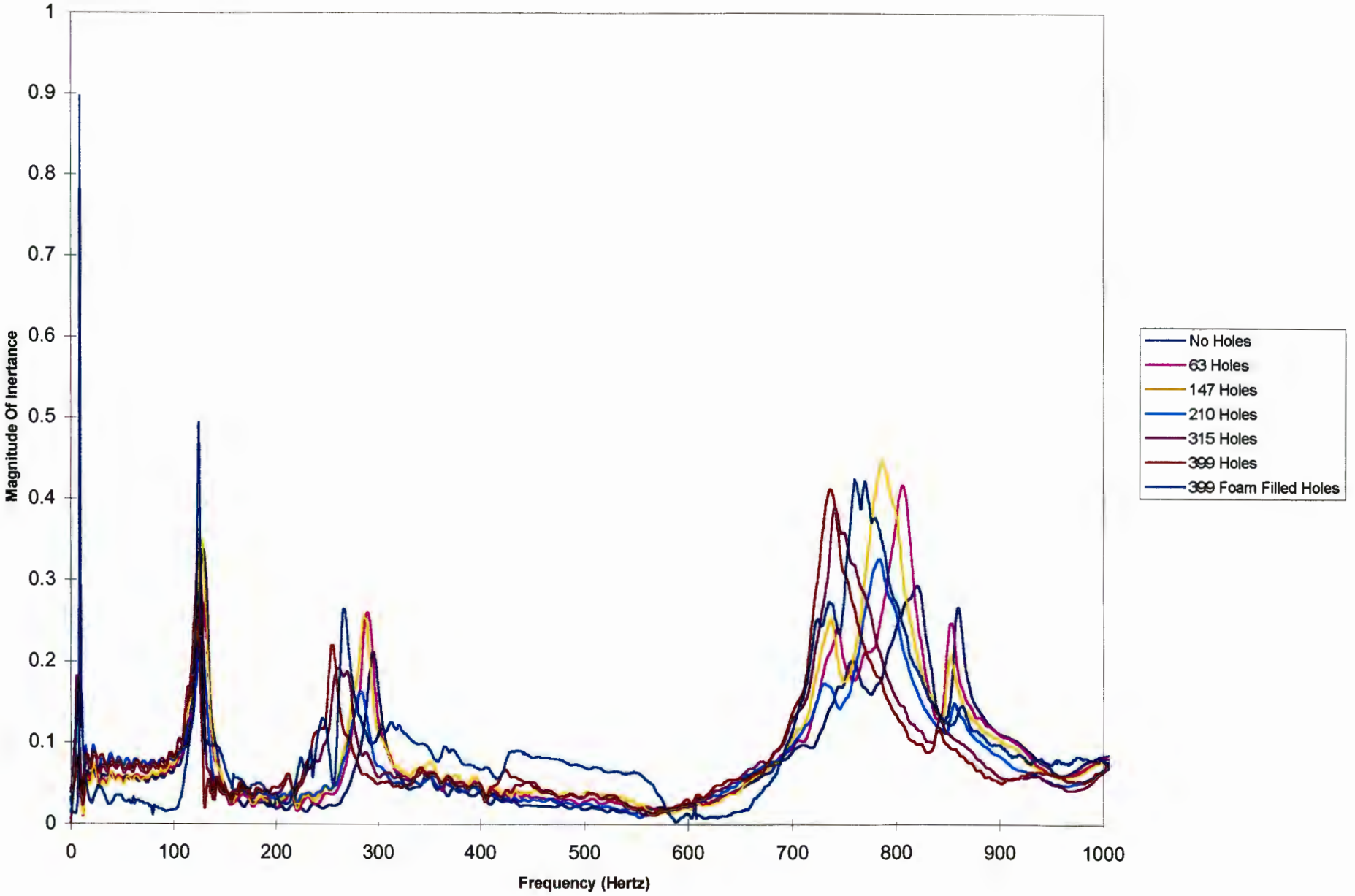

Frequency Response Function Of Degraded Pole C

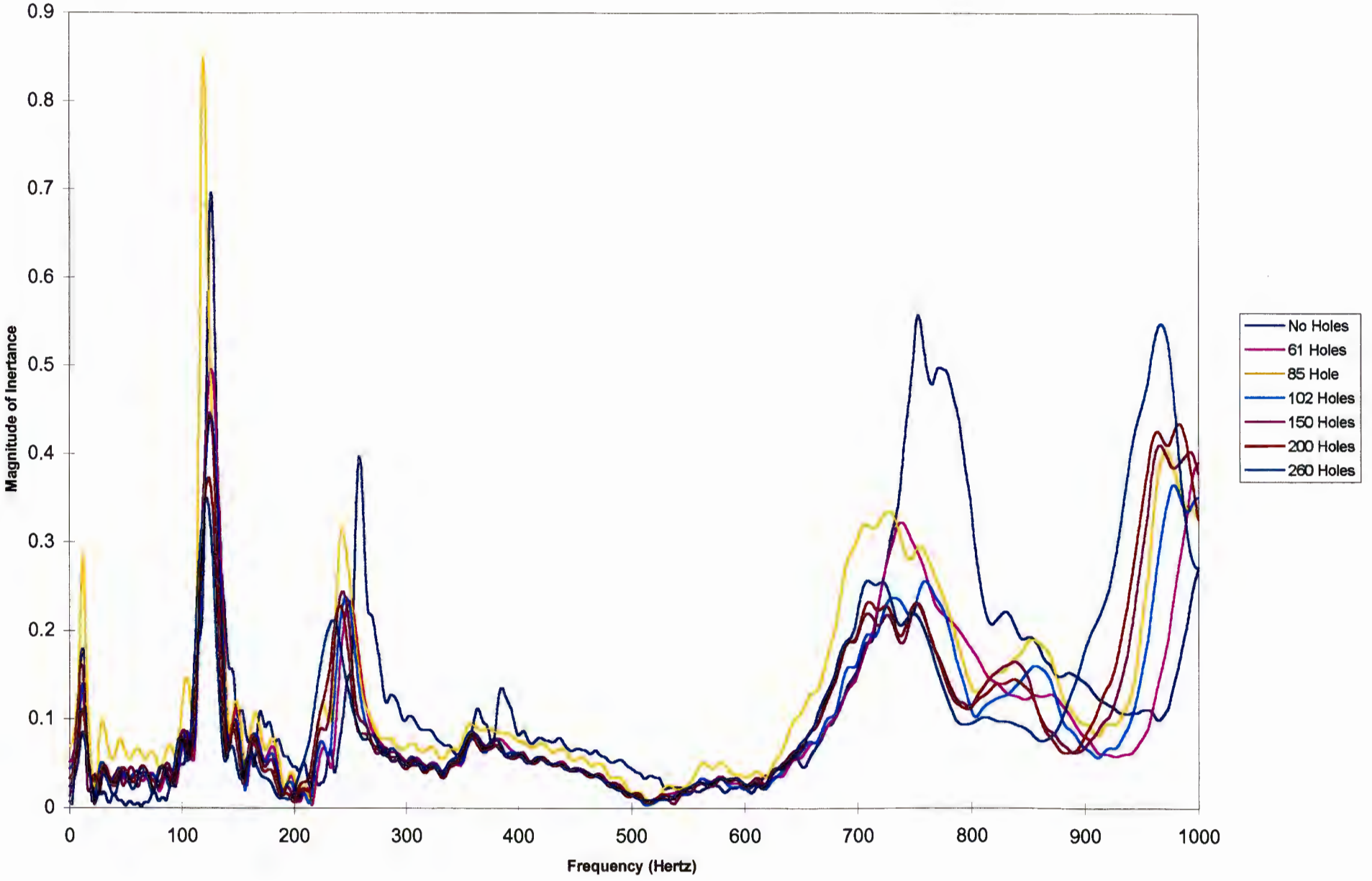

Frequency Response Function Of Degraded Pole E

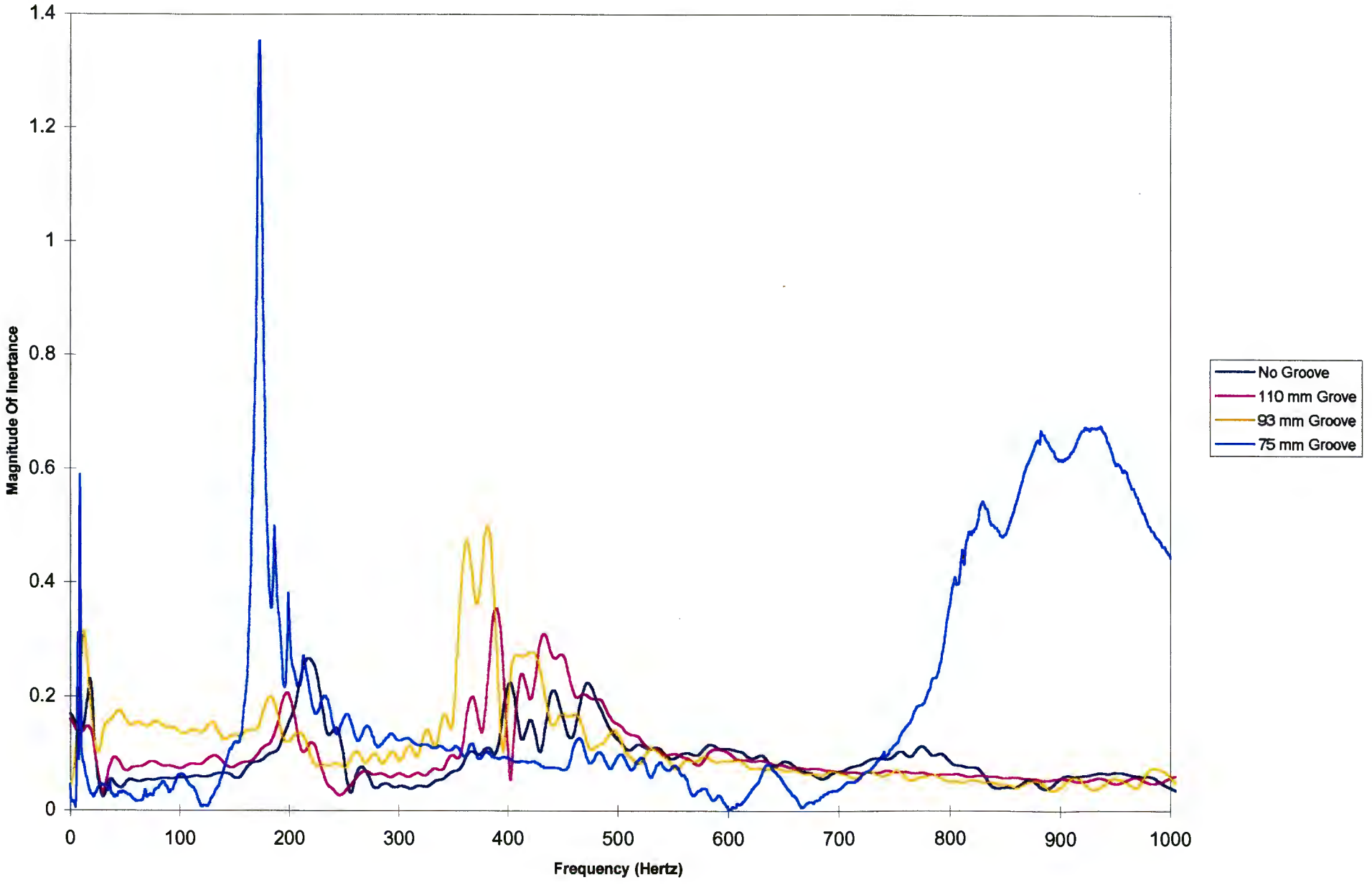

Appendix B

Appendix B

Specifications for the PCB 208B03 Piezoelectric Force Transducer.

(As supplied by PCB Piezotronics)

Specification	Unit	Model 208B03
Range : Compression (1)	lb.	500
Tension	lb.	500
Useful Overange: Compression (2)	lb.	1000
Maximum Force: Compression	lb.	5000
Tension	lb.	750
Resolution	lb.	0.01
Sensitivity (± 10%)	mV/lb.	10
Resonant Frequency	kHz	70
Rise Time	μ seconds	10
Discharge Time Constant	seconds	≥2000
Low Frequency Response	Hz	0.0003

Notes:

- One lb ≈ 4.448 N
- 24 volt DC supply typically required for full overrange

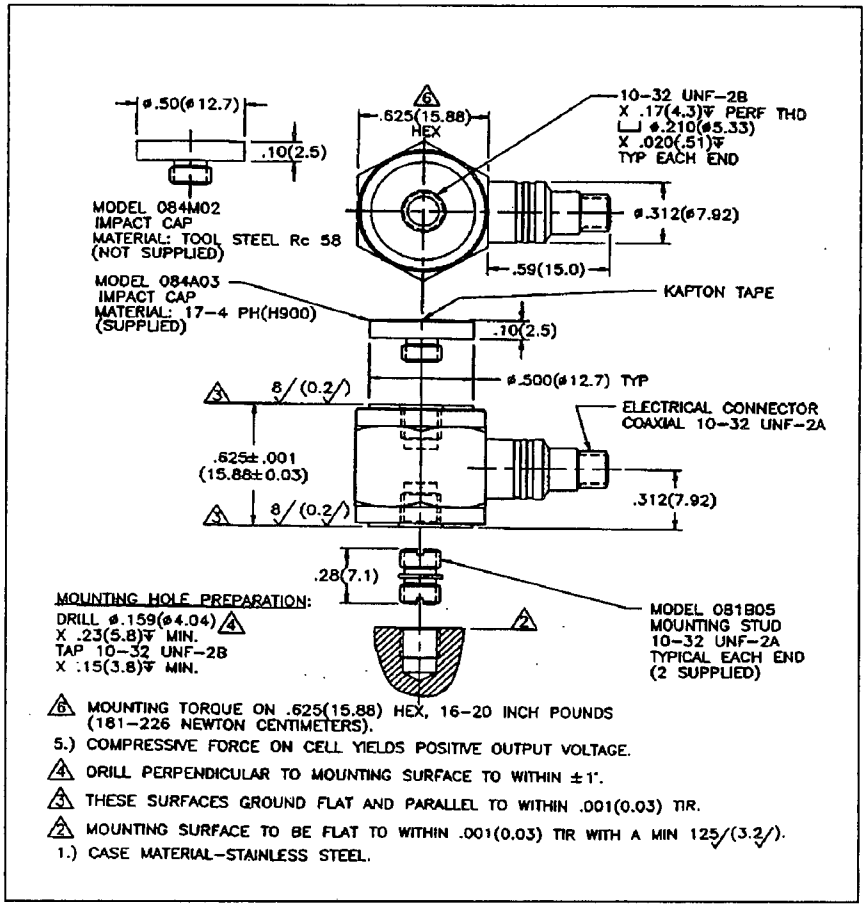

Specifications for the Wilcoxon 736 Accelerometer.

(As supplied by Wilcoxon Research)

Specification	Units	Model 736
Dynamic		
Sensitivity ±5% at 25 °C	mV/g	100
Acceleration Range	g peak	50
Amplitude Nonlinearity	%	1
Frequency Response ±5% ±3 dB	Hz	6 - 15000 2 - 25000
Electrical		
Power Requirement	VDC mA	18 - 30 2 - 10
Environmental		
Temperature Range	°C	-50 - +120
Vibration Limit	g peak	500
Shock Limit	g peak	5000

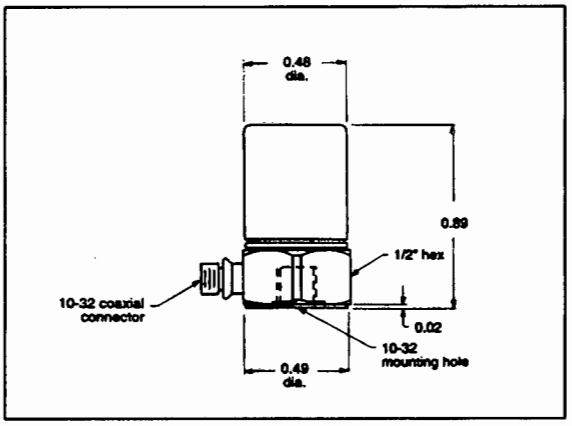

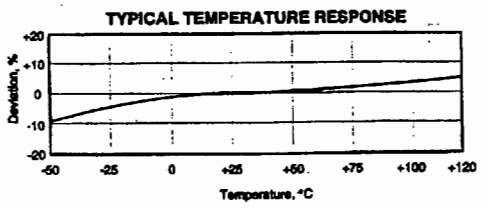

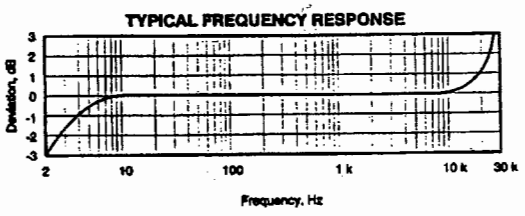

Calculation of the Spring Constant of the Helical Spring Used in the Experiments

In order to calculate the spring constant of the spring used in this experiment, the spring was tested under known compression forces and the displacements were measured. This allowed the calculation of the spring constant using Hooke's Law.

The dimensions of the spring were as follows:
Free Length : 52 mm
Experimental Compressed Length : 40.3 mm

The following table shows the tested data:

Length	Compression Force	Calculated Spring Constant
0.011 m	79.26 N	7205.45 N.m
0.014 m	100.65 N	7189.29 N.m
0.020 m	144.15 N	7207.50 N.m

The average Spring Constant from the tests was calculated as 7200.75 N.m

Hewlett-Packard Spectrum Analyser

Current Limiting Power Supplies Used In Conjunction With Transducers

Appendix C

Appendix C

Example of the ESKOM "Wind-on-pole" Calculation with regards to Typical Pole Design

If one considers the design of a typical single pole as shown below with the following dimensions and design requirements:

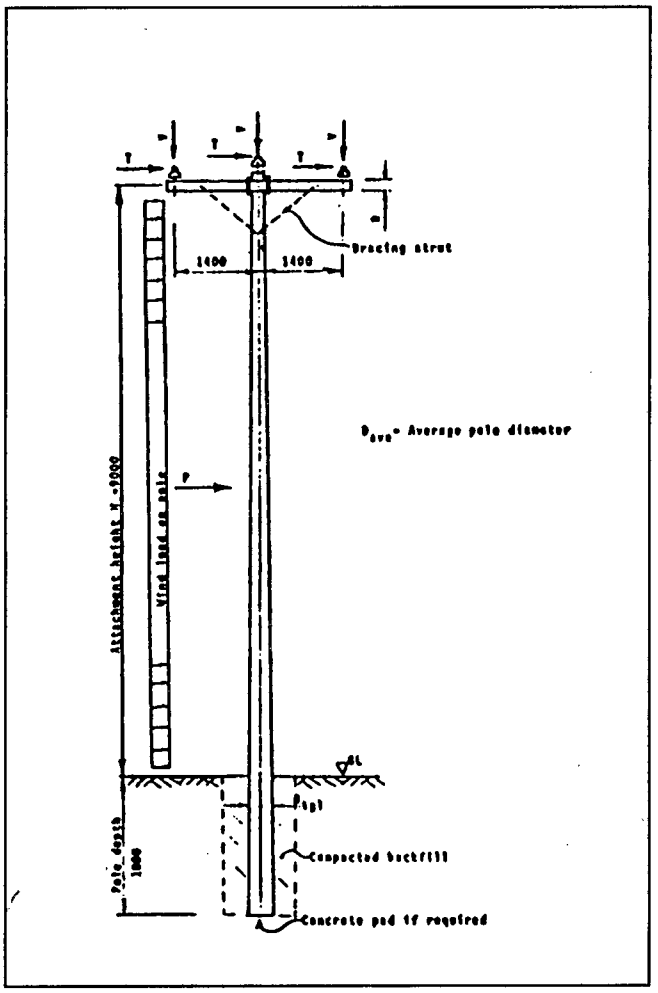

Length : 9.0 m : L

Planting Depth : 1.8 m : P

Cross Bar Length : 2.8 m : Z

The conductors shall have the following properties:

Weight : 4.22 N/m : W

Outside Diameter :14.3 mm : d

Rated Breaking Strength : 36.5 kN

No earth conductor required and the wind and dead load of hardware will be ignored.

The design spans are given by:

Wind span : 130 m : L_w

Weight span : 150 m : L_{wgt}

Nominal span : 110 m : L_{nom}

The force exerted by the wind on the conductor:

T = wind pressure x wind span reduction factor x wind span x diameter

T = 700 Pa x 0.6 x L_w x d

T = 0.781 kN

The force exerted by the wind on the pole:

P = wind pressure x wind span reduction factor x height x diameter average

P = 700 Pa x 0.6 x H x D_{ave}

P=0.76 kN

The maximum bending moment of the pole which is back-filled, occurs below ground level. As has been discussed, a rule of thumb is to assume this point of maximum bending to be a quarter of the pole depth below ground level. Both this and a more exact method will be shown.

Assuming that the planting depth is 1.8 m, then the maximum bending moment is:

M = 3 x T x (L + 1.8/4) + P x (L/2 + 1.8/4)

M =25.9 kNm

The section modulus of the pole at that point is then:

$Z = (\pi \times D^3 \times t \times g \times l)/32$

$Z = 0.001274\ m^3$

Bending Stress:

$f = M / Z$

$f = 20.3$ MPa

This is then compared with the required standard and the safety factor calculated.

Safety factor = 55 / 20.3 = 2.71

This is the same as the required 2.7 safety factor specified.

A more exact method is to approximate the soil pressure and the bending moment (using the passive pressure method) of a pole as shown in the diagram below.

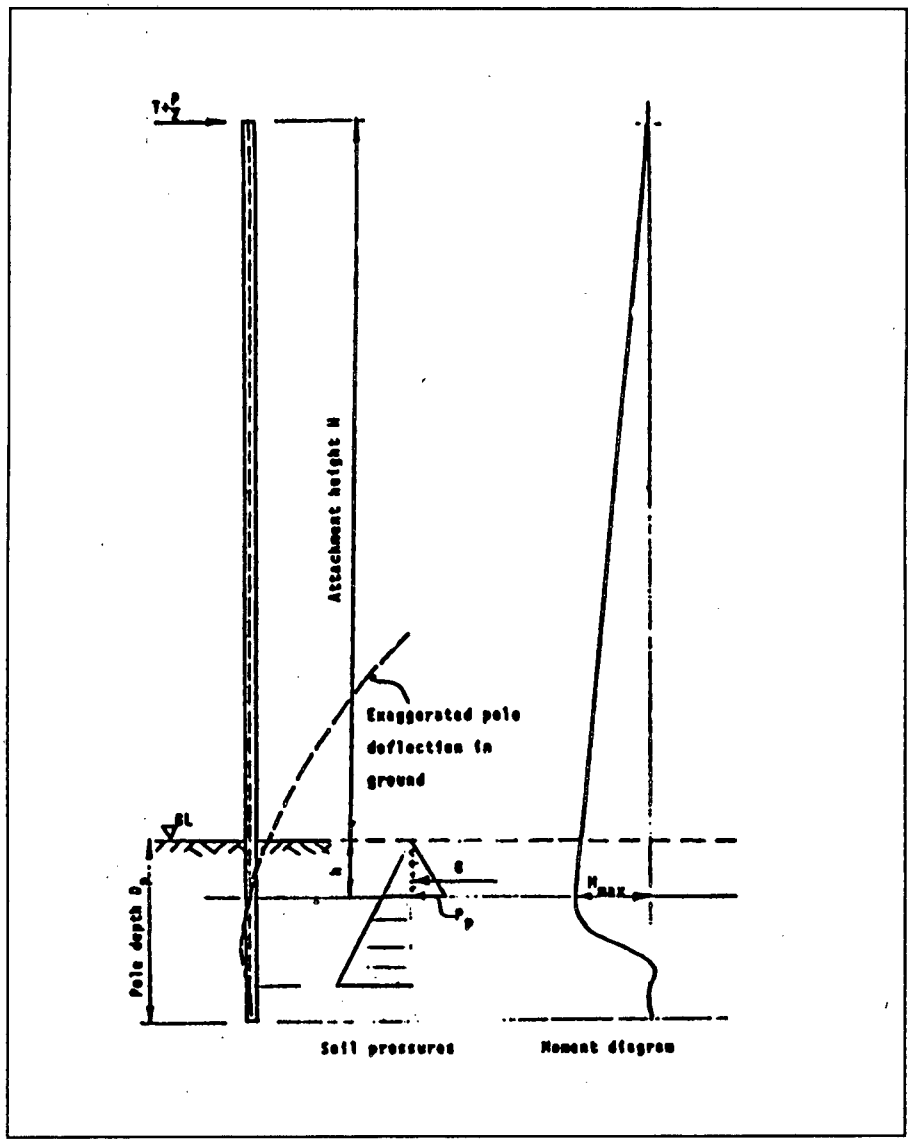

The point of maximum bending can be determined by calculating the depth of soil required to resist the applied horizontal load T using a safety factor of 2. The total depth must furthermore not be less than 1.5 times the distance to the point of maximum bending.

Using average soil parameters as follows:

The internal angle of friction = ϕ =30°

The saturated soil density = S =10 kN/m^3

A safety factor = SF = 2

And ignoring cohesion and friction between the pole and soil

$$G = \frac{1}{2} P_P h D_{tgl}$$

where P_p = passive soil reaction = $\frac{1}{SF} K_p S h$

$P_p = 15h$ kN/m

where $K_p = \frac{1+\sin\phi}{1-\sin\phi}$ = passive reaction coefficient

Thus G = 1.76 h^2

Then for:

$$T + \frac{P}{2} = G$$

therefore h = 1.24 m

and the minimum depth is 1.86 m, which is very close to the assumed planting depth of 1.8 m.

The maximum bending in the pole is then:

$$M = 2.72(H + h) - G\frac{h}{3}$$

M = 26.7 kNm

which compares very well with the 25.9 kNm calculated using the assumed depth.

Crossarm design

The size of the cross arm is governed by the weight of the conductors and hardware

The maximum bending moment induced in a crossarm is:

$$M = Vl$$

where l is half the crossarm length.

The section modulus for a 100 mm diameter pole is:

$$Z = \frac{\pi \cdot D^3}{32}$$

and the bending stresses

$$f_b = \frac{M}{Z}$$

which in this case is 9.2 MPa

and results in a safety factor of 6 and is more than the required 4.5.

Appendix D

Appendix D

The Comparison between the Exact Solution and the Derived Shape Function for use in Rayleigh's Equation.

The general properties and physical characteristics of the "specimen" for the comparison were assumed to have the following values.

Given: $E := 13 \cdot 10^9$ $\rho 1 := 650$

$d := 0.22$ $I := \frac{d^4}{64} \cdot \pi$

$l := 1.7$ $A := \frac{d^2}{4} \cdot \pi$

The Exact Solution:

$\beta_1 := \frac{1.875104}{l}$ $\beta_2 := \frac{4.694091}{l}$ $\beta_3 := \frac{7.854757}{l}$ $\beta_4 := \frac{10.995541}{l}$

$\omega_1 := (\beta_1 \cdot l)^2 \cdot \sqrt{\frac{E \cdot I}{\rho 1 \cdot A \cdot l^4}}$ $\omega_1 = 299.248$

$\omega_2 := (\beta_2 \cdot l)^2 \cdot \sqrt{\frac{E \cdot I}{\rho 1 \cdot A \cdot l^4}}$ $\omega_2 = 1.875 \cdot 10^3$

$\omega_3 := (\beta_3 \cdot l)^2 \cdot \sqrt{\frac{E \cdot I}{\rho 1 \cdot A \cdot l^4}}$ $\omega_3 = 5.251 \cdot 10^3$

$\omega_4 := (\beta_4 \cdot l)^2 \cdot \sqrt{\frac{E \cdot I}{\rho 1 \cdot A \cdot l^4}}$ $\omega_4 = 1.029 \cdot 10^4$

The Rayleigh Solution:

$$W(x)= \quad C\cdot\left[\sin(\beta_n\cdot x)-\sinh(\beta_n\cdot x)-\left(\frac{\sin(\beta_n\cdot l)+\sinh(\beta_n\cdot l)}{\cos(\beta_n\cdot l)+\cosh(\beta_n\cdot l)}\right)\cdot\left(\cos(\beta_n\cdot x)-\cosh(\beta_n\cdot x)\right)\right]$$

$$W''(x)=C\cdot\left[-\sin(\beta_n\cdot x)\cdot(\beta_n)^2-\sinh(\beta_n\cdot x)\cdot(\beta_n)^2-\frac{\left(\sin(\beta_n\cdot l)+\sinh(\beta_n\cdot l)\right)}{\left(\cos(\beta_n\cdot l)+\cosh(\beta_n\cdot l)\right)}\cdot\left[-\cos(\beta_n\cdot x)\cdot(\beta_n)^2-\cosh(\beta_n\cdot x)\cdot(\beta_n)^2\right]\right]$$

$C := 1 \qquad n := 1$

$$G(x) := C\cdot\left[\sin(\beta_n\cdot x)-\sinh(\beta_n\cdot x)-\left(\frac{\sin(\beta_n\cdot l)+\sinh(\beta_n\cdot l)}{\cos(\beta_n\cdot l)+\cosh(\beta_n\cdot l)}\right)\cdot\left(\cos(\beta_n\cdot x)-\cosh(\beta_n\cdot x)\right)\right]$$

$$H(x) := C\cdot\left[-\sin(\beta_n\cdot x)\cdot(\beta_n)^2-\sinh(\beta_n\cdot x)\cdot(\beta_n)^2-\frac{\left(\sin(\beta_n\cdot l)+\sinh(\beta_n\cdot l)\right)}{\left(\cos(\beta_n\cdot l)+\cosh(\beta_n\cdot l)\right)}\cdot\left[-\cos(\beta_n\cdot x)\cdot(\beta_n)^2-\cosh(\beta_n\cdot x)\cdot(\beta_n)^2\right]\right]$$

$$\omega A := \sqrt{\frac{E\cdot I\cdot\int_0^{1.7}(H(x))^2\,dx}{\rho 1\cdot A\cdot\int_0^{1.7}G(x)^2\,dx}}$$

$\omega A = 299.248$

$n := 2$

$$G(x) := C \cdot \left[\sin(\beta_n \cdot x) - \sinh(\beta_n \cdot x) - \left(\frac{\sin(\beta_n \cdot l) + \sinh(\beta_n \cdot l)}{\cos(\beta_n \cdot l) + \cosh(\beta_n \cdot l)} \right) \cdot (\cos(\beta_n \cdot x) - \cosh(\beta_n \cdot x)) \right]$$

$$H(x) := C \cdot \left[-\sin(\beta_n \cdot x) \cdot (\beta_n)^2 - \sinh(\beta_n \cdot x) \cdot (\beta_n)^2 - \frac{(\sin(\beta_n \cdot l) + \sinh(\beta_n \cdot l))}{(\cos(\beta_n \cdot l) + \cosh(\beta_n \cdot l))} \cdot \left[-\cos(\beta_n \cdot x) \cdot (\beta_n)^2 - \cosh(\beta_n \cdot x) \cdot (\beta_n)^2 \right] \right]$$

$$\omega B := \sqrt{\frac{E \cdot I \cdot \int_0^{1.7} (H(x))^2 \, dx}{\rho 1 \cdot A \cdot \int_0^{1.7} G(x)^2 \, dx}} \qquad \omega B = 1.875 \cdot 10^3$$

$n := 3$

$$G(x) := C \cdot \left[\sin(\beta_n \cdot x) - \sinh(\beta_n \cdot x) - \left(\frac{\sin(\beta_n \cdot l) + \sinh(\beta_n \cdot l)}{\cos(\beta_n \cdot l) + \cosh(\beta_n \cdot l)} \right) \cdot (\cos(\beta_n \cdot x) - \cosh(\beta_n \cdot x)) \right]$$

$$H(x) := C \cdot \left[-\sin(\beta_n \cdot x) \cdot (\beta_n)^2 - \sinh(\beta_n \cdot x) \cdot (\beta_n)^2 - \frac{(\sin(\beta_n \cdot l) + \sinh(\beta_n \cdot l))}{(\cos(\beta_n \cdot l) + \cosh(\beta_n \cdot l))} \cdot \left[-\cos(\beta_n \cdot x) \cdot (\beta_n)^2 - \cosh(\beta_n \cdot x) \cdot (\beta_n)^2 \right] \right]$$

$$\omega C := \sqrt{\frac{E \cdot I \cdot \int_0^{1.7} (H(x))^2 \, dx}{\rho 1 \cdot A \cdot \int_0^{1.7} G(x)^2 \, dx}} \qquad \omega C = 5.251 \cdot 10^3$$

$n := 4$

$$G(x) := C \cdot \left[\sin(\beta_n \cdot x) - \sinh(\beta_n \cdot x) - \left(\frac{\sin(\beta_n \cdot l) + \sinh(\beta_n \cdot l)}{\cos(\beta_n \cdot l) + \cosh(\beta_n \cdot l)} \right) \cdot \left(\cos(\beta_n \cdot x) - \cosh(\beta_n \cdot x) \right) \right]$$

$$H(x) := C \cdot \left[-\sin(\beta_n \cdot x) \cdot (\beta_n)^2 - \sinh(\beta_n \cdot x) \cdot (\beta_n)^2 - \frac{\left(\sin(\beta_n \cdot l) + \sinh(\beta_n \cdot l) \right)}{\left(\cos(\beta_n \cdot l) + \cosh(\beta_n \cdot l) \right)} \cdot \left[-\cos(\beta_n \cdot x) \cdot (\beta_n)^2 - \cosh(\beta_n \cdot x) \cdot (\beta_n)^2 \right] \right]$$

$$\omega D := \sqrt{\frac{E \cdot I \cdot \int_0^{1.7} (H(x))^2 \, dx}{\rho 1 \cdot A \cdot \int_0^{1.7} G(x)^2 \, dx}}$$

$\omega D = 1.029 \cdot 10^4$

Exact Solution

$\omega_1 = 299.248$

$\omega_2 = 1.875 \cdot 10^3$

$\omega_3 = 5.251 \cdot 10^3$

$\omega_4 = 1.029 \cdot 10^4$

Rayleigh's Solution

$\omega A = 299.248$

$\omega B = 1.875 \cdot 10^3$

$\omega C = 5.251 \cdot 10^3$

$\omega D = 1.029 \cdot 10^4$

Appendix E

Appendix E

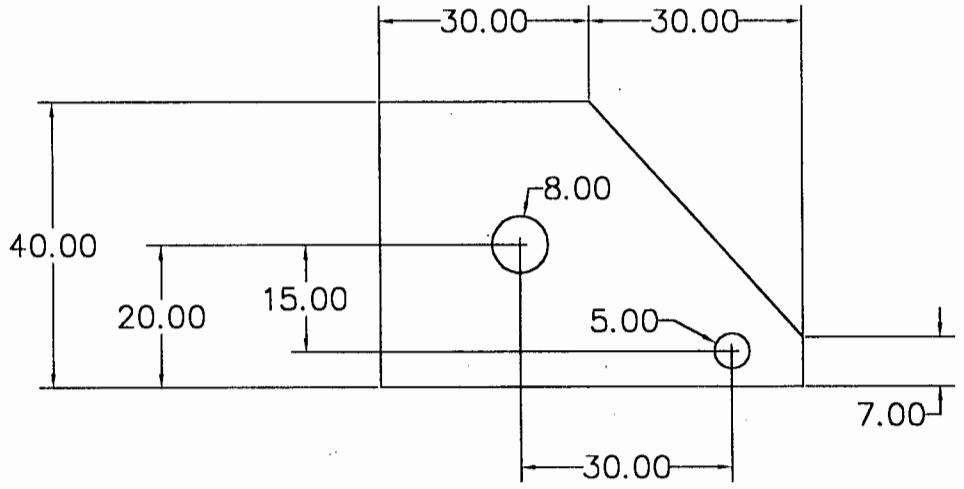

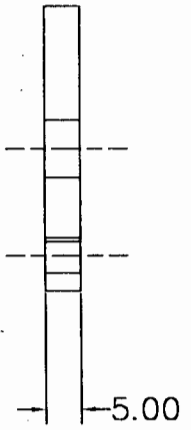

Hole Diameters: 8.00 +0.02/−0.00 5.00 +0.02/−0.00
Material : Mild Steel
UNIVERSITY OF CAPE TOWN Department of Mechanical Engineering
SLIDE PLATE
Date : February 1996 Drawn by : B.P.Prestage

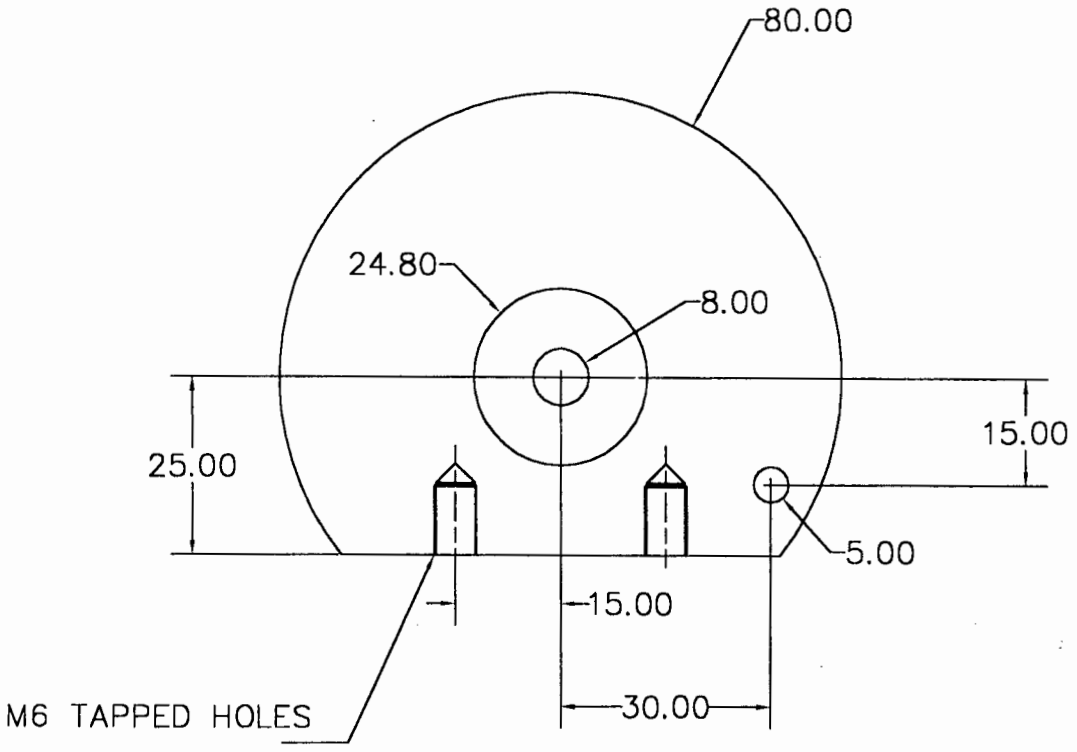

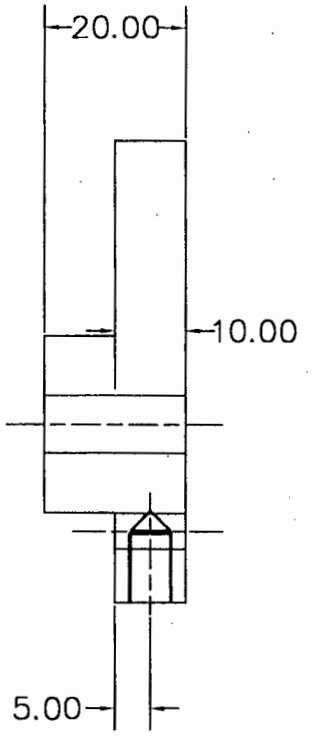

Hole Diameters: 8.00 +0.02/−0.00 5.00 +0.02/−0.00
Material : Mild Steel
UNIVERSITY OF CAPE TOWN Department of Mechanical Engineering
SLIDE SUPPORT (Furthest from pole)
Date : February 1996 Drawn by : B.P.Prestage

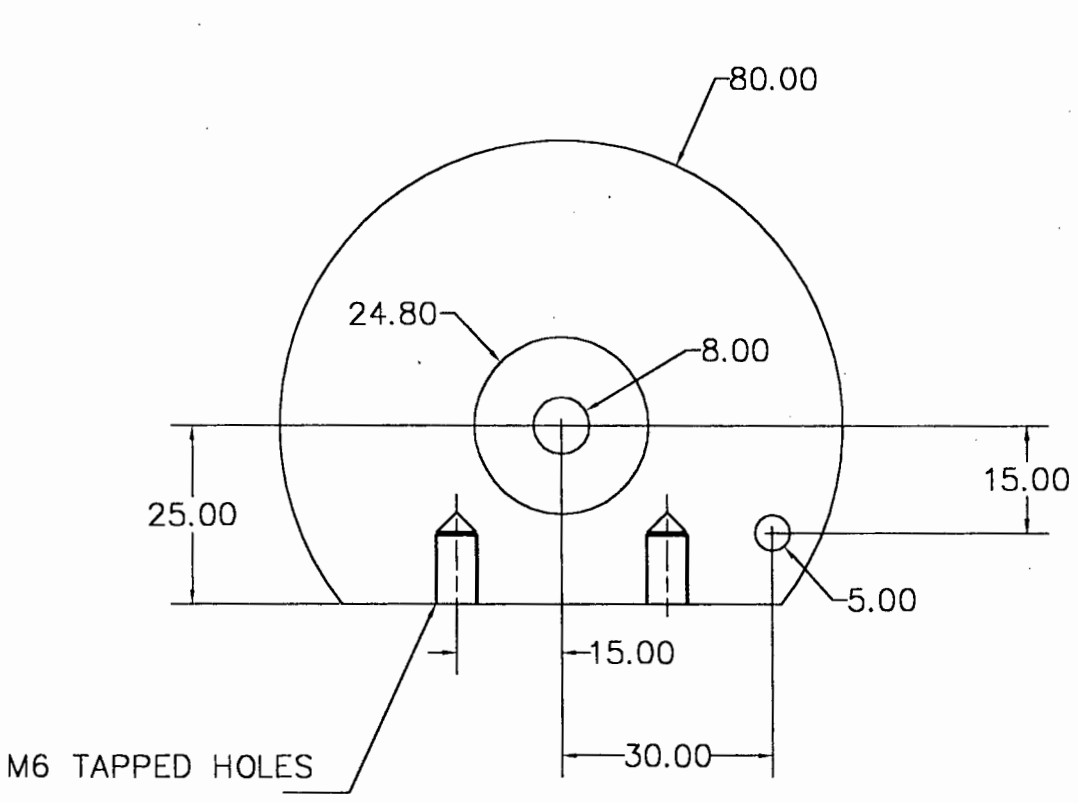

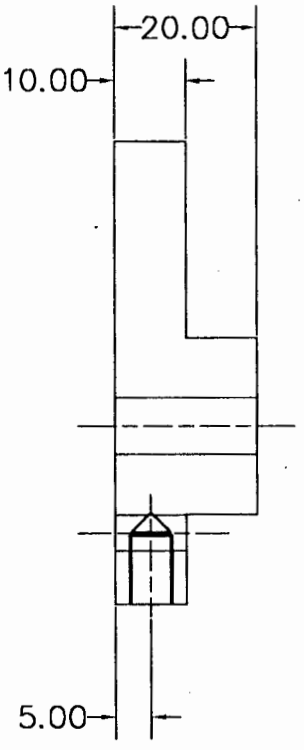

Hole Diameters: 8.00 +0.02/−0.00 5.00 +0.02/−0.00
Material : Mild Steel
UNIVERSITY OF CAPE TOWN Department of Mechanical Engineering
SLIDE SUPPORT (Closest to pole)
Date : February 1996 Drawn by : B.P.Prestage

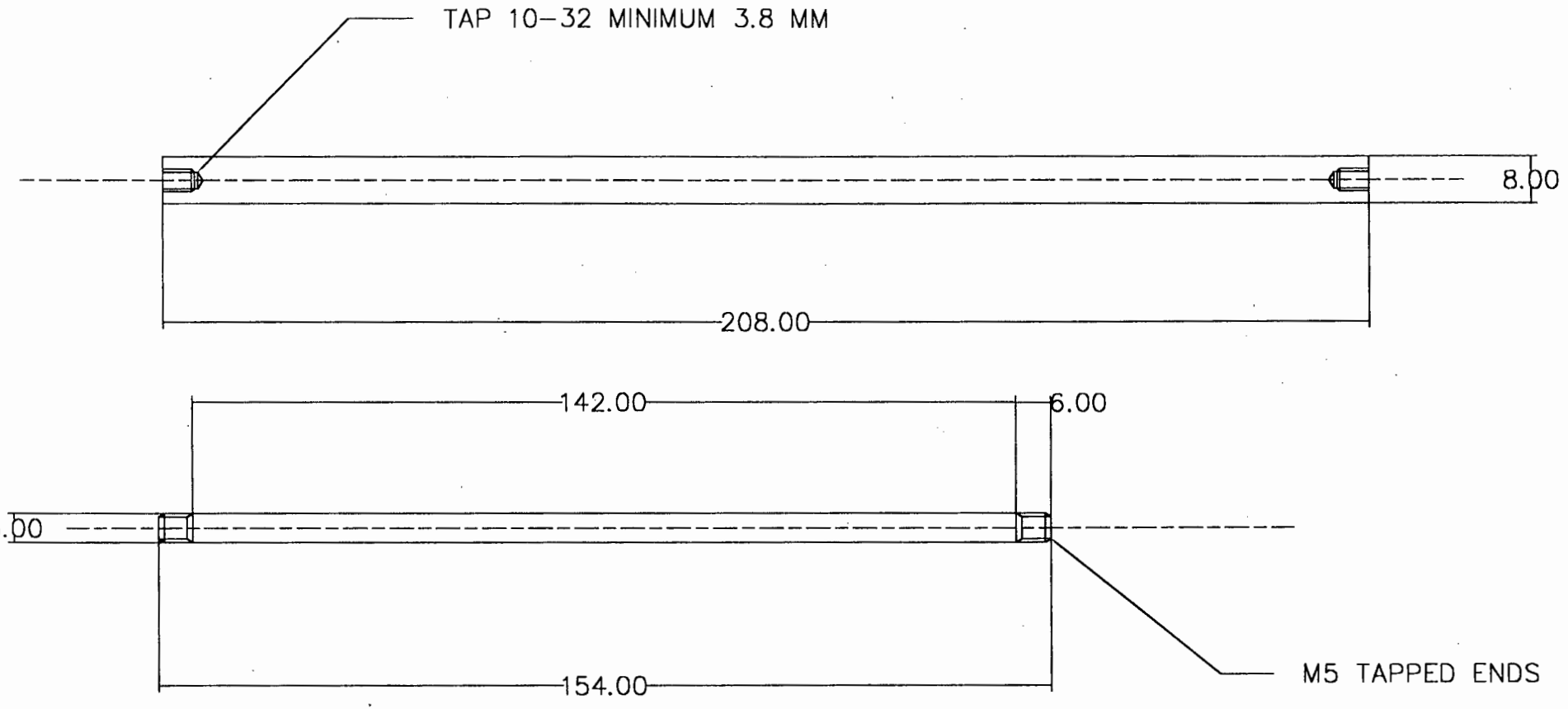

One off. each
Material : Silver Steel
UNIVERSITY OF CAPE TOWN Department of Mechanical Engineering
SLIDER SHAFTS
Date : February 1996 Drawn by : B.P.Prestage

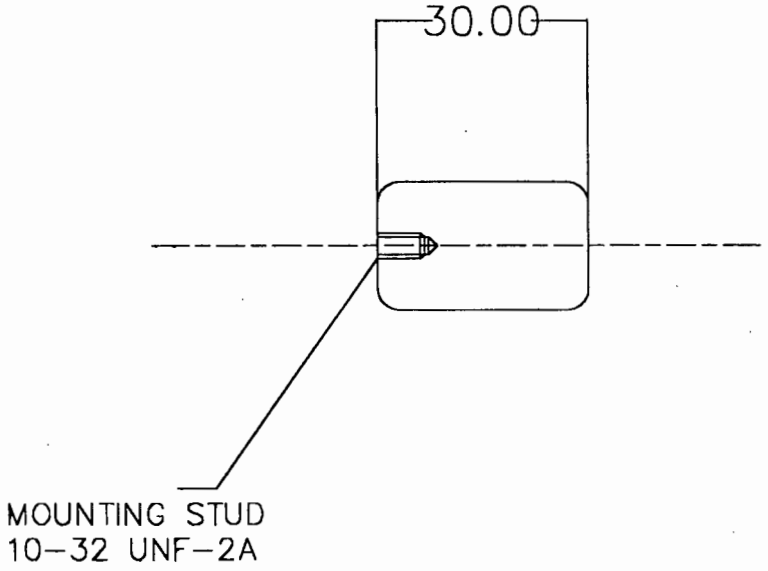

Material : Mild Steel
UNIVERSITY OF CAPE TOWN Department of Mechanical Engineering
SLIDER KNOB
Date : February 1996 Drawn by : B.P.Prestage

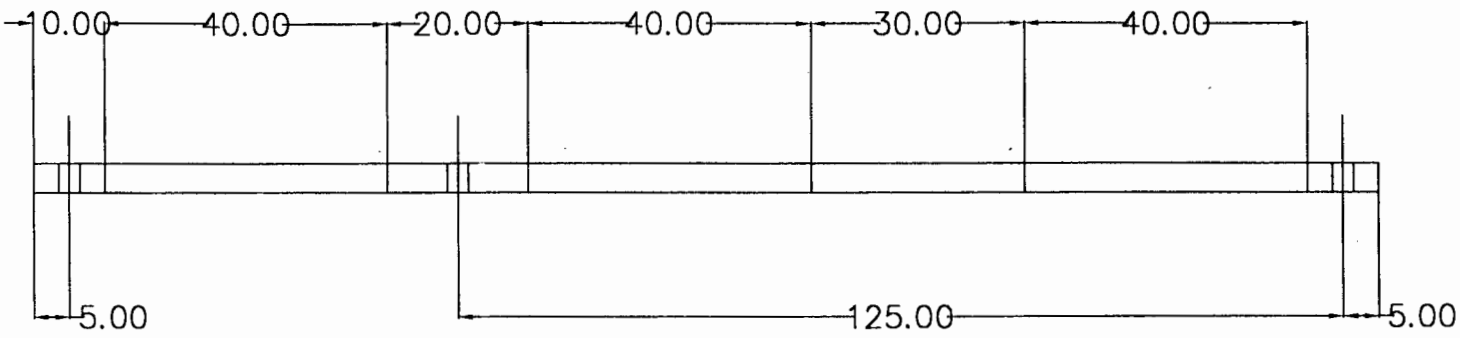

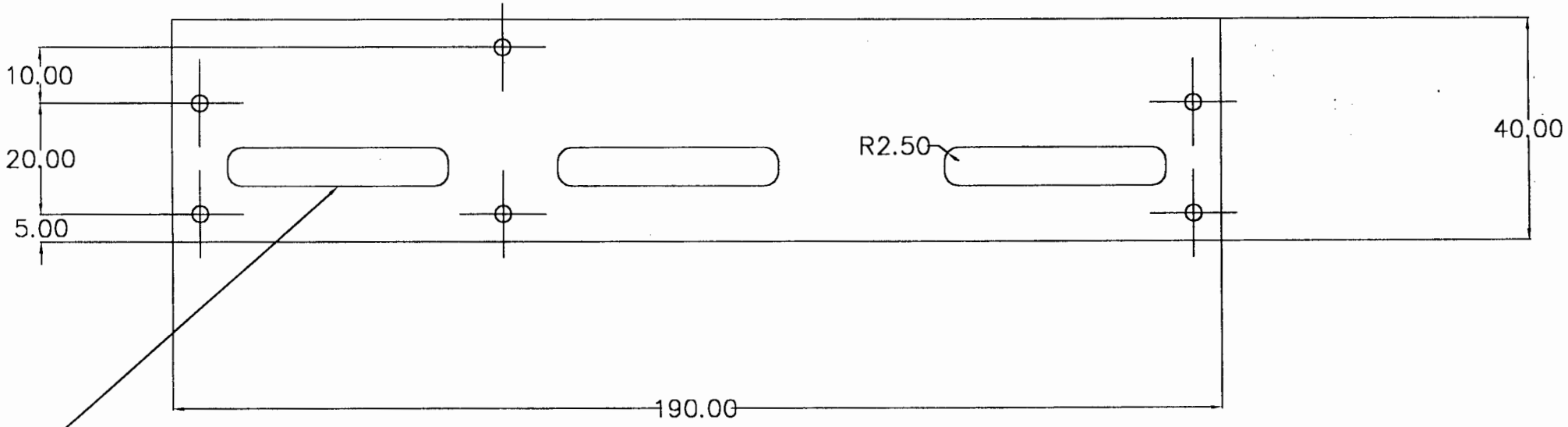

GROOVES 40 MM LONG 7.5 MM WIDE WITH R 2.5 ENDS

Two off. each
Material : Mild Steel
UNIVERSITY OF CAPE TOWN Department of Mechanical Engineering
SIDE SUPPORTS FOR STRAPS
Date : February 1996 Drawn by : B.P.Prestage

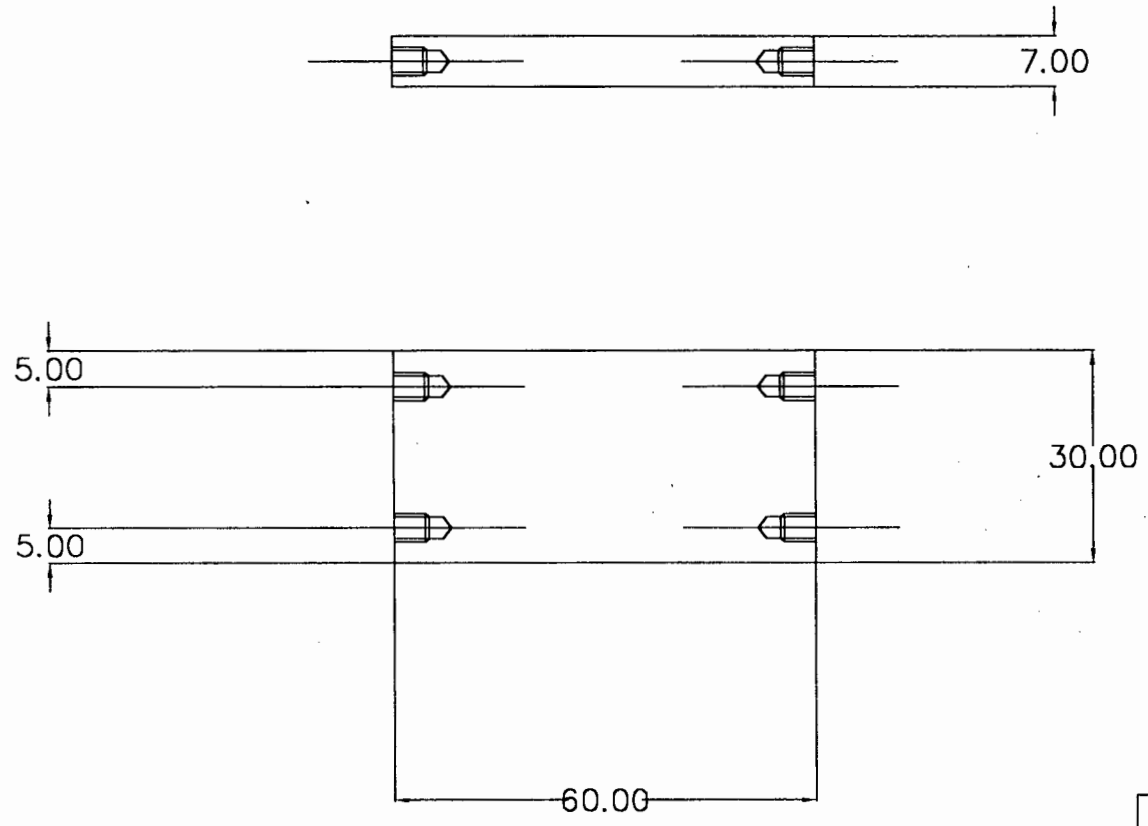

Two off. each
Material : Mild Steel
UNIVERSITY OF CAPE TOWN Department of Mechanical Engineering
TOP BRACE FOR SIDE SUPPORTS
Date : February 1996 Drawn by : B.P.Prestage

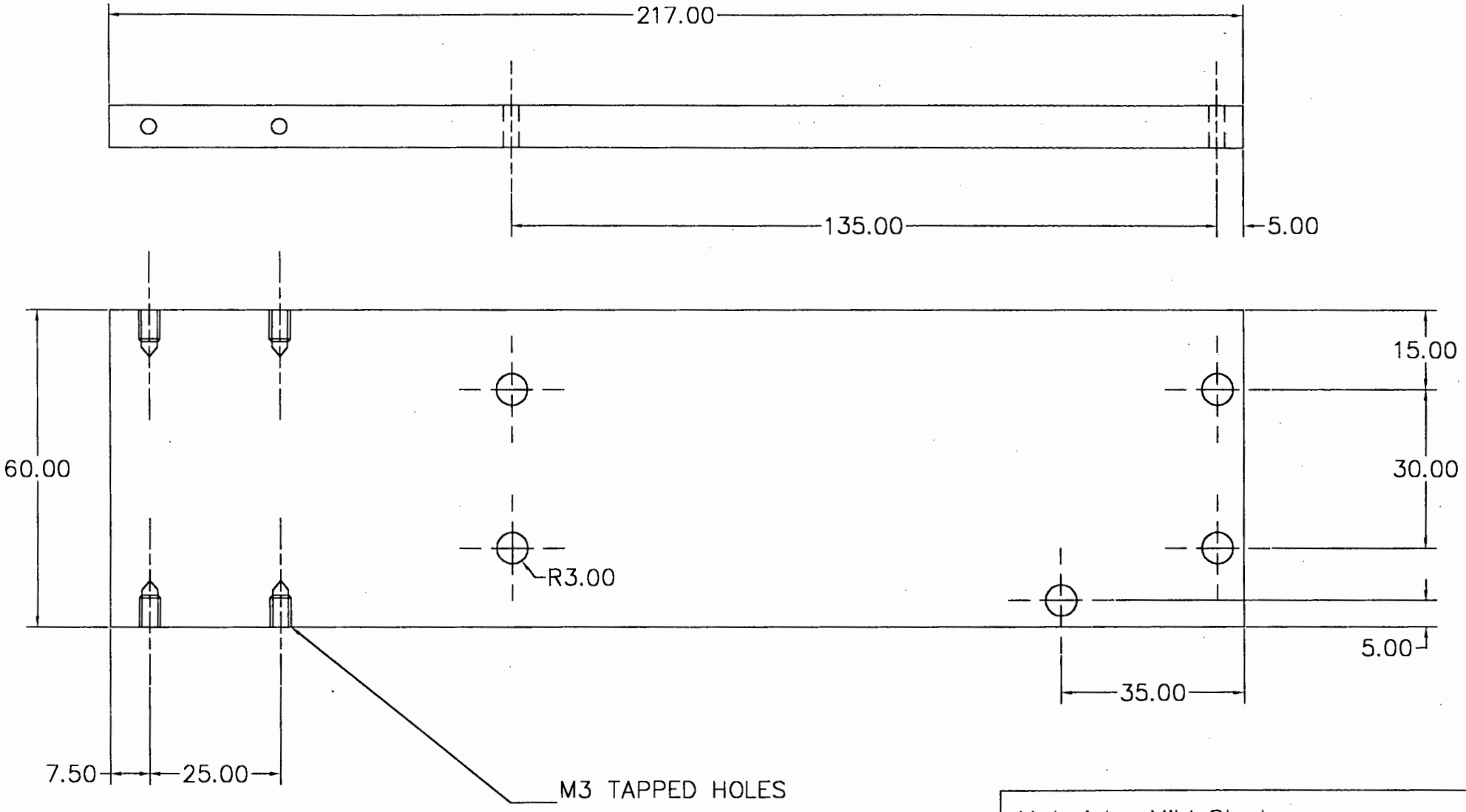

Material : Mild Steel
UNIVERSITY OF CAPE TOWN Department of Mechanical Engineering
BASE PIECE
Date : February 1996 Drawn by : B.P.Prestage

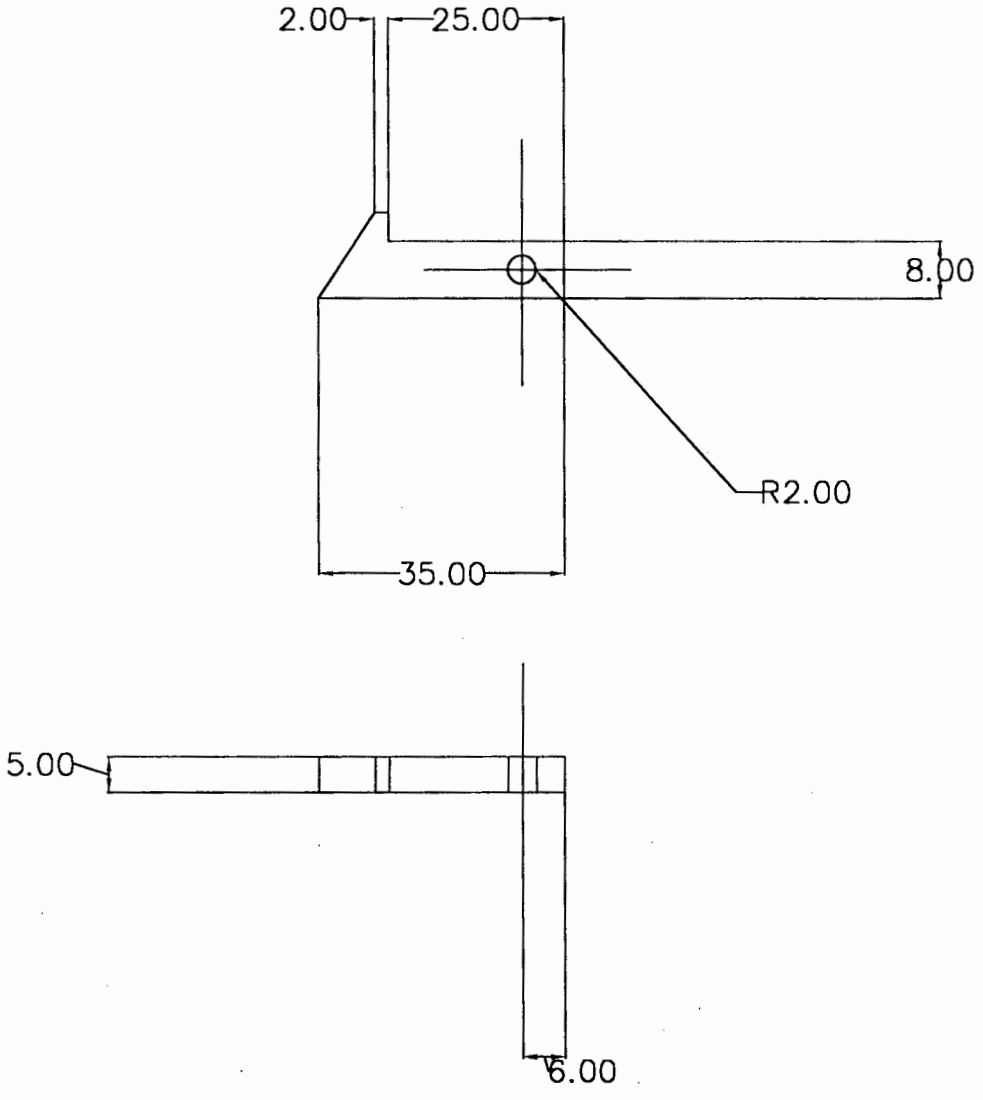

Material : Mild Steel
UNIVERSITY OF CAPE TOWN Department of Mechanical Engineering
TRIGGER
Date : February 1996 Drawn by : B.P.Prestage

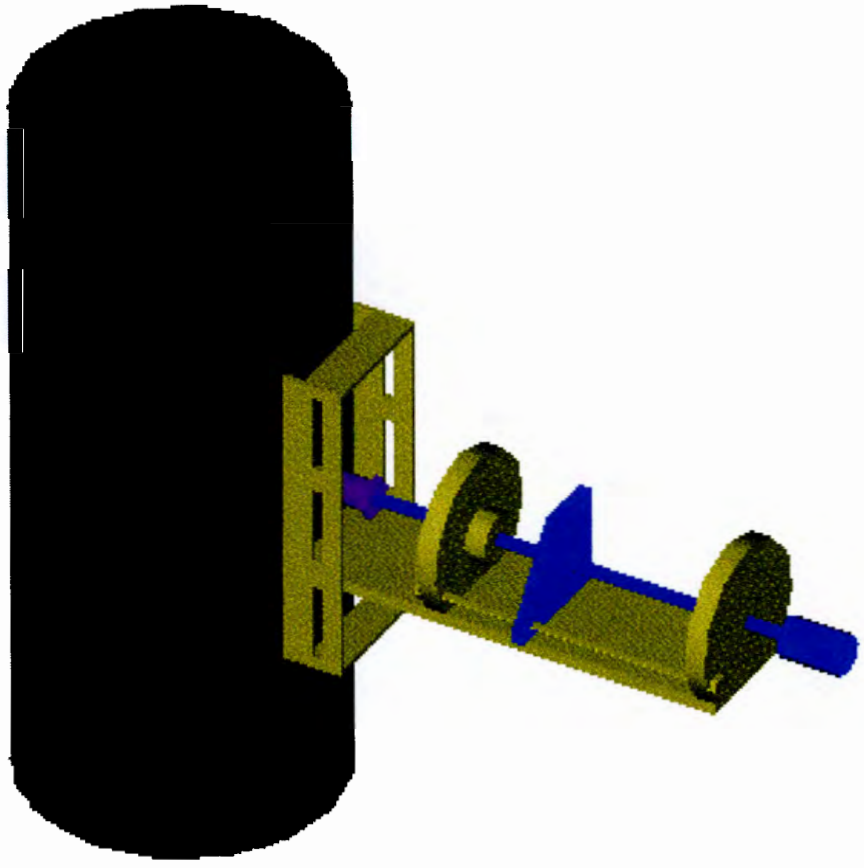

UNIVERSITY OF CAPE TOWN
Department of Mechanical Engineering

ASSEMBLY DRAWING SHOWING IMPACTOR STRAPPED TO POLE

Date : February 1996
Drawn by : B.P.Prestage

Appendix F

Appendix F

Pole A

Pole A

Pole B

Pole B

Pole C

Pole C

Pole D

Pole D

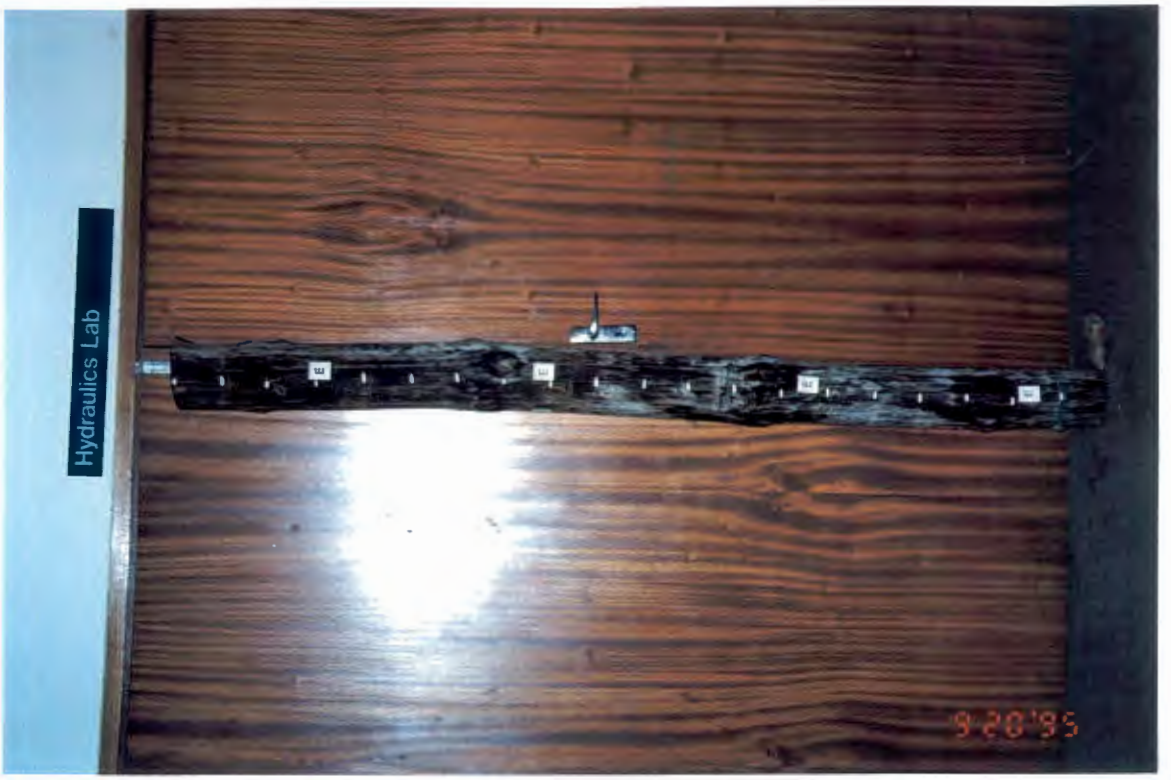

Pole E

Pole E

Pole F

Pole F

Pole G

Pole G

Pole F Showing Centre Crack and Decay

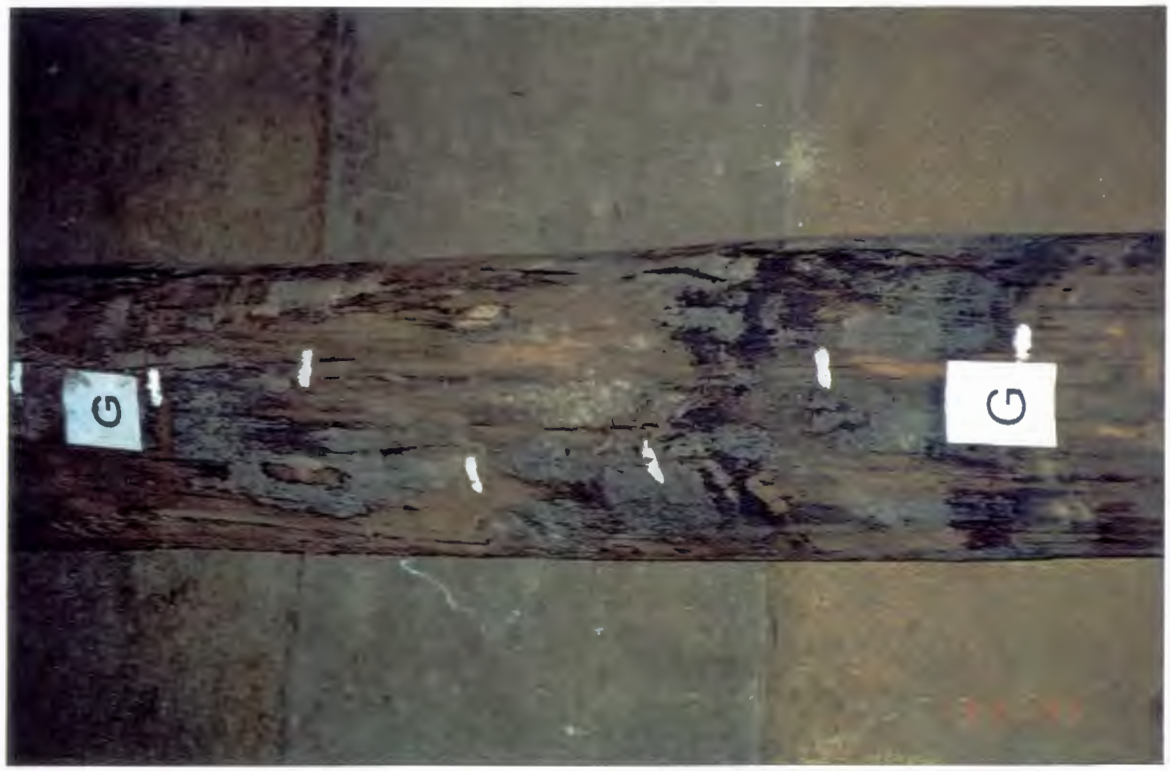

Pole G Showing Decay

slide is then loaded and held in place by the trigger mechanism. Figure 16 illustrates the impactor used in the experimental procedure.

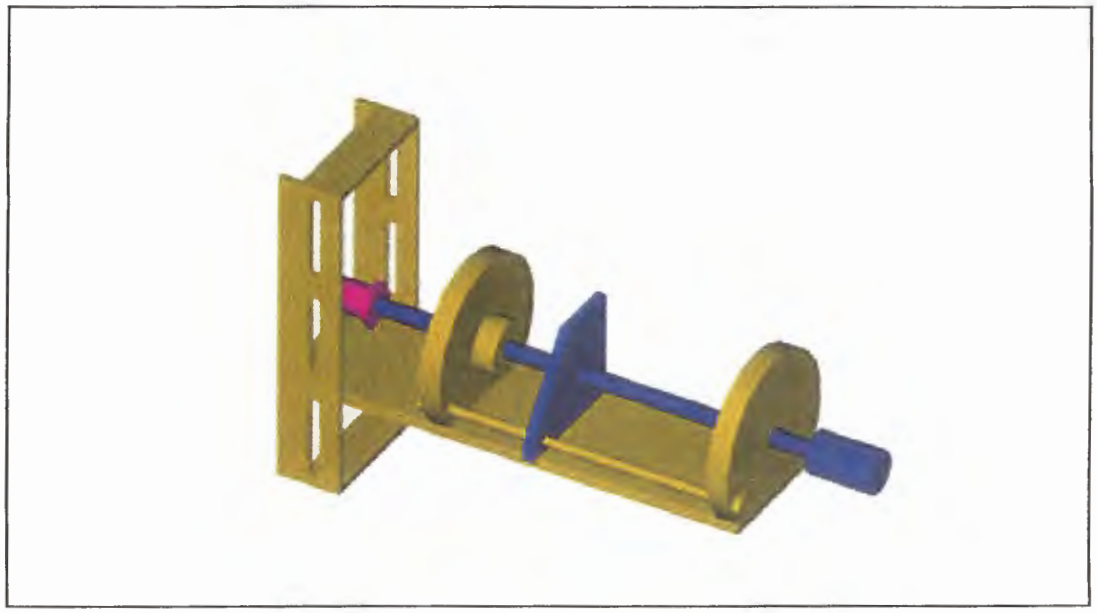

Figure 16: Diagram of Impactor

Photograph 1: The Isolation of the Experiment from External Vibration.